THE GENERALISED CONFORMAL FIELD EQUATIONS NEAR SPATIAL INFINITY

Georgios Doulis

a thesis submitted for the degree of

Doctor of Philosophy

at the University of Otago, Dunedin,

New Zealand.

Contents

Introduction

In late 1915, during the madness of Word World I, somewhere in Europe a ray of hope and logic was rising: Albert Einstein published, in a compact four page article, his celebrated field equation for gravity [18]. These equations—a highly non-linear system of partial differential equations—comprised the hallmark of what would be later known as the general theory of relativity. They represented the completely novel idea of interrelating gravity with the geometry of the underlying space-time. Now curvature becomes the primary concept and gravity reduces to just a (secondary) manifestation of it. Broadly speaking, gravity became an artifact; a mathematical creation that helps us to describe Nature's weakest way of interaction. Because of this, gravity lost its primary status as a "pure" fundamental force of Nature and became a so-called pseudo-force.

By explaining the precession of the perihelion of Mercury—an unsolved problem for almost half a century—and by predicting the bending of light by the Sun, the new theory managed to draw the attention of the scientific community—especially, after its first observational verification by *Sir A. Eddington* during the solar eclipse of 29th of May 1919, where was confirmed that the Sun was, indeed, bending the light rays that were passing close enough from it. Soon after Einstein's original publication the first exact solutions to his equations started to be published. In 1916 a static spherically symmetric [81] and a static charged spherically symmetric [72] solution to his equations were found by Schwarzschild and Reissner, respectively. The de Sitter solution [15] and the (homogeneous and isotropic) cosmological solutions of Friedman [26], [27] soon followed. Thus, the new theory had already—only a decade after its publication—acquired a dominant position in astronomy, cosmology, astrophysics, and the study of the structure of space-time.

In contrast to its rapid development in the aforementioned fields, general relativity progressed slowly in the study of gravitational waves despite the fact that

very early—already in 1918—Einstein showed [19] that his field equations—after a proper linearization—admit the existence of gravitational waves. Their weak, and for that difficult to detect, nature declined physicists' interest on them. As this observationally "unpleasant" property was not already enough, in 1936 Einstein himself abnegated their existence in (the original form of) a paper [20] with Rosen![1]

But things, fortunately, started to change in the late '50s with the introduction of the notion of an isolated system in general relativity. Pioneering work done by people like Pirani [70], Trautman [86], and Bondi et al. [7] was proposing that, by using the aforementioned notion, the study of gravitational phenomena could be done without the "rough" simplification implied by the linearization of the field equations. In essence, this idea was suggesting that the bypassing of the linearization procedure would reveal new features of the field equations. Features that are directly related to the non-linear nature of the equations and remained in the dark because of the (artificial) linearization of Einstein's equations.

An isolated system is, of course, an idealization of Nature's workings. It is, actually, implying that a source of gravitational waves—like a binary system of neutron stars or black holes, a fast spinning neutron star, etc.—can be thought of as being largely separated of other similar sources, where the influence of the latter can be taken into account only in the form of the gravitational radiation emitted by them. In a similar fashion, an observer is placed far away—at "infinity"—from these objects; so the only information the observer gets is encoded in the gravitational radiation that is received from them. But, automatically, this arrangement—i.e. the placement of the observer at a distance where the gravitational phenomena become weak—leads naturally to the notion of an asymptotically flat space-time. This means that the space-time, independently of how much curved is near massive objects, at infinity resembles Minkowski space-time—i.e. its curvature dies off. At these regions the gravitational fields are expected to develop a wave-like behaviour as the space-time is actually becoming Minkowski there. Exactly this feature is that helps us to bypass the artificial linearization of the field equations, as now the emerging of the gravitational waves is led exclusively to the geometry of the space-time under

---

[1]Of course, [20], in its final revised form, published in 1937, contains the Einstein-Rosen solution of Einstein's field equations. But in its original 1936 form entitled "Do Gravitational Waves Exist?", the authors concluded that Einstein's equations were not admitting wavelike solutions. For a more detailed account of this fascinating story, see [46]

consideration.

Based on these assumptions people like Bondi et al. [8], Newman and Penrose [59], and Sachs [75], [76] tried to construct models that describe how fields behave at infinity. But, dealing with infinity is a difficult task, especially when one wants to incorporate it in analytical and numerical calculations that involve limits "as one goes to infinity". Thus, these attempts unavoidably depended heavily on the physical intuition and creativity of their authors, and on previous simplified models. Something was missing! A very important ingredient that would provide a consistent and solid ground treatment to the study of the behaviour of fields near (and at) space-time infinity was obviously missing.

Sir R. Penrose filled the gap by introducing in [62], [63] the notion of *conformal infinity*—which he called *scri*. It is worth quoting from [62] the original reasoning underlying its introduction by Penrose:

> "... Asymptotic questions are those relating to the "neighborhood of infinity". From the point of view of the metric structure of space-time, however, there is no such thing as a point at infinity, since such a point would be an infinite distance from its neighbors. But if we think only in terms of conformal structure of space-time (only ratios of neighboring infinitesimal distances are to have significance), then infinity can be treated as though it were simply an ordinary three-dimensional boundary to a "finite" four-dimensional region. In fact, we can envisage a new "unphysical" metric assigned (but perhaps only locally) to space-time, which is conformal to the original physical metric, and according to which "infinity" is now finite and in most places regular..."

He unveiled, in this way, the basic features of the geometrical structure underlying this particular field of study. Thus, infinity was brought to a finite distance and, as a consequence, the behaviour of gravitational radiation at infinity could be studied now in local terms. This could be achieved by conformally rescaling the (physical) space-time metric under consideration with an appropriately chosen conformal factor, say, Ω. All the information about infinity is now incorporated in the behaviour of this function; having at hand such a "quantitative" representation of infinity makes our efforts to study it a little bit easier. A question concerning the generality of this procedure naturally emerges at this point, i.e. it is always possible

to find a function Ω with the aforementioned property? In [64], [44] it was rigorously shown that this is possible for all the physically interesting exact solutions of Einstein's equations. An extremely pleasant property of the above proposition is that any other conformal rescaling, say by a function ϑ, of the unphysical metric—or equivalently of the already rescaled physical metric—is diffeomorphic to it. This feature give us the freedom to chose Ω in a way that fits better with the specific problem under consideration, i.e. Ω is a "gauge" function.

The next step one has to take, in order to proceed further in the study of the behaviour of gravitational radiation at (and near) space-time infinity, is to express Einstein's equations in the aforementioned conformal picture and, subsequently, to establish their form at infinity—which is now brought to a finite distance. In addition, the above steps must be made in such a way that the choice of Ω must be compatible with the fact that the physical metric has to satisfy Einstein's field equations—a task not so straightforward as it sounds. Various ingenious attempts to address this problem were made, in the three decades following Penrose's original publication [62], by a vast—for the standards of this particular field of study—number of authors: Geroch [39], [40]; Schmidt [77], [78]; Sommers [82]; Persides [67]-[69]; Ashtekar and Hansen [3]; Ashtekar and Romano [4]; Ko, Newman, and Tod [47]; Penrose [64]; Friedrich [28], [29], [32], [33]. Specifically, in [39], [40] and [28], [29], [32], [33] a novel description of both null and spatial infinity was proposed; in [64] and [47] only null infinity was studied; in [77], [78], [82], [67]-[69], [3], [4] Penrose's approach [64] to null infinity was adopted, but spatial infinity was treated in a different way.

In this work, we are going to concentrate our attention on H. Friedrich's approach to space-like and null infinity originally presented in [32] and [33]. His interpretation is based solely on the initial data, the field equations, and the conformal structure of space-time. The key feature in this analysis is the manipulation of the available gauge freedom provided by the conformal structure. Thus, in addition to the extensive exploitation of the gauge nature of the conformal factor Ω—carried out in [28], [29]—Friedrich introduces in [32] another possible freedom arising from the use of a torsionless (non-metric) connection—the so-called Weyl connection—instead of a Levi-Civita connection. By using a Weyl connection to express the field equations Friedrich achieves a considerable simplification of the resulting evolution equations. Specifically, with only exception the symmetric hyperbolic system governing the

evolution of the rescaled Weyl tensor, no spatial derivatives of the unknown quantities are involved anymore in the evolution equations. Numerically, this feature of Friedrich's field equations is extremely pleasant. This set of field equations is known as the *general conformal field equations*. Moreover, in this scheme, the "stiff" problem of the singular behaviour of the conformal fields at space-like infinity is addressed in a rigorous way.

In a string of papers [22]-[24] Frauendiener managed to employ the "ancestors" of the general conformal field equations, namely the *metric conformal field equations*, introduced in [28], [29], into a numerical code and study their behaviour at null infinity. Therein the Cauchy problem especially adapted to the conformal nature of the metric conformal field equations was used for the numerical treatment of asymptotically flat space-times. The "unphysical" space-time plays here the primary role as in Penrose's picture the physical space-time consists a finite portion of it. In this picture the boundaries of the physically interesting parts of the space-time under consideration are given by the equation $\Omega = 0$. In this way, the boundary emerges naturally from the conformal picture and thus it does not have to be artificially introduced. But this nice feature comes with an additional complication: the conformal factor is not known beforehand and for that it must be computed during the evolution.[2]

Taking advantage of Friedrich's result [30] that the hyperboloidal initial value problem is well-posed,[3] the "unphysical" space-time can be foliated in an appropriate way by space-like hypersurfaces that manifest themselves as hyperboloidal hypersurfaces in the physical space-time. The initial data is prescribed on one of these hyperboloidal hypersurfaces and is evolved by the evolution equations. The primary reason for the introduction of the hyperboloidal hypersurfaces was the avoidance of space-like infinity where some of the components of the Weyl tensor are singular; thus, this setting cannot be used to study regions close to space-like infinity.

But, in order to study the gravitational radiation emitted by isolated astrophysical objects in all its generality, we must incorporate in our studies the region of space-time that serve as a connection between the ingoing and outgoing radiation, i.e. space-like infinity i^0. One's main concern is to address the problem at future

---

[2]Einstein's field equations can be used for this purpose.

[3]Namely, given smooth Cauchy initial data there exist a solution of the metric conformal field equations in some small neighbourhood of the initial hypersurface.

null infinity $\mathscr{I}^+$, where the detectors of gravitational waves are placed,[4] but in order to acquire a complete and cohesive picture of the global procedures involved one has also to study what happens at space-like infinity, and especially at the interface between space-like and null infinity. The general conformal field equations provide an ideal arena for such an effort. In [33] Friedrich managed to construct an initial value problem for the conformal representation of the Einstein's equation, which is regular near space-like infinity, through a procedure of which the main ingredient is the blowing up of space-like infinity i^0 to a *cylinder I*. Now, the Cauchy initial data can be prescribed on generic space-like hypersurfaces, i.e. the use of hyperboloidal hypersurfaces is not essential anymore.

As was already mentioned above in this representation of Einstein's field equations, the resulting evolution equations acquire—except of the ones controlling the evolution of the rescaled Weyl tensor—an extremely simple form, where only "time" derivatives occur in their expressions. On the cylinder though, which now represents space-like infinity, even the spatial derivatives in the evolution equations of the rescaled Weyl tensor drop out, forming an intrinsic system of evolution equations on the cylinder. Obviously, the cylinder is a *total* characteristic of the general conformal field equations.

In addition, by specifying the gauge in which the evolution equations acquire the aforementioned very convenient form, one also specifies the form of the conformal factor Ω. Thus, the location of null infinity is now known beforehand and it does not have to be computed during the evolution.

All these features, namely the regularity of the initial data, the fixed location of null infinity, the fact that the whole of the physical space-time can be covered by one computational domain, and the extremely simple form of the evolution equations (especially on the cylinder), make the general conformal field equations extremely suitable for numerical manipulations.

However, as expected,[5] the intrinsic system of evolution equations on the cylinder degenerates at the interface of the cylinder I with null infinity. In general, the solutions generate logarithmic singularities at these regions which are expected to travel along null infinity and spoil its smoothness, making it impossible to read-

---

[4]The metric conformal field equations serve this purpose.

[5]It is a general feature of Einstein's field equations that there exist asymptotically flat data that develop non-smooth singular behaviour at null infinity.

off the gravitational radiation at I^+. In Friedrich's approach this generic singular behaviour of asymptotically flat solutions to Einstein's field equations is successfully reproduced, but in a more manageable way. Now, the appearance of this singular behaviour has been made explicit and its occurrence and precise nature has been related to the structure of the initial data. In other words, there is a possibility that by choosing appropriately the initial data the occurrence of non-smooth features in the solutions at null infinity can be avoided. A possible way out of this problem, that has been investigated already in [33], is to prescribe initial data that respect the regularity conditions proposed therein.

In this work, we will use Friedrich's general conformal fields equations to evolve generic asymptotically Euclidean initial data in the vicinity of space-like infinity. We will begin our endeavour from the simplest possible case: linearised gravitational fields on a Minkowski background. Although simple, this "toy model" encapsulates all the crucial characteristics of the full non-linear system. Namely, the cylinder must be introduced in order to set our initial data regular and the intrinsic to the cylinder evolution equations degenerate at the regions $I^\pm$ that the cylinder meets null infinity. We will try to evolve the initial data as close as possible to the ill-behaved regions $I^\pm$ and study the behaviour of our numerical solutions there. This procedure will be carried out twice by using the linearised general conformal field equations in their first and second order form, where the latter can be derived from the former. Although analytically, the two approaches are equivalent, their numerical implementation could possibly address the same issues differently [49].[6] Spotting these differences and detecting any potential numerical advantages or disadvantages between the two approaches will be also one of our goals here.

In Chapter 1, a short overview of the ideas put forward in [32], [33], which depicts their current understanding by the author, will be attempted. The exposition there closely parallels the discussion in the survey articles [34], [37]. The two following chapters are devoted to the first order representation of the general conformal field equations. Chapter 2 sets the analytical background of the problem, while Chapter 3 deals with the numerical implementation of the system. Chapter 3 also contains all our results regarding numerical solutions for various classes of initial data. The structure of the remaining two chapters is similar, but they are addressing the second

---

[6]In [49], it has been pointed out that the numerical evolution of a system using second order wave equations has several advantages compared to a system of first order equations.

order representation of the general conformal field equations. Again, Chapter 4 is concerned with the analytical work, while in Chapter 5 the analytical setting of Chapter 4 is implemented numerically and our numerical findings are presented.

Chapter 1

The conformal representation of Einstein's field equations

1.1 The conventional picture

Both the desire to study gravitational radiation emanating from an isolated system and the placement of the observer (i.e. of our detectors) at an infinite space-time distance from it, entail that we have to look for vacuum solutions of Einstein's field equations, namely[1]

$$\tilde{R}_{\mu\nu}[\tilde{g}] = 0, \tag{1.1}$$

where with $\tilde{}$ we will denote all the quantities related to a so-called "physical" (Lorentzian) manifold $(\tilde{M}, \tilde{g})$. Since general solutions to this equation are not still (and maybe will not be in the near future) available, we have to think of an alternative way to attack this problem.

A possible way to deal with it is by trying to express (1.1) in the conformal picture. To do that we have to introduce an "unphysical"[2] (conformal) metric $g_{\mu\nu}$, which is related to the "physical" metric $\tilde{g}_{\mu\nu}$ through the relation

$$g_{\mu\nu} = \Omega^2 \tilde{g}_{\mu\nu}, \tag{1.2}$$

where the *conformal factor* Ω is positive. (All the quantities related to the "unphysical" (Lorentzian) manifold (M, g) will be denoted without a $\tilde{}$.) Thus, by using (1.2)

---

[1]The cosmological constant is considered, here, zero.
[2]The use of the terms "physical" and "unphysical" will be justified later, see sec. 1.4.

we can express Einstein's field equations in the conformal scheme:

$$R_{\mu\nu}[g] = \tilde{R}_{\mu\nu}[\tilde{g}] - 2\,\Omega^{-1}\nabla_\mu\nabla_\nu\,\Omega - g_{\mu\nu}\Omega^{-1}\left(\square\,\Omega - 3\,\Omega^{-1}\nabla_\rho\,\Omega\nabla^\rho\,\Omega\right), \qquad (1.3)$$

where $\square \equiv \nabla_\rho\nabla^\rho$ and ∇ is the Levi-Civita connection of g. By observing (1.1) and assuming that Ω is given, expression (1.3) can be considered, in a local coordinate system x^μ, as a second order partial differential equation for g, i.e.

$$\partial_{[\rho}\,\Gamma_{\nu]}{}^\rho{}_\mu + \Gamma_\lambda{}^\rho{}_{[\rho}\,\Gamma_{\nu]}{}^\lambda{}_\mu = -\,\Omega^{-1}\nabla_\mu\nabla_\nu\,\Omega - \frac{1}{2}\,g_{\mu\nu}\Omega^{-1}\left(\square\,\Omega - 3\,\Omega^{-1}\nabla_\rho\,\Omega\nabla^\rho\,\Omega\right),$$

where $\Gamma_\mu{}^\rho{}_\nu = \frac{1}{2}\,g^{\rho\lambda}(\partial_\nu\,g_{\lambda\mu} + \partial_\mu\,g_{\lambda\nu} - \partial_\lambda\,g_{\mu\nu})$. Despite this nice feature, equation (1.3) has two major drawbacks arising from the nature of the particular problem we want to address—namely the structure of asymptotically flat space-times. The first one is closely related to our desire to study the behaviour of gravitational fields near infinity, i.e. where $\Omega \to 0$.[3] Obviously, the r.h.s of (1.3) is *singular* in this limit. The second difficulty arises from the fact that in general the function Ω is not given a priori and for that it has to be calculated somehow.

1.2 Metric conformal field equations

It follows, from the discussion above, that the conformal setting (1.3) of Einstein's equations is not the most appropriate for our purposes here. Thus, to proceed further, one must find a conformal representation of (1.1) that i) does not involve any Ω^{-1} terms and ii) ascertains the value of Ω solely from Einstein's equations.

A conformal representation that respects both these requirements was put forward by Friedrich in [28], [29]. The nature of our problem—i.e. solving Einstein's vacuum field equations (1.1) in a conformal scheme—clearly indicates that we have to involve, somehow, in our equations the *Weyl* tensor

$$C^\mu{}_{\nu\lambda\rho} = R^\mu{}_{\nu\lambda\rho} - 2\left(g^\mu{}_{[\lambda}L_{\rho]\nu} - g_{\nu[\lambda}L_{\rho]}{}^\mu\right), \qquad (1.4)$$

where the *Schouten* tensor

$$L_{\mu\nu} = \frac{1}{2}\left(R_{\mu\nu} - \frac{1}{6}\,R\,g_{\mu\nu}\right) \qquad (1.5)$$

---

[3]This statement will be also warranted in sec. 1.4.

was introduced. Such a statement follows quite naturally from the fact that the Weyl tensor is the only non-zero component of the curvature tensor in the absence of matter. In addition, the Weyl tensor governs the propagation of gravitational radiation emitted from isolated systems and describes its behaviour through the peeling-off property.[4]

A possible starting point is the *second Bianchi identity*

$$\nabla_{[\kappa} R^{\mu}{}_{|\nu|\lambda\rho]} = 0, \tag{1.6}$$

which is satisfied by all curvature tensors. Using (1.4) one can express the Bianchi identity in terms of the Weyl and Schouten tensors:

$$\nabla_{[\kappa} C^{\mu}{}_{|\nu|\lambda\rho]} = 2\left(g_{\nu[\lambda}\nabla_{\kappa}L_{\rho]}{}^{\mu} - g^{\mu}{}_{[\lambda}\nabla_{\kappa}L_{\rho]\nu}\right),$$

which, after a contraction of the first two l.h.s indices, takes—in four dimensions—the more compact form

$$\nabla_{\mu} C^{\mu}{}_{\nu\lambda\rho} = \nabla_{\lambda} L_{\rho\nu} - \nabla_{\rho} L_{\lambda\nu}. \tag{1.7}$$

The generality of the above formula is apparent: it holds for any tensor satisfying the decomposition (1.4). Consequently, a similar relation must also hold for quantities defined on the "physical" space-time, namely $\tilde{\nabla}_{\mu} C^{\mu}{}_{\nu\lambda\rho} = \tilde{\nabla}_{\lambda}\tilde{L}_{\rho\nu} - \tilde{\nabla}_{\rho}\tilde{L}_{\lambda\nu}$. (Where obviously $C^{\mu}{}_{\nu\lambda\rho} = \tilde{C}^{\mu}{}_{\nu\lambda\rho}$.) The r.h.s of the last formula vanishes if Einstein's vacuum field equations (1.1) are taken into account (obviously the Schouten tensor (1.5) vanishes when (1.1) is satisfied):

$$\tilde{\nabla}_{\mu} C^{\mu}{}_{\nu\lambda\rho} = 0. \tag{1.8}$$

In order to relate the r.h.s of (1.7) with (1.8) one can use the transformation law

$$\Gamma_{\mu}{}^{\kappa}{}_{\lambda} = \tilde{\Gamma}_{\mu}{}^{\kappa}{}_{\lambda} + \delta^{\kappa}{}_{\mu}\Omega^{-1}\nabla_{\lambda}\Omega + \delta^{\kappa}{}_{\lambda}\Omega^{-1}\nabla_{\mu}\Omega - g^{\kappa\sigma}g_{\lambda\mu}\Omega^{-1}\nabla_{\sigma}\Omega \tag{1.9}$$

of the connection coefficients under the conformal rescaling (1.2) and reproduce the very important relation

$$\nabla_{\mu}(\Omega^{-1} C^{\mu}{}_{\nu\lambda\rho}) = \Omega^{-1}\tilde{\nabla}_{\mu} C^{\mu}{}_{\nu\lambda\rho},$$

---

[4]The peeling-off property states that in asymptotically flat space-times the curvature tensor exhibits the characteristic asymptotic behaviour $\mathcal{O}(r^{n-5})$, $n = 0, \ldots, 4$, for each one of its five independent complex components in the 2-spinor formulation [65], [66]. (Where r is the affine distance from the source of gravitational radiation.) For further details see [76], [64].

which through (1.8) gives the so-called *Bianchi equation*

$$\nabla_\mu d^\mu{}_{\nu\lambda\rho} = 0, \tag{1.10}$$

where

$$d^\mu{}_{\nu\lambda\rho} = \Omega^{-1} C^\mu{}_{\nu\lambda\rho} \tag{1.11}$$

is the *rescaled Weyl tensor* (or gravitational field). The importance of (1.10) follows from its conformally invariant nature and the fact that it controls (in vacuum space-times) the behaviour of the only non-vanishing component of the curvature tensor. Using (1.10) in the form $\nabla_\mu C^\mu{}_{\nu\lambda\rho} = d^\mu{}_{\nu\lambda\rho}\nabla_\mu\Omega$ and (1.11) one can express (1.4) and (1.7) in terms of the rescaled Weyl tensor:

$$R^\mu{}_{\nu\lambda\rho} = \Omega\, d^\mu{}_{\nu\lambda\rho} + 2\left(g^\mu{}_{[\lambda}L_{\rho]\nu} - g_{\nu[\lambda}L_{\rho]}{}^\mu\right), \tag{1.12}$$

and

$$\nabla_\lambda L_{\rho\nu} - \nabla_\rho L_{\lambda\nu} = d^\mu{}_{\nu\lambda\rho}\nabla_\mu\Omega \tag{1.13}$$

respectively. With equations (1.10), (1.12), and (1.13) the first objective set at the beginning of the present section has been achieved, namely we managed to construct an alternative to (1.3) that does not contain any Ω^{-1} terms. If one assumes that Ω is given, then the rescaled Weyl and Schouten tensors can be obtained by solving (1.10) and (1.13), respectively. Inserting the results in (1.12) we end up with a (regular at $\Omega = 0$) second order partial differential equation for the metric tensor. Unfortunately, in general Ω is not known beforehand; thus, it must be somehow computed.

Therefore, our next task is to compute Ω using Einstein's equations. As usual our terminus a quo will be equation (1.3); its trace provides the rescaling law for the Ricci scalar under transformations of the type (1.2):

$$R[g] = \Omega^{-2}\tilde{R}[\tilde{g}] - 6\,\Omega^{-1}\left(\Box\Omega - 2\,\Omega^{-1}\nabla_\rho\Omega\nabla^\rho\Omega\right). \tag{1.14}$$

Using (1.5) and (1.14)—where the vanishing of $\tilde{R}[\tilde{g}]$ follows from (1.1)—one can express (1.3) in terms of the scalar quantity

$$s \equiv \frac{1}{4}\,\Box\Omega + \frac{1}{24}\,R\,\Omega \tag{1.15}$$

and the Schouten tensor, i.e.

$$\nabla_\mu\nabla_\nu\Omega = -\Omega\,L_{\mu\nu} + s\,g_{\mu\nu}. \tag{1.16}$$

18

The above expression can be used for describing the dynamical evolution of the conformal factor Ω. While an equation specifying the dynamics of the Schouten tensor is already available, see (1.13), a similar expression for s is still missing. In order to fill the gap one can use the twice contracted second Bianchi identity $\nabla^\lambda L_{\lambda\mu} = \frac{1}{6}\nabla_\mu R$ and substitute $L_{\lambda\mu}$ and R with their expressions in terms of s:

$$L_{\lambda\mu} = -\Omega^{-1}\nabla_\lambda\nabla_\mu\Omega + \Omega^{-1}s\,g_{\lambda\mu},$$
$$R = -6\,\Omega^{-1}\Box\Omega + 24\,\Omega^{-1}s.$$

If, in addition, the commutator $[\nabla_\rho, \nabla_\mu]\,V_\lambda = V_\kappa\,R^\kappa{}_{\lambda\mu\rho}$ of the covariant derivative ∇_ρ and the expression (relating the Ricci tensor with $L_{\lambda\mu}$ and s)

$$R_{\lambda\mu} = 2\,L_{\lambda\mu} + 4\,\Omega^{-1}\,s\,g_{\lambda\mu} - \Omega^{-1}\Box\Omega\,g_{\lambda\mu}$$

are used, then a quite elegant formula dictating the dynamics of s can be obtained:

$$\nabla_\mu s = -L_{\lambda\mu}\,\nabla^\lambda\Omega. \tag{1.17}$$

Finally, expressing the contracted Einstein's field equations (1.14), with $\tilde{R} = 0$, in terms of the scalar (1.15), one acquires an equation that constrains the quantities Ω and s:

$$2\,\Omega\,s - \nabla_\rho\Omega\,\nabla^\rho\Omega = 0. \tag{1.18}$$

Obviously, expressions (1.16)-(1.18) are regular at the limit $\Omega \to 0$ and can be used for specifying the value of Ω. Consequently, with these equations at hand the second requirement set at the beginning of the present section is also fulfilled.

Summarizing, the equations (1.12), (1.13), (1.10), (1.16), (1.17), and (1.18)

$$R^\mu{}_{\nu\lambda\rho} = 2\left(g^\mu{}_{[\lambda}\,L_{\rho]\nu} - g_{\nu[\lambda}\,L_{\rho]}{}^\mu\right) + \Omega\,d^\mu{}_{\nu\lambda\rho}, \tag{1.19}$$
$$\nabla_\lambda\,L_{\rho\nu} - \nabla_\rho\,L_{\lambda\nu} = d^\mu{}_{\nu\lambda\rho}\,\nabla_\mu\,\Omega, \tag{1.20}$$
$$\nabla_\mu\,d^\mu{}_{\nu\lambda\rho} = 0, \tag{1.21}$$
$$\nabla_\mu\nabla_\nu\,\Omega = -\Omega\,L_{\mu\nu} + s\,g_{\mu\nu}, \tag{1.22}$$
$$\nabla_\mu\,s = -L_{\lambda\mu}\,\nabla^\lambda\Omega, \tag{1.23}$$
$$2\,\Omega\,s - \nabla_\rho\Omega\,\nabla^\rho\Omega = 0, \tag{1.24}$$

derived above, form the so-called *metric conformal field equations* for the unknowns

$$g_{\mu\nu}, \quad \Omega, \quad s, \quad L_{\mu\nu}, \quad d^\mu{}_{\nu\lambda\rho}. \tag{1.25}$$

The above set of equations is equivalent to the vacuum conformal field equations (1.3) and, as desired, does not exhibit singular terms in the limit $\Omega \to 0$. In the above representation the choice of the unknowns (1.25)—which is dictated by the specific problem we want to address—absorbs the singular terms and leaves us with a regular set of field equations.

In [28], [29] Friedrich shows rigorously how one can use the metric conformal field equations (1.19)-(1.24) to describe the behaviour of gravitational fields near (and at) null infinity. But, to build a global space-time one, while passing from past null $\mathscr{I}^-$ to future null $\mathscr{I}^+$ infinity, has to cross through space-like infinity i^0. As it will be shown later, dealing with space-like infinity is not possible in this setting because of the singular behaviour of some components of the rescaled Weyl tensor at i^0. Despite this unpleasant feature, the metric conformal field equations play a very crucial role in Friedrich's theory, namely they are used for deriving the conformal constraints on the initial hypersurface $\tilde{S}$. We will close this section by making some remarks about the way one can restrict the gauge freedom related to the conformal factor.

The conformal nature of (1.19)-(1.24) guarantees their invariance under a rescaling of the conformal factor Ω. Thus, even when Ω is known, it conserves its gauge nature: a rescaling of Ω by a smooth positive function ϑ leaves invariant the metric conformal field equations. For example, under a rescaling of the form $\Omega' = \vartheta\,\Omega$ the rescaled Weyl tensor transforms like $d'^{\mu}{}_{\nu\lambda\rho} = \vartheta^{-1}\,d^{\mu}{}_{\nu\lambda\rho}$ and, consequently, the Bianchi equation (1.21) remains invariant:

$$\nabla'_{\mu}\,d'^{\mu}{}_{\nu\lambda\rho} = \vartheta^{-1}\nabla_{\mu}\,d^{\mu}{}_{\nu\lambda\rho} = 0.$$

In a similar way, one can check that the rest of the metric conformal field equations remain also invariant. In order to remove the freedom of choosing the conformal factor one has to find a consistent and quite general way to specify the value of ϑ. The transformation law (1.14) suggests a possible way to do that. Specifically, applying (1.14) for the rescaling $g_{\mu\nu} = \vartheta^{-2}g'_{\mu\nu}$ of the metric tensor—which naturally follows from $\Omega' = \vartheta\,\Omega$—one is legitimate to write

$$R[g] = \vartheta^2 R'[g'] - 6\,\vartheta\left(\Box\vartheta^{-1} - 2\,\vartheta\,\nabla_{\rho}\vartheta^{-1}\nabla^{\rho}\vartheta^{-1}\right),$$

which simplifies to

$$\vartheta^2 R'[g'] = R[g] - 6\,\vartheta^{-1}\Box\vartheta.$$

The fact that, for a given R', the above equation can be always solved locally unveils the gauge nature of the unphysical Ricci scalar R. It is entirely arbitrary and to our disposal; its choice will depend on the problem under consideration and on the compatibility with the choice of the other gauge dependent quantities. The above expression, accompanied with an appropriate choice of initial conditions, fixes uniquely the value of ϑ.

As it was already mentioned, although the conformal representation described in this section is an entirely novel approach to the problem described by (1.1), it is not the most appropriate for studies of space-like infinity in the context of isolated self-gravitating systems. The blow-up of some components of the rescaled Weyl tensor while approaching space-like infinity poses restrictions on the use of equations (1.19)-(1.24). A way to bypass this obstacle and to achieve a considerable simplification of the resulting equations was proposed by Friedrich in [32], [33]. In addition to these two extremely pleasant characteristics, the new representation possesses all the nice features of the metric conformal field equations.

1.3   General conformal field equations

The novel new idea put forward in [32] is related to the use of a connection better adapted to the conformal structure: the *Weyl connection*. Thus, both the freedom to choose the conformal factor and the connection is now available; a fact that gives us the opportunity to exploit the full gauge freedom available in the conformal scheme.

1.3.1   Weyl connection

To bring in the basic ideas introduced in [32] we have to define a connection that respects the conformal structure,[5] i.e. it is an invariant of the conformal structure. A possible choice is a Weyl connection $\hat{\nabla}$, which can be viewed as a generalization of the more familiar Levi-Civita connection in the sense that it does not satisfy the second requirement of the *fundamental theorem of Riemannian geometry* (see,

---

[5]A (pseudo-)conformal structure $CO(p,q)$ on a manifold (M,g) of dimensions $n = p + q$ is a set of conformally equivalent (1.2) (pseudo-)Riemannian metrics of the same signature, see [1]. Here, we will not distinguish between pseudo-conformal and conformal structures as only Lorentzian metrics will be considered.

e.g., [11]). In particular, whilst a Weyl connection satisfies the first requirement of torsionless it fails to fulfill the second, which guarantees the preservation of the metric tensor while parallel transported—in other words a Weyl connection is in general *not* metric-compatible.

In order to study the implications of the metric-incompatibility one has to consider how it influences the parallel transport of the inner product of two tangent vectors. Let's assume that at every point p of the "unphysical" manifold (M, g) one can define an inner product on the tangent space $T_p(M)$ for any two vectors $Y, Z \in T_p(M)$:

$$g(Y, Z) \equiv g_{\mu\nu}(p) Y^\mu Z^\nu. \tag{1.26}$$

Thus, the length of a tangent vector and the angle between two tangent vectors at the same point readily follow

$$|Y| = \sqrt{|g(Y, Y)|}, \tag{1.27}$$

$$\cos \angle(Y, Z) = \frac{g(Y, Z)}{|Y||Z|}. \tag{1.28}$$

As expected, under a conformal rescaling (1.2) of the metric, i.e. $g \mapsto \Omega^2 g$, the length (1.27) is not preserved

$$|Y| \mapsto \Omega |Y| \tag{1.29}$$

and the angle (1.28) remains unchanged

$$\cos \angle(Y, Z) \mapsto \cos \angle(Y, Z).$$

A result that clearly demonstrates the angle-preserving nature of the conformal rescaling (1.2).

Let's try now to parallel transport the inner product (1.26) along a smooth curve $x(\lambda)$ in the manifold (M, g). If the connection ∇ is metric-compatible to g and the tangent vectors Y, Z are parallel transported along $x(\lambda)$ with respect to ∇, i.e. $\nabla_{\dot{x}} Y = \nabla_{\dot{x}} Z = 0$, then it can be easily shown that ∇ parallel transports (1.26):

$$\nabla_{\dot{x}} g(Y, Z) = 0, \tag{1.30}$$

where $\dot{x} \equiv dx/d\lambda$. The above result unveils the direct correspondence between the metric-compatibility of a connection and the parallel transport of (1.26) with respect

to it. In a similar fashion one can try to parallel transport the length (1.27) and the angle (1.28) defined on $T_p(M)$; the resulting formulas read, respectively, as follows

$$\nabla_{\dot{x}} |Y| = \frac{\nabla_{\dot{x}} g(Y,Y)}{2\,|Y|}, \tag{1.31}$$

$$\nabla_{\dot{x}} \cos \angle(Y,Z) = \frac{\nabla_{\dot{x}} g(Y,Z)}{|Y||Z|} - \frac{g(Y,Z)}{2\,|Y||Z|} \left(\frac{\nabla_{\dot{x}} g(Y,Y)}{|Y|^2} + \frac{\nabla_{\dot{x}} g(Z,Z)}{|Z|^2} \right). \tag{1.32}$$

Obviously, when (1.30) is satisfied—i.e. when ∇ is metric-compatible to g—the r.h.s of (1.31) and (1.32) vanishes; thus, their parallel transport is guaranteed.

What are the implications of using a metric-incompatible connection for (1.30)-(1.32)? To examine this issue in depth, one has first to investigate the behaviour of (1.30) under conformal rescalings of the metric tensor. We assume again that ∇ is metric-compatible to g and the tangent vectors $Y, Z \in T_p(M)$ are parallel transported with respect to it. By inserting (1.2)—i.e. $g \mapsto \Omega^2\,\tilde{g}$, where ~ is used as a reminder of the incompatibility of ∇ and $\tilde{g}$—in (1.30) one obtains, up to a scalar factor, the extremely important expression

$$\nabla_{\dot{x}} \tilde{g}(Y,Z) = -2\,\tilde{g}(Y,Z)\,\Omega^{-1}\nabla_{\dot{x}}\,\Omega, \tag{1.33}$$

which is clearly in agreement with the well-known fact that a metric-incompatible connection cannot parallel transport inner products of the form (1.26). Let's see now how the length and angle on a tangent space are influenced by the use of a metric-incompatible connection. Substituting $g \mapsto \Omega^2 g$, $\nabla_{\dot{x}}\,g(Y,Z) \mapsto -2\,g(Y,Z)\,\Omega^{-1}\nabla_{\dot{x}}\,\Omega$, and (1.29) in (1.31) and (1.32) one surprisingly obtains

$$\nabla_{\dot{x}} |Y| = -|Y|\,\Omega^{-2}\nabla_{\dot{x}}\,\Omega, \tag{1.34}$$

$$\nabla_{\dot{x}} \cos \angle(Y,Z) = 0. \tag{1.35}$$

Quite remarkably, the use of a metric-incompatible connection does not parallel transport inner products in such a way that guarantees the parallel transport of the angle (1.28), but not of the length (1.27)! Expressions (1.33)-(1.35) demonstrate how well the metric-incompatible connection is adapted to the (angle-preserving) conformal structure.

If, in addition to its metric-incompatibility, we assume that our connection is non-metric, then the expression (1.33) can be further generalized (see [1]) to

$$\nabla_{\dot{x}} \tilde{g}(Y,Z) = -2\,\dot{x}\tilde{f}\,\tilde{g}(Y,Z), \tag{1.36}$$

23

where $\tilde{f} = \tilde{f}_\rho \, dx^\rho$ is an arbitrary 1-form residing on $(\tilde{M}, \tilde{g})$. By non-metric we mean that our connection is not metric-compatible to any metric tensor in the conformal class (1.2).

Now we are in position to define a Weyl connection for the conformal class (1.2) as follows. A *Weyl* connection $\hat{\nabla}$ is a *torsionless*, not necessarily metric, connection which, according to (1.36), can be defined by the expression

$$\hat{\nabla}_\rho \, \tilde{g}_{\mu\nu} = -2 \, \tilde{f}_\rho \, \tilde{g}_{\mu\nu}, \tag{1.37}$$

where the 1-form $\tilde{f}$ is defined as above. Alternatively, a Weyl connection can be viewed, according to (1.35), as a torsion-free, possibly non-metric, affine connection on a manifold (M, g) with the property that any parallel transport with respect to it preserves the angle between vectors tangent to the manifold (M, g). In the special case that $\tilde{f}$ is exact we can always choose a conformal factor in such a way that the connection $\hat{\nabla}$ becomes locally a Levi-Civita connection of a metric in the conformal class. For example, if (1.2) is used in (1.37) to rescale $\tilde{g}_{\mu\nu}$ and $\tilde{f}$ takes the form $\tilde{f}_\rho = \Omega^{-1} \tilde{\nabla}_\rho \Omega$,[6] then it readily follows that $\hat{\nabla}_\rho \, g_{\mu\nu} = 0$, namely the connection $\hat{\nabla}$ becomes the Levi-Civita connection ∇ of the metric tensor $g_{\mu\nu}$. In the general case that $\tilde{f}$ is inexact one can show, by inserting (1.2) in (1.37), that when $\tilde{f}$ transforms, under (1.2), as

$$f_\rho = \tilde{f}_\rho - \Omega^{-1} \nabla_\rho \Omega \tag{1.38}$$

to another 1-form f_ρ on (M, g), then a relation similar to (1.37)

$$\hat{\nabla}_\rho \, g_{\mu\nu} = -2 \, f_\rho \, g_{\mu\nu}$$

holds. Thus, it can be inferred that the expression (1.37) holds independently of which metric in the conformal class is used—unveiling in this way its conformally invariant character.

For later reference we display here some very useful results concerning the Weyl connection. Using definition (1.37) the transformation law (1.9) can be generalized to

$$\hat{\Gamma}_\mu{}^\rho{}_\nu = \tilde{\Gamma}_\mu{}^\rho{}_\nu + S(\tilde{f})_\mu{}^\rho{}_\nu, \text{ where } S(\tilde{f})_\mu{}^\rho{}_\nu = \delta^\rho{}_\mu \, \tilde{f}_\nu + \delta^\rho{}_\nu \, \tilde{f}_\mu - g^{\rho\sigma} g_{\nu\mu} \, \tilde{f}_\sigma.$$

In the special case that $\tilde{f}$ is exact it follows easily that the above expression reduces to (1.9). In addition, the conformally invariant combination $g^{\rho\sigma} g_{\nu\mu}$ of the metric

---

[6]This choice of $\tilde{f}_\rho$ guarantees that the 1-form $\tilde{f}$ is exact: $\tilde{f} = \tilde{\nabla}_\rho \ln \Omega \, dx^\rho = d \ln \Omega$.

tensors guarantees that the above transformation law holds for any metric in the conformal class (1.2). Summarizing, one can write

$$
\begin{aligned}
\hat{\Gamma}_\mu{}^\rho{}_\nu &= \tilde{\Gamma}_\mu{}^\rho{}_\nu + S(\tilde{f})_\mu{}^\rho{}_\nu, \quad \text{i.e.} \quad \hat{\nabla} - \tilde{\nabla} = S(\tilde{f}), \\
\hat{\Gamma}_\mu{}^\rho{}_\nu &= \Gamma_\mu{}^\rho{}_\nu + S(f)_\mu{}^\rho{}_\nu, \quad \text{i.e.} \quad \hat{\nabla} - \nabla = S(f), \\
\Gamma_\mu{}^\rho{}_\nu &= \tilde{\Gamma}_\mu{}^\rho{}_\nu + S(\Omega^{-1}d\,\Omega)_\mu{}^\rho{}_\nu, \quad \text{i.e.} \quad \nabla - \tilde{\nabla} = S(\Omega^{-1}d\,\Omega),
\end{aligned}
\tag{1.39}
$$

where

$$
S(l)_\mu{}^\rho{}_\nu = \delta^\rho{}_\mu l_\nu + \delta^\rho{}_\nu l_\mu - g_{\mu\nu} g^{\rho\lambda} l_\lambda
\tag{1.40}
$$

for a general (exact or not) 1-form l_μ.

1.3.2   Derivation of the general conformal field equations

In the subsequent derivation of the general conformal field equations we will, as in the case of the metric conformal field equations, assume that the "physical" metric $\tilde{g}$ satisfies Einstein's vacuum field equations (1.1), but will use another positive definite conformal factor Θ.[7] Thus, the transformation law (1.2) will be replaced by

$$
g_{\mu\nu} = \Theta^2 \tilde{g}_{\mu\nu},
\tag{1.41}
$$

where Θ is a positive definite function.

As we already pointed out a Weyl connection, introduced in the preceding section, will be used in the derivation of the general conformal field equations. For this we have to introduce the Weyl counterparts of the decomposition (1.12), the contracted Bianchi identity (1.13), and the Bianchi equation (1.10). In order to express (1.12) in terms of a Weyl connection we have, firstly, to write the Riemann tensor as a function of the connection coefficients and use (1.39) to get

$$
R^\mu{}_{\nu\lambda\rho} = \hat{R}^\mu{}_{\nu\lambda\rho} - 2\left(g^\mu{}_{[\rho} \nabla_{\lambda]} f_\nu + \nabla_{[\rho} f^\mu g_{\lambda]\nu} - g^\mu{}_\nu \nabla_{[\rho} f_{\lambda]} - \right.
$$
$$
\left. -g^\mu{}_{[\rho} f_{\lambda]} f_\nu + g_{\nu[\rho} f_{\lambda]} f^\mu + g^\mu{}_{[\rho} g_{\lambda]\nu} f_\sigma f^\sigma \right).
\tag{1.42}
$$

The transformation laws for the Ricci tensor $\hat{R}_{\nu\rho} = \hat{R}^\mu{}_{\nu\mu\rho}$ and the Ricci scalar $\hat{R} = g^{\nu\rho} \hat{R}_{\nu\rho}$ immediately follow

$$
R_{\nu\rho} = \hat{R}_{\nu\rho} + 3\nabla_\rho f_\nu - \nabla_\nu f_\rho - 2 f_\nu f_\rho + g_{\nu\rho}(\nabla_\lambda f^\lambda + 2 f_\lambda f^\lambda),
\tag{1.43}
$$
$$
R = \hat{R} + 6\nabla_\lambda f^\lambda + 6 f_\lambda f^\lambda.
$$

---

[7]The need of introducing different conformal factors will be justified later, see secs. 1.6 and 1.7.

Relation (1.43) provides some information about the nature of $\hat{R}_{\nu\rho}$; by anti-symmetrizing it one gets $\hat{R}_{[\nu\rho]} = 4\,\nabla_{[\rho}\,f_{\nu]}$, a result that clearly indicates that the Ricci tensor is not symmetric! Inserting (1.42) into (1.4) one can write

$$C^{\mu}{}_{\nu\lambda\rho} = \hat{R}^{\mu}{}_{\nu\lambda\rho} - 2\left(g^{\mu}{}_{[\lambda}L_{\rho]\nu} - g^{\mu}{}_{[\lambda}\nabla_{\rho]}\,f_{\nu} + g^{\mu}{}_{[\lambda}\,f_{\rho]}\,f_{\nu} - \frac{1}{2}\,g^{\mu}{}_{[\lambda}\,g_{\rho]\nu}\,f_{\sigma}\,f^{\sigma}\right) +$$

$$+2\left(g_{\nu[\lambda}L_{\rho]}{}^{\mu} - g_{\nu[\lambda}\nabla_{\rho]}\,f^{\mu} + g_{\nu[\lambda}\,f_{\rho]}\,f^{\mu} - \frac{1}{2}\,g_{\nu[\lambda}\,g^{\mu}{}_{\rho]}\,f_{\sigma}\,f^{\sigma}\right) - g^{\mu}{}_{\nu}\,\nabla_{[\lambda}\,f_{\rho]},$$

where the conformal invariant nature of the Weyl tensor guarantees that $\hat{C}^{\mu}{}_{\nu\lambda\rho} = C^{\mu}{}_{\nu\lambda\rho}$. Obviously, one can define

$$\hat{L}_{\rho\nu} = L_{\rho\nu} - \nabla_{\rho}\,f_{\nu} + f_{\rho}\,f_{\nu} - \frac{1}{2}\,g_{\rho\nu}\,f_{\sigma}\,f^{\sigma} \tag{1.44}$$

and express the above decomposition in the more compact form

$$C^{\mu}{}_{\nu\lambda\rho} = \hat{R}^{\mu}{}_{\nu\lambda\rho} - 2\left(g^{\mu}{}_{[\lambda}\hat{L}_{\rho]\nu} - g_{\nu[\lambda}\hat{L}_{\rho]}{}^{\mu} - g^{\mu}{}_{\nu}\,\hat{L}_{[\lambda\rho]}\right). \tag{1.45}$$

(Note that $\hat{L}_{[\lambda\rho]} = -\nabla_{[\lambda}\,f_{\rho]}$.) Relation (1.45) with the help of definition (1.11) can be expressed in the form

$$\hat{R}^{\mu}{}_{\nu\lambda\rho} = \Theta\,d^{\mu}{}_{\nu\lambda\rho} + 2\left(g^{\mu}{}_{[\lambda}\hat{L}_{\rho]\nu} - g_{\nu[\lambda}\hat{L}_{\rho]}{}^{\mu} - g^{\mu}{}_{\nu}\,\hat{L}_{[\lambda\rho]}\right). \tag{1.46}$$

Inserting (1.5) in (1.44) and using the aforementioned result $\hat{R}_{[\nu\rho]} = 4\,\nabla_{[\rho}\,f_{\nu]}$, the form of the Schouten tensor in the Weyl representation can be easily derived

$$\hat{L}_{\rho\nu} = \frac{1}{2}\left(\frac{1}{2}\,\hat{R}_{[\rho\nu]} + \hat{R}_{(\rho\nu)} - \frac{1}{6}\,g_{\rho\nu}\,\hat{R}\right).$$

Let's turn, now, to (1.13) and try to express it in terms of quantities in the Weyl representation. Using (1.44) and the commutation rule $2\,\nabla_{[\lambda}\nabla_{\rho]}f_{\nu} = f_{\mu}R^{\mu}{}_{\nu\rho\lambda}$, it is fairly straightforward to show that

$$\nabla_{[\lambda}L_{\rho]\nu} = \nabla_{[\lambda}\hat{L}_{\rho]\nu} + \frac{1}{2}\,f_{\mu}R^{\mu}{}_{\nu\rho\lambda} - \nabla_{[\lambda}\left(f_{\rho]}f_{\nu}\right) + f_{\sigma}\,\nabla_{[\lambda}\left(g_{\rho]\nu}f^{\sigma}\right).$$

If, in addition, we replace, through (1.39), the Levi-Civita connection appearing in the first term on the r.h.s, and use (1.45) and (1.42) to simplify the resulting expression, we end up with

$$\nabla_{[\lambda}L_{\rho]\nu} = \hat{\nabla}_{[\lambda}\hat{L}_{\rho]\nu} - \frac{1}{2}\,f_{\mu}C^{\mu}{}_{\nu\rho\lambda}. \tag{1.47}$$

Substituting (1.47) into (1.13), the latter one can be written in the form

$$\hat{\nabla}_\lambda \hat{L}_{\rho\nu} - \hat{\nabla}_\rho \hat{L}_{\lambda\nu} = d^\mu{}_{\nu\lambda\rho} \nabla_\mu \Theta + \Theta f_\mu d^\mu{}_{\nu\lambda\rho},$$

where the definition (1.11) was used and Ω was replaced by Θ. Finally, by introducing the smooth 1-form

$$d_\mu \equiv \Theta \, \tilde{f}_\mu = \Theta \, f_\mu + \nabla_\mu \Theta, \tag{1.48}$$

which is just a reformulation of the 1-form $\tilde{f}_\mu$ that, in contrast to $\tilde{f}_\mu$ (see (1.38) with Ω replaced by Θ), is not singular in the limit $\Theta \to 0$, one can produce the Weyl version of the contracted Bianchi identity (1.13), i.e.

$$\hat{\nabla}_\lambda \hat{L}_{\rho\nu} - \hat{\nabla}_\rho \hat{L}_{\lambda\nu} = d_\mu \, d^\mu{}_{\nu\lambda\rho}. \tag{1.49}$$

In order to express (1.10) in terms of a Weyl connection we have to use (1.39), (1.40), and the first Bianchi identity $d_{\mu[\nu\lambda\rho]} = 0$. In this way the following result can be obtain

$$\hat{\nabla}_\mu d^\mu{}_{\nu\lambda\rho} = f_\mu \, d^\mu{}_{\nu\lambda\rho}. \tag{1.50}$$

So far, with equations (1.46), (1.49), and (1.50) we have managed to generalize the relations (1.12), (1.13), and (1.10), respectively, in the case that transitions to Weyl connections are allowed in our theory.

It is essential, especially for the manipulation of fields near space-like infinity, to express the conformal field equations in terms of an appropriately chosen *orthonormal* frame field. Let's begin by defining a non-coordinate vierbein $\mathbf{e}_k = (\mathbf{e}_0, \mathbf{e}_1, \mathbf{e}_2, \mathbf{e}_3)$ and its dual basis $\boldsymbol{\theta}^k$ on the tangent $T_p(M)$ and cotangent $T_p^*(M)$ space, respectively, of the "unphysical" manifold (M, g). (Obviously, the relation $\langle \boldsymbol{\theta}^k, \mathbf{e}_l \rangle = \eta^k{}_l$ must hold.) As usual we can relate the non-coordinate bases $\boldsymbol{\theta}^k$ and $\mathbf{e}_k$ to an as yet unspecified coordinate system x^μ through the frame coefficients $\mathrm{e}^\mu{}_k = \langle \mathrm{dx}^\mu, \mathbf{e}_k \rangle$, namely $\mathbf{e}_k = \mathrm{e}^\mu{}_k \, \partial_\mu$ and $\boldsymbol{\theta}^k = \mathrm{e}_\mu{}^k \, \mathrm{dx}^\mu$.[8] In addition, we require $\mathbf{e}_k$ to be orthonormal with respect to the "unphysical" metric g, i.e.

$$g_{ik} = g(\mathbf{e}_i, \mathbf{e}_k) = g_{\mu\nu} \, \mathrm{e}^\mu{}_i \, \mathrm{e}^\nu{}_k = \eta_{ik}. \tag{1.51}$$

(Latin and Greek indices are used to denote the non-coordinate and coordinate basis, respectively.) In the following, ∇_k and $\hat{\nabla}_k$ will denote the covariant derivatives of

---

[8]Notice that $\mathrm{e}_\mu{}^k$ is the inverse of $\mathrm{e}^\mu{}_k$; therefore, $\mathrm{e}^\mu{}_k \mathrm{e}_\nu{}^m = \eta_k{}^m \eta^\mu{}_\nu$ and $\det(\mathrm{e}^\mu{}_k) > 0$ must hold.

the corresponding connections in the direction of $\mathbf{e}_k$, i.e. $\nabla_k \equiv \nabla_{\mathbf{e}_k} = \mathrm{e}^\mu{}_k \nabla_\mu$; the connection coefficients of $\hat{\nabla}_k$ in this frame field are defined by $\hat{\nabla}_i \mathbf{e}_k = \hat{\Gamma}_i{}^j{}_k \mathbf{e}_j$, and similarly for ∇.

Recall that a Weyl connection is torsion-free. This property together with the non-holonomic nature of the non-coordinate basis can be nicely accommodated by the formalism introduced above. For any two vectors $X, Y \in T_p(M)$ the torsion-free condition can be expressed as

$$\hat{\nabla}_X Y - \hat{\nabla}_Y X - [X, Y] = 0,$$

where the square brackets are used to denote the Lie bracket of the fields. Choosing $X = \mathbf{e}_p$ and $Y = \mathbf{e}_q$ the above condition becomes

$$[\mathbf{e}_p, \mathbf{e}_q] = \hat{\nabla}_{\mathbf{e}_p} \mathbf{e}_q - \hat{\nabla}_{\mathbf{e}_q} \mathbf{e}_p = (\hat{\Gamma}_p{}^j{}_q - \hat{\Gamma}_q{}^j{}_p) \mathbf{e}_j, \tag{1.52}$$

which is consistent with the non-vanishing of the Lie bracket of our non-holonomic basis $[\mathbf{e}_p, \mathbf{e}_q] = \gamma_p{}^j{}_q \mathbf{e}_j$, where the structure constants are given by $\gamma_p{}^j{}_q = \hat{\Gamma}_p{}^j{}_q - \hat{\Gamma}_q{}^j{}_p$.

In a similar fashion one can express the curvature tensor

$$\hat{R}(X, Y)Z = \hat{\nabla}_X \hat{\nabla}_Y Z - \hat{\nabla}_Y \hat{\nabla}_X Z - \hat{\nabla}_{[X,Y]} Z,$$

where $X, Y, Z \in T_p(M)$, appearing on the l.h.s of (1.46) in terms of the orthonormal frame field and its connection coefficients. Choosing $X = \mathbf{e}_p$, $Y = \mathbf{e}_q$, and $Z = \mathbf{e}_j$ we can write

$$\hat{\nabla}_p \hat{\nabla}_q \mathbf{e}_j - \hat{\nabla}_q \hat{\nabla}_p \mathbf{e}_j - \hat{\nabla}_{[\mathbf{e}_p, \mathbf{e}_q]} \mathbf{e}_j = \hat{\nabla}_p (\hat{\Gamma}_q{}^i{}_j \mathbf{e}_i) - \hat{\nabla}_q (\hat{\Gamma}_p{}^k{}_j \mathbf{e}_k) - \gamma_p{}^k{}_q \hat{\nabla}_k \mathbf{e}_j =$$
$$= (\hat{\nabla}_p \hat{\Gamma}_q{}^i{}_j) \mathbf{e}_i + \hat{\Gamma}_q{}^k{}_j \hat{\Gamma}_p{}^i{}_k \mathbf{e}_i - (\hat{\nabla}_q \hat{\Gamma}_p{}^i{}_j) \mathbf{e}_i - \hat{\Gamma}_p{}^k{}_j \hat{\Gamma}_q{}^i{}_k \mathbf{e}_i - \gamma_p{}^k{}_q \hat{\Gamma}_k{}^i{}_j \mathbf{e}_i$$

and

$$\hat{R}^i{}_{jpq} = (\hat{\nabla}_p \hat{\Gamma}_q{}^i{}_j) + \hat{\Gamma}_q{}^k{}_j \hat{\Gamma}_p{}^i{}_k - (\hat{\nabla}_q \hat{\Gamma}_p{}^i{}_j) - \hat{\Gamma}_p{}^k{}_j \hat{\Gamma}_q{}^i{}_k - \gamma_p{}^k{}_q \hat{\Gamma}_k{}^i{}_j,$$

where $\gamma_p{}^k{}_q$ are the structure constants introduced above.

Now, we can express all the tensor fields involved in the equations (1.46), (1.49), and (1.50) in terms of the above frame field and its connection coefficients. In addition, by adding the torsion-free condition (1.52) in the above system, we can construct an equivalent system of equations for the conformal field equations (1.3), with unknowns

$$\mathrm{e}^\mu{}_k, \quad \hat{\Gamma}_i{}^j{}_k, \quad \hat{L}_{ij}, \quad d^i{}_{jkl}, \tag{1.53}$$

28

which reads

$$[\mathbf{e}_p \, , \mathbf{e}_q] = (\hat{\Gamma}_p{}^l{}_q - \hat{\Gamma}_q{}^l{}_p) \, \mathbf{e}_l, \tag{1.54}$$

$$\mathbf{e}_p \, (\hat{\Gamma}_q{}^i{}_j) - \mathbf{e}_q \, (\hat{\Gamma}_p{}^i{}_j) - \hat{\Gamma}_k{}^i{}_j \, (\hat{\Gamma}_p{}^k{}_q - \hat{\Gamma}_q{}^k{}_p) + \hat{\Gamma}_p{}^i{}_k \, \hat{\Gamma}_q{}^k{}_j - \hat{\Gamma}_q{}^i{}_k \, \hat{\Gamma}_p{}^k{}_j =$$
$$= 2(g^i{}_{[p} \hat{L}_{q]j} - g^i{}_j \hat{L}_{[p\,q]} - g_{j\,[p} \hat{L}_{q]}{}^i) + \Theta \, d^i{}_{jpq}, \tag{1.55}$$

$$\hat{\nabla}_p \, \hat{L}_{qj} - \hat{\nabla}_q \hat{L}_{pj} = d_i \, d^i{}_{jpq}, \tag{1.56}$$

$$\nabla_i \, d^i{}_{jkl} = 0, \tag{1.57}$$

In the last equation the connection ∇ is used instead of $\hat{\nabla}$ for the sake of brevity, but no harm is done as always one can express it in terms of a Weyl connection—see the discussion leading to (1.50). The notation used to express the first couple of terms in the l.h.s of (1.55) follows $\mathbf{X}(h) \equiv \nabla_{\mathbf{X}} h$, where h is a scalar function. (Indices on $\hat{\Gamma}$ in these specific two terms denote components; they are not abstract indices.) The first three equations (1.54)-(1.56) are the *structural equations* of our system as they define its torsion and curvature. The last equation is called *Bianchi equation* and, as we will see in the following, plays central role in our theory. For later reference, we notice that the 1-from f entering the definition (1.48) takes, in our frame, the form

$$f_i = f_\mu \, \mathrm{e}^\mu{}_i = \frac{1}{4} \hat{\Gamma}_i{}^k{}_k. \tag{1.58}$$

It can be readily checked that the above relation follows from the identity $\nabla_i \, g_{l\,k} = \Gamma_i{}^j{}_k \, g_{j\,l} + \Gamma_i{}^j{}_l \, g_{j\,k} = 0$.

Although the system (1.54)-(1.57) is regular at the limit $\Theta \to 0$, it does not provide any equations for Θ and d_i. This feature follows directly from the gauge nature of the two fields: the former is related to the freedom of choosing the conformal factor in (1.41), while the latter can be traced back to the freedom of choosing the connection. Thus, by confining the available gauge freedom provided by our system, one could expect to produce differential equations describing the behaviour of Θ and d_i. We have to remark here that the two gauge freedoms are not totally unrelated. According to (1.48) when $\Theta = 0$ holds, then $d_i = \nabla_i \Theta$ must also hold. (It will become clearer in the following why the choice $\Theta = 0$ is so important in our theory.)

1.3.3   Conformal Gauss gauge

Obviously, the lack of differential equations for Θ and d_i in the equations (1.54)-(1.57) unveils their gauge nature. One possible way of specifying these quantities is by using the notion of *conformal geodesics*. Specifically, the conformal geodesics will be used to introduce a coordinate system, see [35], and subsequently propagate the initial data along them. Interestingly, the introduction of such coordinates along the conformal geodesics suffices to provide equations governing the behaviour of the gauge fields Θ and d_i.

A brief presentation of the theory of conformal geodesics follows—for a more detailed discussion see [38], [35], [79]. In general, conformal geodesics are related to the conformal structure in a similar way that the metric geodesics are related to the metric structure. A conformal geodesic is a space-time curve $x^\mu(\tau)$ of $(\tilde{M}, \tilde{g})$ that solves, together with a 1-form $\tilde{f}_\rho$ along it, the system of ordinary differential equations

$$\tilde{\nabla}_{\dot{x}}\, \dot{x}^\mu + S(\tilde{f})_\rho{}^\mu{}_\lambda\, \dot{x}^\rho \dot{x}^\lambda = 0, \tag{1.59}$$

$$\tilde{\nabla}_{\dot{x}}\tilde{f}_\mu - \frac{1}{2}S(\tilde{f})_\mu{}^\rho{}_\lambda\, \tilde{f}_\rho \dot{x}^\lambda - \tilde{L}_{\nu\mu}\, \dot{x}^\nu = 0, \tag{1.60}$$

where $\tilde{L}_{\nu\mu}$ is the 4-dimensional physical Schouten tensor and S is given by (1.40). Conformal geodesics are conformally invariant as they do not depend on the metric chosen in the conformal class to express them. In addition, they are also independent of the connection used to formulate their constitutive equations (1.59)-(1.60). Namely, if we assume that x^μ and $\tilde{f}_\rho$ are solutions of (1.59)-(1.60), then the pair x^μ, $\tilde{f}_\rho - b_\rho$ is also a solution of the same equations but with $\tilde{\nabla}$ replaced by $\hat{\nabla} = \tilde{\nabla} + S(b)$ and $\tilde{L}$ by $\hat{L}$, i.e.

$$\hat{\nabla}_{\dot{x}}\, \dot{x}^\mu + S(\tilde{f} - b)_\rho{}^\mu{}_\lambda\, \dot{x}^\rho \dot{x}^\lambda = 0,$$

$$\hat{\nabla}_{\dot{x}}(\tilde{f} - b)_\mu - \frac{1}{2}S(\tilde{f} - b)_\mu{}^\rho{}_\lambda\, (\tilde{f} - b)_\rho\, \dot{x}^\lambda - \hat{L}_{\nu\mu}\, \dot{x}^\nu = 0,$$

where b_ρ is just another 1-form along the conformal geodesics. Choosing $b = \tilde{f}$ the above equations decouple and simplify significantly to

$$\hat{\nabla}_{\dot{x}}\, \dot{x}^\mu = 0, \quad \hat{L}_{\nu\mu}\, \dot{x}^\nu = 0.$$

If, in addition, we assume that a frame field $\mathbf{e}_k$ is parallel transported along the

geodesics, then we end up with the complementary equation

$$\hat{\nabla}_{\dot{x}} \, \mathrm{e}^{\mu}{}_{k} = 0,$$

which when expressed (through the first transformation law of (1.39)) in terms of the physical Levi-Civita connection takes the form

$$\tilde{\nabla}_{\dot{x}} \, \mathrm{e}^{\mu}{}_{k} + S(\tilde{f})_{\rho}{}^{\mu}{}_{\lambda} \, \mathrm{e}^{\rho}{}_{k} \, \dot{x}^{\lambda} = 0. \tag{1.61}$$

Obviously, the use of the Weyl connection considerably simplified the conformal geodesics equations (1.59)-(1.61) and enabled us to write them in the following decoupled and more compact form

$$\hat{\nabla}_{\dot{x}} \, \dot{x}^{\mu} = 0, \tag{1.62}$$

$$\hat{L}_{\nu\mu} \, \dot{x}^{\nu} = 0, \tag{1.63}$$

$$\hat{\nabla}_{\dot{x}} \, \mathrm{e}^{\mu}{}_{k} = 0. \tag{1.64}$$

We are going now to define a gauge through the construction of *conformal Gauss coordinates*, where the time-like coordinate lines will be conformal geodesics that start orthogonally from a given space-like hypersurface in $(\tilde{M}, \tilde{g})$. In this spirit, we denote by $\tilde{S}$ this space-like hypersurface and choose on it a function $\Theta|_{\tilde{S}} = \Theta_{\star}$, a frame field $\mathrm{e}^{\mu}{}_{k\star}$, and a 1-form $\tilde{f}_{\star}$ such that the orthogonality condition $\tilde{g}_{\mu\nu} \, \mathrm{e}^{\mu}{}_{i\star} \, \mathrm{e}^{\nu}{}_{k\star} = \Theta_{\star}^{-2} \eta_{ik}$ is satisfied and $\mathrm{e}^{\mu}{}_{0\star}$ is orthogonal to $\tilde{S}$. (The $\star$ quantities are independent of τ and, thus, constant along the conformal geodesics.) Thus, according to the theory of conformal geodesics (see [38] and references therein), through each point $x_{\star} \in \tilde{S}$ there exists a *unique* conformal geodesic satisfying on $\tilde{S}$ the initial conditions $\dot{x}^{\mu} = \mathrm{e}^{\mu}{}_{0\star} \perp \tilde{S}$, $\tilde{f} = \tilde{f}_{\star}$.[9] If the initial data are smooth enough, then these curves can define a caustic-free congruence in a neighbourhood U of $\tilde{S}$. Then, by solving (1.64) we can obtain on U a smooth frame field $\mathrm{e}^{\mu}{}_{k}$ that satisfies the initial condition $\mathrm{e}^{\mu}{}_{k} = \mathrm{e}^{\mu}{}_{k\star}$ and preserves the orthogonality condition $\tilde{g}_{\mu\nu} \, \mathrm{e}^{\mu}{}_{i} \, \mathrm{e}^{\nu}{}_{k} = \Theta^{-2} \eta_{ik}$. Finally, dragging along the conformal geodesics local coordinates $\mathrm{x}^{\mu} = (\tau, \mathrm{x}^1, \mathrm{x}^2, \mathrm{x}^3)$, where the last three live on $\tilde{S}$, one obtains a coordinate system. The above setting defines a *conformal Gauss gauge*, i.e.

$$\dot{x}^{\mu} = \mathrm{e}^{\mu}{}_{0} = \partial_{\tau}, \quad \hat{\Gamma}_{0}{}^{i}{}_{k} = 0, \quad \hat{L}_{0k} = 0, \tag{1.65}$$

---

[9]This condition does not necessarily imply that on any successive time slice $\tau = const. > 0$ the tangent vector $\dot{x}^{\mu} = \mathrm{e}^{\mu}{}_{0}$ along the conformal geodesics is orthogonal to the slice; the tangent vector must be orthogonal only to the initial time slice $\tau = 0$.

where the last two conditions follow from (1.62)-(1.64), when expressed in terms of $\dot{x}^\mu = \mathrm{e}^\mu{}_0$.

Although (1.65) restricts, as will be shown shortly, part of the freedom introduced by d_i, there is still no differential equation for the conformal factor Θ. As we mentioned previously, see (1.51), a proper manipulation of space-like infinity implies the use of an orthonormal frame field, i.e. $g_{\mu\nu}\mathrm{e}^\mu{}_i\mathrm{e}^\nu{}_k = \eta_{ik}$. By requiring our frame to be orthonormal with respect to g and orthogonal with respect to $\tilde{g}$, we introduce a conformal factor Θ that satisfies (1.41). Now, we can fix Θ's value in the following sense. By repeatedly differentiating the orthogonality condition $\tilde{g}_{\mu\nu}\,\mathrm{e}^\mu{}_i\,\mathrm{e}^\nu{}_k = \Theta^{-2}\eta_{ik}$, and observing (1.59)-(1.61), one can prove [32] that Θ obeys the differential equation $\tilde{\nabla}^{(3)}_{\dot{x}}\Theta = 0$ with solution

$$\Theta(\tau) = \Theta_\star + \tau\,\dot{\Theta}_\star + \frac{\tau^2}{2}\,\ddot{\Theta}_\star, \tag{1.66}$$

where $\dot{\Theta}_\star = \Theta_\star\,\tilde{f}_{\mu\star}\,\dot{x}^\mu_\star$ and $\ddot{\Theta}_\star = \frac{1}{2}\,\Theta_\star\,(g^{\mu\nu}\tilde{f}_\mu\,\tilde{f}_\nu)_\star$ are given initial data on $\tilde{S}$. Thus, through (1.66) the conformal factor is completely specified by the initial data on $\tilde{S}$. The above result is of great importance as it can be used to locate the conformal boundary of the space-time under consideration. (We will see in the next section that $\Theta \to 0$ at infinity.)

Using (1.65) one can confine the remaining freedom introduced by the Weyl connection by specifying the components of the 1-form d_i. Observing (1.58) one can write (1.48) in the form

$$d_i = d_\mu \mathrm{e}^\mu{}_i = \frac{1}{4}\,\Theta\,\hat{\Gamma}_i{}^k{}_k + \nabla_i\Theta.$$

Taking the components of the above expression, in the gauge (1.65), we calculate for $i = 0$:

$$d_0 = \nabla_0\,\Theta = \dot{\Theta} \tag{1.67}$$

and for $i = a$ (for a detailed proof see [32]):

$$\tilde{\nabla}_{\dot{x}}\,d_a = 0 \Rightarrow d_a = const.$$

(Lower case Latin indices from the beginning of the alphabet will be used, from now on, to denote quantities living on the 3-dimensional initial hypesurface in the non-coordinate frame.) Thus, by fixing d_a on the initial hypersurface $\tilde{S}$ we can specify

32

its value once and for all, i.e.

$$d_a = \Theta_\star \, \tilde{f}_{\mu\star} \, \mathrm{e}^\mu{}_{a\star}. \tag{1.68}$$

There is still some freedom left in the choice of the initial condition for (1.67). The standard choice made in the literature is to assume that on $\tilde{S}$ the derivative of the conformal factor Θ in the direction of the future directed "unphysical" g-unit normal vector $\mathrm{e}^\mu{}_0$ vanishes:

$$d_{0\star} = 0. \tag{1.69}$$

An immediate implication of this choice is the vanishing—see (1.67)—of the linear term in (1.66).

The relations (1.54)-(1.57) supplemented by (1.66), (1.67), and (1.68) consist the so-called *general conformal field equations*, which provide a complete system for the unknowns (1.53). All the equations are regular at the limit $\Theta \to 0$, the conformal factor and the connection are determined solely by the conformal structure and only the initial data on S are given by hand. Apparently, these features meet all the requirements set at the beginning of our endeavour.

1.4   Asymptotically simple space-times

In the preceding sections we were greatly concerned about the behaviour of our field equations when the conformal factor (Ω or Θ) tended to zero,[10] but we have not still justified rigorously this concern. The present section serves this purpose.

It has been already mentioned that we are primarily interested in the behaviour of gravitational fields at (and near) space-time infinity. A comprehensive study of the behaviour of gravitational fields at infinity, in the context of isolated systems, requires a precise and rigorous definition of a limiting procedure that provides detailed information on the decay of the metric and the curvature tensor. For analytical and, especially, numerical studies a quantitative description of the limiting procedure is required. In [62], [63] Penrose showed that such a description is possible in the conformal picture.

---

[10]Actually, both the metric and general conformal field equations were designed to be regular at this limit.

Proposition: *Far fields of isolated gravitational systems behave like those of asymptotically flat space-times.*

Penrose not only managed to reproduce previous results of [8], [59], [75], [76], but developed a powerful technique that can be also applied to more general curved space-times. The key idea is to replace, through (1.41), the original physical space-time described by the metric $\tilde{g}$ by a new "unphysical" one described by g. If the conformal factor is assumed to vanish at infinity, then, under certain conditions, the "unphysical" metric can be extended in a regular way to infinity—this implies though that the physical metric becomes infinite there. The points where the conformal factor vanishes represent infinity for the physical space-time and, thus, provide a "finite" boundary for it. Now, the behaviour of fields at infinity can be studied in terms of this more realizable and better manageable (with local techniques) boundary. A detailed description of Penrose's idea follows [66].

Definition 1 *A smooth manifold $(\tilde{M}, \tilde{g})$ is called k–asymptotically simple if both a C^{k+1} smooth (space- and time-) oriented manifold (M, g) with boundary $\mathscr{I} = \partial M$ and a smooth function Θ exist such that*

i) $\tilde{M} = M^o (\equiv int\, M)$,

ii) $g_{\mu\nu} = \Theta^2 \tilde{g}_{\mu\nu}$ in $\tilde{M}$,

iii) Θ and $g_{\mu\nu}$ are C^k–smooth throughout M,

iv) $\Theta > 0$ in $\tilde{M}$ and $\Theta = 0$, $\nabla_\mu \Theta \neq 0$ on $\mathscr{I}$,

v) every null geodesic in $\tilde{M}$ acquires a past and future endpoint on $\mathscr{I}$.

According to conditions i) and ii) one can think of the physical space-time $(\tilde{M}, \tilde{g})$ as a part of a larger "unphysical" space-time (M, g) with boundary $\mathscr{I} = \partial M$. Condition iii) implies that both the conformal factor and the "unphysical" metric g can be extended in a well-defined way through the boundary while $\tilde{g}$ cannot. Condition iv) states that Θ in the limit $|r| \to \infty$ should fall-off as $1/|r|$, where r is an affine parameter along any null direction; moreover, from this condition, in the case of asymptotically flat space-times—where (1.1) holds—can be inferred that $\mathscr{I}$ is a null hypersurface. Finally, condition v) implies that $\tilde{M}$ is null geodesically complete

and that all of null infinity is included in $\mathscr{I}$. Of course, in space-times where singularities occur—e.g. Schwarzschild space-time—this condition does not hold as null geodesics are oftentimes trapped or absorbed by the singularity. In these cases a weaker version—the so-called weakly asymptotically simple space-times—of the above definition is adopted.
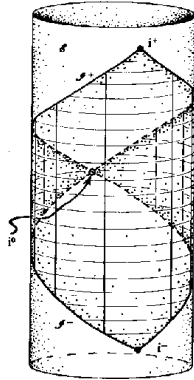

Figure 1.1: Penrose's conformally compactified picture of the simplest asymptotically flat space-time, i.e. Minkowski space-time. Minkowski space-time is conformally related to the interior of the "square" that is embedded into Einstein's static universe represented by the cylinder. The locations of space-like infinity i^0, null infinity $\mathscr{I}^{\pm}$, future and past temporal infinity $i^{\pm}$ are clearly indicated. (The figure is taken from [66].)

Here we are interested in isolated systems that satisfy near infinity the vacuum field equations (1.1). Because of this we are going to deal exclusively with asymptotically flat space-times. An asymptotically simple space-time becomes asymptotically flat when (1.1) is satisfied in a neighbourhood of infinity. Thus, **Definition 1** supplemented with the sixth condition

$$vi) \quad \tilde{R}_{\mu\nu}[\tilde{g}] = 0$$

can be used to define asymptotically flat space-times.

It must be noted here that, in the context of asymptotically flat space-times, in Penrose's picture [63] there are three more points i^+, i^-, and i^0 representing future, past, and spatial infinity, respectively. Both future $\mathscr{I}^+$ and past $\mathscr{I}^-$ null infinity have the topology of a three dimensional cylinder $S^2 \times E^1$. $\mathscr{I}^+$ is bounded at its past and future ends by i^0 and i^+, respectively. In a similar way $\mathscr{I}^-$ is bounded

by i^- and i^0. In addition, $\mathscr{I}^-$ and $\mathscr{I}^+$ are linked through i^0, see Fig. 1.1 for a graphical representation.

The above limiting procedure proposed by Penrose, beside the fact that manages to bring rigorously to light the geometrical features underlying the notion of asymptotically flat space-times, is completely coordinate independent, and for that extremely flexible in its manipulations.

1.5 Evolution equations

To exemplify the simplification power emerging from the conformal Gauss gauge we are going now to extract from (1.54)-(1.57) the evolution equations for those components of the unknowns (1.53) that are not explicitly determined by the gauge conditions (1.65). To do that we have to set $p = 0$ in (1.54)-(1.57) and use (1.65), thus one can obtain the symmetric hyperbolic system

$$\partial_\tau \, \mathrm{e}^\mu{}_q = -\hat{\Gamma}_q{}^l{}_0 \, \mathrm{e}^\mu{}_l, \tag{1.70}$$

$$\partial_\tau \, \hat{\Gamma}_q{}^i{}_j = -\hat{\Gamma}_k{}^i{}_j \, \hat{\Gamma}_q{}^k{}_0 + g^i{}_0 \, \hat{L}_{qj} + g^i{}_j \, \hat{L}_{q0} - g_{j0} \, \hat{L}_q{}^i + \Theta \, d^i{}_{j\,0q}, \tag{1.71}$$

$$\partial_\tau \, \hat{L}_{qj} + \hat{\Gamma}_q{}^k{}_0 \, \hat{L}_{kj} = d_i \, d^i{}_{j\,0q}, \tag{1.72}$$

$$\nabla_i \, d^i{}_{jkl} = 0. \tag{1.73}$$

A direct comparison of the above set of evolution equations with the corresponding set of equations (see, e.g., [22]) evaluated from the so-called metric conformal field equations—in this approach [28], [29] Friedrich makes use only of the freedom emanating from the conformal factor Θ—unveils the extent of simplification achieved by the artificial introduction of the "gauge" object d_i through the use of the Weyl connection. Not only their form is simpler and more compact but, in addition, as one can readily confirm by inspecting (1.70)-(1.72), all spatial derivatives of the unknown quantities $\mathrm{e}^\mu{}_k, \hat{\Gamma}_k{}^i{}_j, \hat{L}_{ij}$ disappear. This fact makes their analytical and numerical treatment considerably simpler. In fact, the apparent simplicity of (1.70)-(1.72), actually reduces the study of the evolution system to the analysis of the properties of the Bianchi equation (1.73).

Extracting symmetric hyperbolic equations from the Bianchi equation (1.73) requires a little bit more effort. The easier way to do that is in the context of the 2-spinor formulation [65], [66], where (1.73) splits readily into (3) constraint and

(5) symmetric hyperbolic evolution equations [33]. It turns out that, although the constraints can be prescribed uniquely on a given space-like hypersurface, there is a plethora of different evolution schemes, see [34], [37]. This extremely pleasant feature makes the Bianchi equation highly adjustable to different geometrical settings. In this work, we will use the so-called "boundary adapted" evolution system, first introduced in [32]. The constraints can always be expressed in the form [33]

$$F^\mu \partial_\mu \phi = H(\Gamma)\,\phi,$$

where the 3×5 matrices F and H are functions of the frame and connection coefficients, respectively. The column vector ϕ with entries $(\phi_0, \phi_1, \phi_2, \phi_3, \phi_4)^\mathrm{T}$ denotes the components of the totally symmetric spinor field ϕ_{ABCD}, which, in the 2-spinor formalism, is used to represent the rescaled conformal Weyl tensor (1.11). (The notation $\phi_k = \phi_{A+B+C+D}$ is employed here.) In a similar fashion the boundary adapted evolution system can be written (after an appropriate transformation of ϕ, see [32]) in the symmetric hyperbolic form

$$I\,\partial_\tau \phi + A^\mu \partial_\mu \phi = B(\Gamma)\,\phi,$$

where I is the 5×5 identity matrix, A^μ and B are 5×5 matrices that are functions of the frame and connection coefficients, respectively, and ϕ is defined as above. In addition, the matrices A^μ are Hermitian and $I + A^0$ is positive definite.[11] In general, all possible evolution schemes can be expressed as a symmetric hyperbolic system of the above form (see [34], [37]).

Another extremely appealing feature of the system (1.70)-(1.73) is that, according to [32], it preserves the constraints when is used to propagate Cauchy initial data.

1.6   Constraint equations

To complete the study of the conformal field equations one has to take care of the conformal constraints evaluated on the initial space-like hypersurface $\tilde{S}$. Interestingly, in [33] Friedrich uses different conformal factors, namely Θ and Ω, to analyse the evolution and constraint equations, respectively. He introduces a smooth and

---

[11]Features that guarantee the symmetric hyperbolicity of the above system.

positive function κ on the initial hypersurface $\tilde{S}$ to relate the two conformal factors through the expression $\Theta|_{\tau=0} = \kappa^{-1}\Omega$. Using the freedom introduced by κ one can gain control on the behaviour of Θ (see (1.66)) near space-like infinity. In this way the points where Θ is vanishing can be controlled and consequently, according to condition iv) of **Definition 1**, the location of $\mathscr{I}$. Another equally crucial, if not more important, use of the function κ is to "absorb" the singular behaviour of some components of the rescaled Weyl tensor near space-like infinity.

1.6.1 Derivation of the conformal constraints

It turns out more convenient to derive the conformal constraints in the metric, instead of the general, formulation of the conformal field equations. Thus, the transformation law (1.2), for a positive definite function Ω, will be again used in this section and the Weyl connection will be replaced by the more familiar Levi-Civita connection ∇. Recall that in sec. 1.2 the metric conformal field equations for the unknowns

$$ g_{\mu\nu}, \quad \Omega, \quad s, \quad L_{\mu\nu}, \quad d^{\mu}{}_{\nu\lambda\rho} $$

were derived in the form

$$ R^{\mu}{}_{\nu\lambda\rho} = 2\left(g^{\mu}{}_{[\lambda}\,L_{\rho]\nu} - g_{\nu[\lambda}\,L_{\rho]}{}^{\mu}\right) + \Omega\,d^{\mu}{}_{\nu\lambda\rho}, $$

$$ \nabla_{\lambda}\,L_{\rho\nu} - \nabla_{\rho}\,L_{\lambda\nu} = d^{\mu}{}_{\nu\lambda\rho}\,\nabla_{\mu}\,\Omega, $$

$$ \nabla_{\mu}\,d^{\mu}{}_{\nu\lambda\rho} = 0, $$

$$ \nabla_{\mu}\nabla_{\nu}\,\Omega = -\Omega\,L_{\mu\nu} + s\,g_{\mu\nu}, $$

$$ \nabla_{\mu}\,s = -L_{\lambda\mu}\,\nabla^{\lambda}\Omega, $$

$$ 2\,\Omega\,s - \nabla_{\rho}\Omega\,\nabla^{\rho}\Omega = 0, $$

where $s = \frac{1}{4}\,\Box\,\Omega + \frac{1}{24}\,R\,\Omega$ and $L_{\mu\nu} = \frac{1}{2}(R_{\mu\nu} - \frac{1}{6}\,g_{\mu\nu}R)$. This set of equations is equivalent to the vacuum conformal field equations (1.3) and, as the general conformal field equations, do not exhibit singular terms in the limit $\Omega \to 0$.

To derive the conformal constraints on the initial hypersurface $\tilde{S}$, we have to consider again a vierbein $\mathbf{e}_k = (\mathbf{e}_0, \mathbf{e}_1, \mathbf{e}_2, \mathbf{e}_3)$ that satisfies (1.51), i.e. the orthonormality relation $g_{\mu\nu}\mathrm{e}^{\mu}{}_i\mathrm{e}^{\nu}{}_k = \eta_{ik} = \mathrm{diag}(1,-1,-1,-1)$, in a neighbourhood of $\tilde{S}$. Moreover, we demand $\mathbf{n} \equiv \mathbf{e}_0$ to be g-normal to the initial space-like hypersurface $\tilde{S}$, i.e. $\mathbf{e}_0 \perp \tilde{S}$. The reduction of (1.19)-(1.24) on $\tilde{S}$ is performed with respect to

the above defined normal vector $\mathbf{n}$. Thus, according to (1.51), the reduction of the space-time metric $g_{\mu\nu}$ on $\tilde{S}$ yields the inner metric

$$h_{ab} = -\delta_{ab} = \mathrm{diag}(-1, -1, -1)^{12} \tag{1.74}$$

and the following expression for the second fundamental form

$$\chi_{ab} = g_{\mu\nu}\, \mathrm{e}^{\mu}{}_{b} \nabla_{\mathbf{e}_a} n^{\nu} = g_{\mu\nu}\, \mathrm{e}^{\mu}{}_{b}\, \Gamma_a{}^{j}{}_{0}\, \mathrm{e}^{\nu}{}_{j} = \Gamma_a{}^{j}{}_{0}\, g_{jb} = -\Gamma_a{}^{j}{}_{b}\, g_{j0}.^{13} \tag{1.75}$$

We denote the derivative of the conformal factor Ω in the direction of the future directed g-unit normal vector $\mathbf{n}$ as $\Sigma \equiv \nabla_0 \Omega$. The "unphysical" induced metric h_{ab} and the second fundamental form χ_{ab} are related to their physical counterparts by

$$h_{ab} = \Omega^2 \tilde{h}_{ab} \quad \text{and} \quad \chi_{ab} = \Omega\,(\tilde{\chi}_{ab} + \Sigma\, \tilde{h}_{ab}), \tag{1.76}$$

respectively. Contracting the latter expression one gets the transformation law for the trace of the second fundamental form

$$\Omega\, \chi = \tilde{\chi} + 3\,\Sigma. \tag{1.77}$$

In addition, we denote the orthogonal projections with respect to $\mathbf{n}$ of the fields $L_{\mu\nu}$ and $d^{\mu}{}_{\nu\lambda\rho}$, i.e.

$$L_{\mu\nu}\, n^{\nu}, \quad d^{\mu}{}_{\nu\lambda\rho}\, n^{\nu} n^{\rho}, \quad d^{\mu}{}_{\nu\lambda\rho}\, n^{\nu},$$

expressed in terms of the spatial components of $\mathbf{e}_k$, as follows

$$L_{ab} \equiv L_{\mu\nu} \mathrm{e}^{\mu}{}_{a} \mathrm{e}^{\nu}{}_{b}, \;\; L_a \equiv L_{a0}, \;\; w_{abcd} \equiv d_{abcd}, \;\; w_{ab} \equiv d_{a0b0}, \;\; w^{*}_{ab} \equiv d^{*}_{a0b0}, \;\; w_{abc} \equiv d_{a0bc},$$

where with $*$ we denote the dual of the rescaled Weyl tensor. The tensors w_{ab} and w^{*}_{ab} are the electric and magnetic part, respectively, of the rescaled Weyl tensor d_{abcd} on $\tilde{S}$.

Now we are ready to perform the reduction. Using the space-like version of Gauss' [71], [91]

$$R^{a}{}_{bcd} = r^{a}{}_{bcd} + \chi_{bd}\, \chi_c{}^{a} - \chi_{bc}\, \chi_d{}^{a}$$

and Codazzi's

$$R_{a0bc} = D_b \chi_{ac} - D_c \chi_{ab}$$

---

[12] Where, as before, lower case Latin indices from the beginning of the alphabet take values 1, 2, 3.

[13] The identity $\Gamma_i{}^{j}{}_{k}\, g_{jl} + \Gamma_i{}^{j}{}_{l}\, g_{jk} = 0$ was used in the last equality.

equations, one can reduce (1.19) to

$$r_{ab} = \Omega\, w_{ab} + L_{ab} + h_{ab}\, L_c{}^c - \chi_{ab}\, \chi_c{}^c + \chi_{ac}\chi_b{}^c \quad {}^{14} \tag{1.78}$$

and

$$D_b\, \chi_{ac} - D_c\, \chi_{ab} = \Omega\, w_{abc} + h_{ab}\, L_c - h_{ac}\, L_b, \tag{1.79}$$

respectively. Here $r^a{}_{bcd}$, r_{ab} and D stand, respectively, for the Riemann and Ricci tensor of h_{ab} and the covariant derivative on $\tilde{S}$. In the above derivation the identities $w_{abcd} = 2\left(h_{a[c}w_{d]b} + h_{b[d}w_{c]a}\right)$ and $w_c{}^c = 0$ were extensively used. Relation (1.24) reduces trivially to

$$2\,\Omega\, s - \Sigma^2 - \nabla_a\Omega\,\nabla^a\Omega = 0.$$

Multiplying (1.23) with $\mathrm{e}^\mu{}_a$ one gets

$$\mathrm{e}^\mu{}_a\nabla_\mu\, s\, (\equiv D_a\, s) = -\mathrm{e}^\mu{}_a L_{\lambda\mu}\nabla^\lambda\Omega = -L_{ba}\, D^b\Omega - L_a\,\Sigma.$$

Equation (1.22) reduces to

$$-\Omega\, L_{ab} + s\, h_{ab} = \mathrm{e}^\mu{}_a\mathrm{e}^\nu{}_b\nabla_\mu\nabla_\nu\,\Omega = \mathrm{e}^\mu{}_a\nabla_\mu(\mathrm{e}^\nu{}_b\nabla_\nu\,\Omega) - \mathrm{e}^\mu{}_a(\nabla_\mu\mathrm{e}^\nu{}_b)\nabla_\nu\,\Omega =$$
$$= D_aD_b\Omega - (\nabla_{\mathbf{e}_a}\mathrm{e}^\nu{}_b)\nabla_\nu\,\Omega = D_aD_b\Omega - \Gamma_a{}^i{}_b\,\mathrm{e}^\nu{}_i\nabla_\nu\,\Omega \overset{(1.75)}{=}$$
$$= D_aD_b\Omega + \chi_{ab}\, g^{0i}\,\mathrm{e}^\nu{}_i\nabla_\nu\,\Omega = D_aD_b\Omega + \chi_{ab}\,\Sigma$$

and

$$-\Omega\, L_a = \mathrm{e}^\mu{}_a n^\nu\nabla_\mu\nabla_\nu\,\Omega = \mathrm{e}^\mu{}_a\nabla_\mu(n^\nu\nabla_\nu\,\Omega) - \mathrm{e}^\mu{}_a(\nabla_\mu\, n^\nu)\nabla_\nu\,\Omega =$$
$$= D_a\Sigma - (\nabla_{\mathbf{e}_a}n^\nu)\nabla_\nu\,\Omega = D_a\Sigma - \Gamma_a{}^i{}_0\,\mathrm{e}^\nu{}_i\nabla_\nu\,\Omega \overset{(1.75)}{=}$$
$$= D_a\Sigma - \chi_{ab}\, g^{bi}\,\mathrm{e}^\nu{}_i\nabla_\nu\,\Omega = D_a\Sigma - \chi_a{}^c\nabla_c\,\Omega.$$

The other two metric conformal field equations (1.20) and (1.21) can be reduced in

---

[14]This, actually, is the contracted form of $r^a{}_{bcd} = \Omega\, w^a{}_{bcd} + 2\left(h^a{}_{[c}\, L_{d]b} - h_{b[c}\, L_{d]}{}^a\right) - \chi_{bd}\,\chi_c{}^a + \chi_{bc}\chi_d{}^a$.

a similar fashion. Finally, one gets

$$2\,\Omega\,s - \Sigma^2 - D_a\,\Omega\,D^a\,\Omega = 0, \tag{1.80}$$

$$D_a\,D_b\,\Omega = -\,\Sigma\,\chi_{ab} - \Omega\,L_{ab} + s\,h_{ab}, \tag{1.81}$$

$$D_a\,\Sigma = \chi_a{}^c\,D_c\,\Omega - \Omega\,L_a, \tag{1.82}$$

$$D_a\,s = -L_{ba}\,D^b\Omega - \Sigma\,L_a, \tag{1.83}$$

$$D_a\,L_{bc} - D_b\,L_{ac} = w_{ecab}\,D^e\Omega - \Sigma\,w_{cab} - \chi_{ac}\,L_b + \chi_{bc}\,L_a, \tag{1.84}$$

$$D_a\,L_b - D_b\,L_a = w_{eab}\,D^e\Omega + \chi_a{}^c\,L_{bc} - \chi_b{}^c\,L_{ac}, \tag{1.85}$$

$$D^c w_{cab} = \chi^c{}_a\,w_{bc} - \chi^c{}_b\,w_{ac}, \tag{1.86}$$

$$D^a w_{ab} = \chi^{ac}\,w_{abc}. \tag{1.87}$$

Expressions (1.84) and (1.85) follow from (1.20), while (1.86) and (1.87) follow from (1.21). Equations (1.78)-(1.87) comprise the so-called *conformal constraints*. If the solutions $\tilde{h}_{ab}$ and $\tilde{\chi}_{ab}$ to the vacuum constraints are, somehow, known and the gauge functions Ω, Σ, R have been specified, then the conformal constraints, together with (1.76), can be used to specify the fields

$$s, \ L_{ab}, \ L_a, \ w_{ab}, \ w_{ab}^*.$$

This will be our objective in the following sections.

1.6.2   The situation near space-like infinity

In order to solve the conformal constraint equations (1.78)-(1.87) we have to assume some appropriate boundary conditions on $\tilde{S}$. Space-like infinity will be used for this purpose. One possible way to bring space-like infinity into the picture is by attaching a point i—which must not be confused with its space-time counterpart i^0—on $\tilde{S}$ to represent space-like infinity for any object living on the initial hypersurface $\tilde{S}$.

Since we are primarily concerned here with the study of isolated gravitational systems, and consequently of asymptotically flat space-times, it is natural to demand that near i the initial hypersurface $\tilde{S}$ is *asymptotically Euclidean*. Thus, following [13] the above requirement can be expressed as follows.

Assumption 1 *We assume that for the manifold $(\tilde{S}, \tilde{h})$ there exists a compact subset M of $\tilde{S}$ such that $\tilde{S} - M$ is the disjoint union of a finite number of open sets U_i,*

41

each of which is diffeomorphic to the exterior of a ball $\mathcal{B}$ in the three dimensional Euclidean space $\mathbb{E}^3$. In addition, it is assumed that on the exterior of $\mathcal{B}$ we can always introduce Cartesian coordinates y^a with $|y|^2 = \sum_{a=1}^{3}(y^a)^2$ and express the metric coefficients in the form

$$\tilde{h}_{ab} = -\delta_{ab} + \mathcal{O}\left(\frac{1}{|y|}\right) \quad as \quad |y| \to \infty.$$

A manifold $(\tilde{S}, \tilde{h})$ that satisfies the criteria of **Assumption 1** will be called from now on asymptotically Euclidean. Moreover, it will be assumed that, in the Cartesian coordinates y^a introduced above, the second fundamental form behaves like [91]

$$\tilde{\chi}_{ab} = \mathcal{O}\left(\frac{1}{|y|^2}\right) \quad \text{as} \quad |y| \to \infty.$$

Although **Assumption 1** guarantees the euclidicity of the physical initial data near space-like infinity, it tells us nothing about the behaviour of their "unphysical" counterparts. In order to ensure that, in the conformally compactified picture of **Definition 1**, h_{ab} and χ_{ab} are (initially) smooth enough in the neighbourhood of space-like infinity, we have to strengthen our requirements.[15] One way to do that is by demanding the manifold $(\tilde{S}, \tilde{h})$ to be *asymptotically Euclidean and regular* in the following sense introduced by Friedrich in [33].[16]

Definition 2 *A three dimensional smooth manifold $(\tilde{S}, \tilde{h})$ is called asymptotically Euclidean and regular if both a three dimensional, orientable, smooth, compact Riemannian manifold (S, h) with a point $i \in S$ and a smooth function Ω exist such that*

i) $h_{ab} = \Omega^2 \tilde{h}_{ab}$ on $S\backslash\{i\}$,

ii) $\Omega > 0$ on $S\backslash\{i\}$,

iii) $\Omega = 0$, $D_a \Omega = 0$, and $D_a D_b \Omega = -2\,h_{ab}$ at i.

---

[15]We will see in the following that even when the requirements of **Definition 2** are satisfied, some components of the rescaled Weyl tensor are still (initially) singular near space-like infinity.

[16]More precisely, in addition to **Definition 2**, we have also to require that (S, h) has positive Yamabe number, see [33] for the details.

A suitably chosen small enough neighbourhood of the point i corresponds to the asymptotically flat end of $(\tilde{S}, \tilde{h})$, entailing in this way that the point i represents space-like infinity. Condition $iii)$, which implies that Ω falls-off as $1/|y|^2$ as $|y| \to \infty$, guarantees the Minkowskian behaviour of the conformal factor near i.

Introducing locally, in a small convex normal neighbourhood $\mathcal{U}$ of i, a normal Cartesian coordinate system $\mathrm{x}^a = (\mathrm{x}^1, \mathrm{x}^2, \mathrm{x}^3)$ with origin at i, i.e. $\mathrm{x}^a(i) = 0$, and based on an h-orthonormal frame $\mathbf{e}_k$ at i, one can show that condition $iii)$ actually entails that the conformal factor is of the form

$$\Omega = |\mathrm{x}|^2 f(\mathrm{x}),\,^{17}$$

where f is a continuous function with $f(0) = 1$ and $|\mathrm{x}|$ is the h-distance from the point i, namely $|\mathrm{x}| = \sqrt{\sum_{a=1}^{3} (\mathrm{x}^a)^2}$. It is quite straightforward to show that the above choice for the conformal factor Ω leads to the assertions of the condition $iii)$. Let's check the first one

$$\Omega(i) = \lim_{\mathrm{x} \to 0} \left(|\mathrm{x}|^2 f(\mathrm{x}) \right) = 0,$$

where we denote $|\mathrm{x}|^2 = \mathrm{x}^a \mathrm{x}^b \delta_{ab}$. Bearing in mind that $h_{ab} = -\delta_{ab}$ (see (1.74)) and $D_a |\mathrm{x}| = \mathrm{x}^b \delta_{ab}/|\mathrm{x}|$ the second assertion reads

$$D_a \, \Omega(i) = \lim_{\mathrm{x} \to 0} \left(2\, \mathrm{x}^b \, \delta_{ab} \, f(\mathrm{x}) + |\mathrm{x}|^2 D_a f(\mathrm{x}) \right) = 0.$$

Finally, by differentiating the last expression one gets

$$
\begin{aligned}
D_b D_a \, \Omega(i) &= \\
&= \lim_{\mathrm{x} \to 0} \left(2\, \delta_{ab} \, f(\mathrm{x}) + 2\, \Gamma_b{}^c{}_d \, \mathrm{x}^d \delta_{ca} f(\mathrm{x}) - 4\, \mathrm{x}_{(a} D_{b)} f(\mathrm{x}) + |\mathrm{x}|^2 D_b D_a f(\mathrm{x}) \right) = \\
&= 2\, \delta_{ab} \, f(0) = -2\, h_{ab},
\end{aligned}
$$

which clearly reproduces the last assertion of condition $iii)$.

The above choice for Ω can be rewritten in the form

$$|\mathrm{x}|\, \Omega^{-1/2} = f(\mathrm{x})^{-1/2} \Rightarrow \lim_{\mathrm{x} \to 0} |\mathrm{x}|\, \Omega^{-1/2} = \lim_{\mathrm{x} \to 0} f(\mathrm{x})^{-1/2} = f(0)^{-1/2} = 1,$$

which at i implies the condition

$$|\mathrm{x}|\, \theta \to 1 \quad \text{as} \quad |\mathrm{x}| \to 0, \tag{1.88}$$

---

[17]See (1.100) for the explicit form of f.

where $\theta \equiv \Omega^{-1/2}$.

Interestingly, the boundary condition (1.88) suffices to "bridge" (1.74) and **Assumption 1** in the following sense. The spatial metrics $\tilde{h}$ and h are asymptotically Euclidean and flat,[18] respectively, iff the conformal factor $\theta = \Omega^{-1/2}$ satisfies the boundary condition (1.88). Notice that the spatial physical metric in the Cartesian coordinates y^a, introduced in **Assumption 1**, is given by

$$\tilde{h} = \tilde{h}_{ab} \, \mathbf{d}y^a \, \mathbf{d}y^b.$$

Effecting the coordinate inversion $y^a = -\mathrm{x}^a/|\mathrm{x}|^2$, we can express $\tilde{h}$ in terms of the Cartesian normal coordinate system x^a defined above, i.e.

$$\tilde{h} = \frac{1}{|\mathrm{x}|^4} \, \tilde{h}_{ab} \, \mathbf{d}\mathrm{x}^a \, \mathbf{d}\mathrm{x}^b.$$

Under a conformal rescaling of the form (1.2) the physical metric transforms like

$$\tilde{h} = \theta^4 \, h = \theta^4 \, h_{ab} \, \mathbf{d}\mathrm{x}^a \, \mathbf{d}\mathrm{x}^b = -\theta^4 \, \delta_{ab} \, \mathbf{d}\mathrm{x}^a \, \mathbf{d}\mathrm{x}^b.$$

Obviously, the last two expressions imply that

$$\tilde{h}_{ab} = -|\mathrm{x}|^4 \, \theta^4 \, \delta_{ab}.$$

Observing (1.88), the above result clearly indicates that $\tilde{h}_{ab} \to -\delta_{ab}$ as $|\mathrm{x}| \to 0$ (or $|y| \to \infty$), i.e. the physical metric is asymptotically Euclidean, iff $|\mathrm{x}|\theta \to 1$ as $|\mathrm{x}| \to 0$.

1.6.3 Solving the conformal constraints

It turns out that the system (1.78)-(1.87) can be solved, together with the condition (1.88), for the fields $\theta \equiv \Omega^{-1/2}, s, L_{ab}, L_a, w_{ab}, w_{ab}^*$ just by making some simplifying assumptions for the "unphysical" second fundamental form χ_{ab} and the scalar field Σ. No reference to fields living on the physical space-time is required!

To begin with, we will try to extract from the conformal constraints the Hamiltonian and momentum constraints of the "unphysical" fields. It turns out that the constraints provide a solution for the conformal factor θ. Contracting (1.78) and (1.81), solving the former for $L_a{}^a$ and substituting it into the latter one obtains

$$s = \frac{1}{3} \left(\Delta_h \Omega + \Sigma \, \chi_a{}^a + \frac{\Omega}{4} \left(r + (\chi_a{}^a)^2 - \chi_{ab} \, \chi^{ab} \right) \right),$$

---

[18]Namely, they respect **Assumption 1** and (1.74).

where $\Delta_h \equiv D_a D^a$. Inserting the above expression into (1.80) we end up with the Hamiltonian constraint

$$4\,\Omega\,\Delta_h\Omega + \Omega^2 r - 6\,D_a\Omega D^a\Omega = 6\,\Sigma^2 - \Omega^2((\chi_a{}^a)^2 - \chi_{ab}\,\chi^{ab}) - 4\,\Omega\,\Sigma\,\chi_a{}^a,$$

which, when expressed in terms of $\theta \equiv \Omega^{-1/2}$, simplifies to

$$\left(\Delta_h - \frac{1}{8}\,r\right)\theta = \frac{1}{8}\,\theta\left((\chi_a{}^a)^2 - \chi_{ab}\,\chi^{ab}\right) + \frac{1}{2}\,\theta^3\,\Sigma\,\chi_a{}^a - \frac{3}{4}\,\theta^5\,\Sigma^2.$$

Introducing the smooth symmetric tensor field $\psi_{ab} \equiv \theta^4\,\chi_{ab}$ the Hamiltonian constraint can be written in the form of a generalized Lichnerowicz equation [87]

$$\left(\Delta_h - \frac{1}{8}\,r\right)\theta = \frac{1}{8}\,\theta^{-7}\left((\psi_a{}^a)^2 - \psi_{ab}\,\psi^{ab}\right) + \frac{1}{2}\,\theta^{-1}\,\Sigma\,\psi_a{}^a - \frac{3}{4}\,\theta^5\,\Sigma^2. \qquad (1.89)$$

Contracting (1.79) and using (1.82) to eliminate L_c one obtains the momentum constraint

$$D^a(\Omega^{-2}\chi_{ac}) = \Omega^{-2}\,D_c\,\chi_a{}^a - 2\,\Omega^{-3}\,D_c\,\Sigma,$$

which in terms of θ and ψ_{ab} reads

$$D^a\psi_{ac} = \theta^4\,D_c(\theta^{-4}\psi_a{}^a) - 2\,\theta^6\,D_c\,\Sigma. \qquad (1.90)$$

Following Lichnerowicz's intuition [54] and restricting part of the freedom related to the choice of the conformal factor Ω, one can achieve a considerable simplification of (1.89) and (1.90).

Assumption 2 *We assume that on* $\tilde{S}$

$$\Sigma = 0 \quad and \quad \chi_a{}^a = 0$$

holds.

The former assumption is just a choice of gauge, while the latter ensures that our initial space-like hypersurface has vanishing mean curvature, i.e. it is maximal with respect to g. Under **Assumption 2** expression (1.90) becomes

$$D^a\psi_{ac} = 0, \qquad (1.91)$$

which together with $\psi_a{}^a = 0$ entails that ψ_{ab} is a transverse traceless (TT) tensor [12]. TT tensors are conformally covariant [87], thus ψ_{ab} under rescalings of the form (1.2) remains a TT tensor, i.e. $\tilde{\psi}_{ab}$ is a TT tensor and, consequently, $\tilde{\chi}_a{}^a = 0$ holds. Therefore, our initial space-like hypersurface is also maximal with respect to $\tilde{g}$.[19] Under **Assumption 2** the Hamiltonian constraint (1.89) simplifies vastly and

---

[19]This result also follows from (1.77) and **Assumption 2**.

takes the form of the *Lichnerowicz* equation [54]

$$\left(\Delta_h - \frac{1}{8}\,r\right)\theta = \frac{1}{8}\,\psi_{ab}\,\psi^{ab}\,\theta^{-7}.\tag{1.92}$$

Although (1.91) and (1.92) together with the boundary condition (1.88) can be solved for θ (see [12] and references therein), here we will further simplify (1.92) by considering time reflection symmetric initial data.[20]

Assumption 3 *We assume that on $\tilde{S}$*

$$\chi_{ab} = 0 \quad (and\ consequently)^{21} \quad \tilde{\chi}_{ab} = 0$$

holds.

Now, with **Assumption 3** equation (1.91) is trivially satisfied; thus, in order to determine θ, we have simply to solve the conformally invariant Laplace equation

$$\left(\Delta_h - \frac{1}{8}\,r\right)\theta = 0$$

with the boundary condition (1.88). To avoid lengthy computational arguments[22] Friedrich assumed that the components of h_{ab} are real analytic functions, in $\mathcal{U}$, of the coordinate system x^a specified in sec. 1.6.2.[23] This leads to our next assumption.

Assumption 4 *We assume that*

$$h \ is \ analytic \ near \ i.$$

A detailed description of how to acquire a solution to the above system can be found in [31], [37]. Here, we will just present the result, which looks like

$$\theta \left(\equiv \Omega^{-1/2}\right) = \frac{U}{|\mathrm{x}|} + W \qquad \text{near} \quad i,\tag{1.93}$$

with $U(i) = 1^{24}$ and $W(i) = m/2$ (where m denotes the ADM-mass of the solution). The real analytic function U is determined by the local geometry near i and reads

$$U = \sum_{p=0}^{\infty} U_p |\mathrm{x}|^{2p}\tag{1.94}$$

---

[20] For an extension to non-time reflection symmetric initial data see [14], [89], [90].

[21] Through (1.76) and **Assumption 2**.

[22] For example, **Assumption 4** guarantees the analyticity of the function U, see (1.94).

[23] [90] extents Friedrich's results for non-smooth conformally compactified initial data.

[24] Which follows from (1.88): $\lim_{\mathrm{x}\to 0}(|\mathrm{x}|\,\theta) = \lim_{\mathrm{x}\to 0}(U + |\mathrm{x}|\,W) = U(i) = 1$.

with $U_0 = 1 + \mathcal{O}(|x|^2)$ as $|x| \to 0$; while the function W (also real analytic) is a smooth solution of the conformally invariant Laplace equation displayed above and contains global information about the initial hypersurface S.

Having secured an expression for θ, (1.93), we turn now to the derivation of solutions for the fields $s, L_{ab}, L_a, w_{ab}, w_{ab}^*$ from the conformal constraints (1.78)-(1.87). In the following computations it will be assumed that **Assumptions 2** and **3** are satisfied. The expressions for s and L_a follow trivially from (1.80) and (1.82), respectively. Using the traces of (1.78) and (1.81) to eliminate s from (1.81), one finds an expression for L_{ab}. An expression for w_{ab} is recovered by inserting (1.96) and the trace of (1.78)—which reads $r = 4 L_c{}^c$—into (1.78). Finally, the vanishing of L_a entails that w_{abc} also vanishes; thus, the identity $w_{ad}^* = -\frac{1}{2} w_{abc}\epsilon_d{}^{bc}$ [25] clearly indicates that the magnetic part of the rescaled Weyl tensor vanishes. Therefore, by following the above procedure, one gets the expressions

$$s = \frac{1}{2\,\Omega}\, D_a\,\Omega D^a\Omega, \tag{1.95}$$

$$L_{ab} = -\frac{1}{\Omega}\,(D_a\,D_b\,\Omega - \frac{1}{3}\,h_{ab}\,\Delta_h\Omega) + \frac{1}{12}\,r\,h_{ab}, \tag{1.96}$$

$$L_a = 0, \tag{1.97}$$

$$w_{ab}^* = 0, \tag{1.98}$$

$$w_{ab} = \frac{1}{\Omega^2}\,(D_a\,D_b\,\Omega - \frac{1}{3}\,h_{ab}\,\Delta_h\Omega + \Omega\,s_{ab}) \tag{1.99}$$

for the unknown fields s, L_{ab}, L_a, w_{ab}, and w_{ab}^*. In (1.99) the traceless tensor field $s_{ab} = r_{ab} - \frac{1}{3}\,r\,h_{ab}$ was introduced. It can be confirmed that the rest of the conformal constraints (1.83)-(1.87), which were not used in the derivation of the above results, are also satisfied by (1.95)-(1.99).

1.6.4 Behaviour of the initial data near i

Our Cauchy initial data must be compatible, under our assumptions, with the solutions (1.93)-(1.99) of the conformal constraints (1.78)-(1.87). It is apparent, by observing (1.93)-(1.99), that near space-like infinity Ω dictates the behaviour of the non-vanishing fields s, L_{ab}, w_{ab}. Expression (1.93) entails the form of Ω:

$$\Omega = \frac{|x|^2}{(U + |x|W)^2} \qquad \text{near} \quad i. \tag{1.100}$$

---

[25] ϵ is the totally antisymmetric symbol.

We will be mainly concerned here with the most important, but also the most singular, field we have to prescribe on the initial hypersurface, namely the electric part w_{ab} of the rescaled Weyl tensor. Inserting (1.100) into (1.99), and denoting $\Gamma \equiv |\mathrm{x}|^2$, the field w_{ab} takes the form

$$w_{ab} = w_{ab}^U + w_{ab}^W, \tag{1.101}$$

with

$$\begin{aligned} w_{ab}^U = \frac{1}{|\mathrm{x}|^4} \Big[& 6\,|\mathrm{x}|^2 D_a U D_b U - 4\,U D_a U D_b \Gamma - 2\,|\mathrm{x}|^2\,U D_a D_b U + U^2 D_a D_b \Gamma - \\ & - \frac{1}{3}\left(6\,|\mathrm{x}|^2 D_c U D^c U - 4\,U D_c U D^c \Gamma - 2\,|\mathrm{x}|^2\,U\Delta_h U + U^2 \Delta_h \Gamma\right) h_{ab} + \\ & + |\mathrm{x}|^2\,U^2 s_{ab} \Big] \end{aligned} \tag{1.102}$$

and

$$\begin{aligned} w_{ab}^W = \frac{1}{|\mathrm{x}|^5}\Big[& 12|\mathrm{x}|^4 D_a U D_b W + 6|\mathrm{x}|^5 D_a W D_b W + 2\,|\mathrm{x}|^2 W D_a U D_b \Gamma - \\ & - 6\,|\mathrm{x}|^2 U D_a W D_b \Gamma - \frac{3}{2} U W D_a \Gamma D_b \Gamma - 2\,|\mathrm{x}|^4 W D_a D_b U - \\ & - 2\,|\mathrm{x}|^4 U D_a D_b W - 2\,|\mathrm{x}|^5 W D_a D_b W + |\mathrm{x}|^2 U W D_a D_b \Gamma \Big] - \\ & - \frac{1}{3\,|\mathrm{x}|^5}\Big[12|\mathrm{x}|^4 D_c U D^c W + 6|\mathrm{x}|^5 D_c W D^c W + 2\,|\mathrm{x}|^2 W D_c U D^c \Gamma - \\ & - 6\,|\mathrm{x}|^2 U D_c W D^c \Gamma - \frac{3}{2} U W D_c \Gamma D^c \Gamma - 2\,|\mathrm{x}|^4 W \Delta_h U - 2\,|\mathrm{x}|^4 U \Delta_h W \\ & - 2\,|\mathrm{x}|^5 W \Delta_h W + |\mathrm{x}|^2 U W \Delta_h \Gamma \Big] h_{ab} + \frac{1}{|\mathrm{x}|}(2\,U W + |\mathrm{x}|W^2) s_{ab} \end{aligned} \tag{1.103}$$

In the literature w_{ab}^U is called the *massless* and w_{ab}^W the *massive* part of the rescaled Weyl tensor. The two most singular terms in (1.102) combined behave like

$$D_a D_b \Gamma - \frac{1}{3}\,\Delta_h \Gamma\, h_{ab} = 2\left(\mathrm{x}_c\,\Gamma_a{}^c{}_b + \frac{1}{3}\,\mathrm{x}^f\,\Gamma_c{}^c{}_f\, h_{ab}\right) = \mathcal{O}(|\mathrm{x}|^2) \quad \text{as} \quad |\mathrm{x}| \to 0,$$

where the connection coefficients of the "unphysical" metric $h = \Omega^2\,\tilde{h}$ with Ω and $\tilde{h}$ given by (1.100) and **Assumption 1**, respectively, behave like $\Gamma_a{}^c{}_b = \mathcal{O}(|\mathrm{x}|)$ as $|\mathrm{x}| \to 0$. Similarly, the two most singular terms in (1.103) behave like

$$\begin{aligned} & \frac{1}{2}\,W\left(-3\,D_a \Gamma D_b \Gamma + D_c \Gamma D^c \Gamma\, h_{ab}\right) = \\ & = 2\,W\left(-3\,\mathrm{x}_a \mathrm{x}_b + |\mathrm{x}|^2\,h_{ab}\right) = m\,\mathcal{O}(|\mathrm{x}|^2) \quad \text{as} \quad |\mathrm{x}| \to 0, \end{aligned}$$

48

where m is the ADM-mass of h. The above observations clearly indicate that

$$w^U_{ab} = \mathcal{O}\left(\frac{1}{|x|^2}\right), \quad w^W_{ab} = m\,\mathcal{O}\left(\frac{1}{|x|^3}\right) \quad \text{as} \quad |\text{x}| \to 0. \qquad (1.104)$$

Although, under suitable assumptions on the metric h, the massless part can be regular near i, the massive part always exhibits a singular behaviour of the form $\mathcal{O}(1/|x|^3)$ as $|x| \to 0$, unless the ADM-mass m vanishes.

From the above presentation is apparent that the Cauchy data for the rescaled Weyl tensor are singular in the vicinity of space-like infinity i. In order to continue our investigation of the behaviour of gravitational fields near i, we have to find a way to deal with these singular initial data. In [33] Friedrich proposed a possible way out of this problem. Therein, a suitable rescaling of the "unphysical" metric leads to a finite representation of space-like infinity. In this new picture our Cauchy data become regular—even close to i.

1.7   The finite representation of space-like infinity

Troubled by the aforementioned singular behaviour of the rescaled Weyl tensor and inspired by the result (1.66) Friedrich put forward in [33] a completely novel representation of space-like infinity. In this setting i is not considered anymore a point; an immediate consequence of this statement is that the splitting (1.101) becomes regular at i.

1.7.1   Construction of the cylinder

The basic idea is to *blow up* the point i into a spherical set I^0 such that space-like infinity has now a *finite* representation. Thus, on $\tilde{S}$ space-like infinity is not represented anymore by a point, but by the 2-sphere I^0. Furthermore, one can introduce on $S = \tilde{S} \cup I^0$ a coordinate r that vanishes on I^0, is negative inside I^0, and is positive elsewhere. Evolving I^0 along conformal geodesics that start orthogonally from $\tilde{S}$—this is a very natural thing to do as the data on the initial space-like hypersurface (where I^0 is located) is evolved along conformal geodesics (see sec. 1.3.3)—one constructs a finite *cylinder* I in the following sense.

By choosing the gauge condition (1.69) for the initial value of d_0 the term linear in τ of (1.66) vanishes. In addition, we are legitimate to assume that $\ddot{\Theta}_\star \equiv -2\,\Theta_\star H^{-2}$,

where $H(r)$ is an arbitrary positive function of the coordinate r.[26] According to condition iv) of **Definition 1** the conformal factor Θ must vanish at null infinity $\mathscr{I}^{\pm}$. Because $\Theta_{\star} > 0$ the locations of future and past null infinity are locked by the expression

$$\tau = \pm H(r), \tag{1.105}$$

which under the above assumptions follows naturally from (1.66). The above result indicates that the two branches of null infinity are separated by a *finite* distance $2H(r)$ along the parameter τ. This distance cannot be equal to zero as the homogeneous version of (1.66) does not admit the solution $\tau = 0$. Thus, future and past null infinity do not meet at space-like infinity as before—when space-like infinity was considered a point. Now, they are forced to meet with space-like infinity at the top and bottom base, respectively, of the cylinder I with height $\tau = 2H(0)$. The 2-spheres where $\mathscr{I}^{+}$ and $\mathscr{I}^{-}$ meet the cylinder I—i^{0} is now represented by I—are denoted by I^{+} and I^{-}, respectively. On I and $\mathscr{I}^{\pm}$ the conformal factor vanishes, while on I^{0} and $I^{\pm}$ both the conformal factor and its covariant derivative vanish.

In the above setting the cylinder I can be considered as a blow up of the point i^{0}. A very notable feature of this representation is that the cylinder was not introduced ad hoc or by hand, but emerged naturally from the geometrical structure of our problem: rescaling of our metric on S. In this picture, the part of the neighbourhood of space-like infinity which is outside the cylinder and between $\mathscr{I}^{+}$ and $\mathscr{I}^{-}$ is conformally related to the physical space-time, while the part inside the cylinder and in the cones of $\mathscr{I}^{+}$ and $\mathscr{I}^{-}$ consists the embedding space-time.

To complete the setting of the initial value problem near space-like infinity one has to find a way to extend the data in a regular way on and inside the cylinder, namely in the region where $r \leq 0$. To achieve that Friedrich uses the freedom inherent in the choice of the positive function κ, which was originally introduced to correlate the "evolution" Θ and "constraint" Ω conformal factor through the relation $\Theta|_{\tau=0} = \Theta_{\star} = \kappa^{-1}\Omega$. By choosing $\kappa \equiv r\,\mu(r)$, where μ is a smooth positive function with $\mu(i) = 1$, one achieves i) to bring Θ and d_i, after a proper choice of μ, into a form that is regular on I (where $r \to 0$) and smoothly extensible inside I (where $r < 0$) and ii) to bring the splitting (1.101) into the form $w_{ab} = \kappa^3\,(w_{ab}^U + w_{ab}^W)$, where obviously only non-negative power of r occur; in this way the singular behaviour of

---

[26]In order to simplify our presentation here, we reformulate the constant $\ddot{\Theta}_{\star}$ that appears in (1.66), namely we set $H^{-2} = -\frac{1}{4}\,(g^{\mu\nu}\tilde{f}_{\mu}\tilde{f}_{\nu})_{\star}$. In the following section we will specify H explicitly.

the rescaled Weyl tensor at i is absorbed by κ and, in addition, both the massless and massive part of it can be smoothly extended into the domain $r \leq 0$.

1.7.2 Behaviour of the initial data near I^0

As it was already mentioned, in order to render the expressions (1.104) regular, we have to appropriately rescale the "unphysical" metric h_{ab}. Following [33] we will introduce on S the rescaling

$$h_{ab} \mapsto \bar{h}_{ab} = \kappa^{-2} \, h_{ab}, \tag{1.106}$$

with

$$\kappa(r) = r \, \mu(r), \tag{1.107}$$

where μ is a positive smooth function on S with $\mu(i) = 1$ and r is the radial coordinate introduced in sec. 1.7.1 during the construction of the cylinder. Apparently, (1.106) causes the blowing up of space-like infinity i to I^0 described in sec. 1.7.1. Because of (1.106), κ can be viewed as a rescaling of the conformal factor Ω. Using the initial value of Θ on S to express this operation one can write

$$\Theta|_{\tau=0} = \Theta_\star = \kappa^{-1} \, \Omega \quad \text{on} \quad S.$$

It is worth noticing that with the help of (1.100) the above expression becomes

$$\Theta_\star = \frac{r}{\mu(r)(U + r \, W)^2}, \tag{1.108}$$

where we legitimately denote $r = |\mathrm{x}|$. Notice that the behaviour of $\Theta_\star$ is completely specified by the choice of μ. Inserting (1.69) into (1.66), and having in mind that $\Theta_\star$ is given by (1.108), one gets

$$\Theta(\tau) = \Theta_\star + \frac{\tau^2}{2} \, \ddot{\Theta}_\star, \tag{1.109}$$

where $\ddot{\Theta}_\star = \frac{1}{2} \, \Theta_\star \, (g^{\mu\nu} \tilde{f}_\mu \tilde{f}_\nu)_\star$. To proceed further, we have to specify the 1-form $\tilde{f}_\mu$, which is related to the freedom of choosing the connection, on the initial hypersurface S. Recall that the metric conformal field equations with a Levi-Civita connection, in place of a Weyl connection, were used in the study of the constraints. Thus, because of (1.2) and according to sec. 1.3.1, we can choose[27]

$$\tilde{f}_{\mu\star} = (\Omega^{-1} \, \nabla_\mu \Omega)_\star. \tag{1.110}$$

---

[27] A choice related to the fact that the Weyl connection reduces to the Levi-Civita connection.

Using (1.110) and **Assumption 2** to expand $\ddot{\Theta}_\star$, we get

$$\ddot{\Theta}_\star = -\frac{1}{2}\,\Theta_\star\,(\kappa^2\,\Omega^{-2}\,D_a\Omega\,D^a\Omega)_\star,$$

where the contravariant version of (1.106), namely $h^{ab} \mapsto \kappa^2\,h^{ab}$, was also taken into account. Therefore, the expression (1.109) becomes

$$\Theta(\tau) = \Theta_\star\left(1 - \tau^2\,\frac{\kappa_\star^2}{\omega_\star^2}\right), \tag{1.111}$$

where $\omega \equiv 2\,\Omega/\sqrt{D_a\Omega\,D^a\Omega}$ with Ω and $\Theta_\star$ given by (1.100) and (1.108), respectively. In addition, relations (1.110) and (1.111) entail the form of the 1-form (1.48):

$$d_k(\tau) = (d_0, d_a) = (\dot{\Theta}, \Theta_\star\,\tilde{f}_{\mu\star}\,\mathrm{e}^\mu{}_{a\star}) = \left(-2\,\tau\,\frac{\kappa_\star\,\Omega_\star}{\omega_\star^2}, \kappa_\star^{-1}\,(\nabla_a\,\Omega)_\star\right), \tag{1.112}$$

where (1.67) and (1.68) were used in the second equality. Notice that, with the choice (1.110), the only free function we have in our disposal now is κ (or alternatively μ).

According to **Definition 1**, the vanishing of (1.111) specifies the position of null infinity $\mathscr{I}^\pm$, i.e

$$\tau = \pm\frac{\omega_\star}{\kappa_\star}. \tag{1.113}$$

Comparing with (1.105) it can be readily confirmed that $H(r) = \omega_\star/\kappa_\star$. Thus, the height of the cylinder I is

$$H_{cyl} = 2\,\frac{\omega_\star}{\kappa_\star}\big|_{r=0}. \tag{1.114}$$

Consequently, $\mathscr{I}^+$ and $\mathscr{I}^-$ meet the cylinder at the points H_{cyl} and $-H_{cyl}$, respectively. It is apparent, from (1.113) and (1.114), that only the conformal factor Ω, through ω, and the function μ are involved in the construction of the cylinder. Keeping in mind though that Ω is completely specified by (1.100), then the construction of the cylinder is left entirely to μ. The function μ not only controls the height and the location of the points that null infinity meets the cylinder, but also, as it will be shown in the following chapter, can be used to control the "angle" between $\mathscr{I}^\pm$ and the cylinder.

Now, let's investigate an equally important consequence of the rescaling (1.106): under (1.106) the behaviour of the electric part (1.101) of the rescaled Weyl tensor near i becomes *regular*! This statement follows naturally from the transformation properties of w_{ab} under the rescaling (1.106). We will start from the observation

that, in accordance with (1.106), the "unphysical" space-time metric transforms like $g_{\mu\nu} \mapsto \bar{g}_{\mu\nu} = \kappa^{-2} g_{\mu\nu}$, while, according to its definition (1.11), the rescaled Weyl tensor transforms as $d^{\mu}{}_{\nu\lambda\rho} \mapsto \bar{d}^{\mu}{}_{\nu\lambda\rho} = \kappa\, d^{\mu}{}_{\nu\lambda\rho}$. Combining the last two results one finds

$$\bar{d}_{\mu\nu\lambda\rho} = \kappa^{-1}\, d_{\mu\nu\lambda\rho}.$$

Furthermore, observing that, under (1.106), the g-unit normal vector n^{μ} and the frame coefficients $e^{\mu}{}_a$ transform like

$$\bar{n}^{\mu} = \kappa\, n^{\mu} \quad \text{and} \quad \bar{e}^{\mu}{}_a = \kappa\, e^{\mu}{}_a,$$

we can, according to its definition (see sec 1.3.2), derive the transformation law of w_{ab}, i.e.

$$\bar{w}_{ab} = \kappa^3\, w_{ab}.$$

Thus, the splitting (1.101) becomes

$$\bar{w}_{ab} = \kappa^3 \left(w^U_{ab} + w^W_{ab} \right) \tag{1.115}$$

with w^U_{ab} and w^W_{ab} given by (1.102) and (1.103), respectively. Obviously, the behaviour of the massless and massive component of w_{ab} is now regular:

$$\bar{w}^U_{ab} = \mathcal{O}\left(r\right), \quad \bar{w}^W_{ab} = m\,\mathcal{O}\left(1\right) \quad \text{as} \quad r \to 0. \tag{1.116}$$

In a similar way, it can be proved that the rest of the non-vanishing initial data— i.e. s, L_{ab}, w_{ab} in (1.95)-(1.99)—we have to prescribe on S become also regular near space-like infinity i under the rescaling (1.106).

Chapter 2

Spin-2 system on Minkowski space-time

2.1 Minkowski space-time near space-like infinity

In this chapter we will apply the conformal representation of Einstein's equations, presented in the preceding chapter, in the simplest possible asymptotically flat background: Minkowski space-time. Which, if one considers the complexity of Einstein's field equations, is a very reasonable starting point for our endeavour. Our goal is, after fully understanding what is going on numerically and analytically in this simple case, to proceed gradually to more complicated models: spherical symmetric, axial symmetric etc. On a Minkowski background the structural equations (1.70)-(1.72) are trivially satisfied, thus one has to deal only with the Bianchi equation (1.73).[1] This chapter follows conceptually the presentation of the same topic in [5], [25], [36], and [88].

2.1.1 Conformal compactification

The physical metric representing Minkowski space-time in the natural coordinates y^μ reads

$$\tilde{g} = \eta_{\mu\nu}\, \mathbf{d}y^\mu \, \mathbf{d}y^\nu, \tag{2.1}$$

---

[1]More specifically, as will become apparent in sec. 2.2.2, we will consider here (1.73) in its linearised version.

where $\eta_{\mu\nu} = \mathrm{diag}(1, -1, -1, -1)$. In this representation the region we are mainly interested in, namely the neighbourhood of space-like infinity, lies far away from the origin. In order to get a more quantitative description of the points lying at infinity, we will consider the coordinate inversion [63]

$$y^\mu = -\frac{x^\mu}{x_\lambda x^\lambda}, \tag{2.2}$$

which brings our original metric into the form

$$\tilde{g} = \frac{1}{|x|^4} \eta_{\mu\nu} \, dx^\mu \, dx^\nu, \tag{2.3}$$

where $|x|^2 = x_\lambda x^\lambda$. (The minus sign in (2.2) is to preserve time sense [63].) Notice that with (2.2) points close to infinity in our original coordinates y^μ are now lying in the vicinity of the origin of the new "inverted" coordinates x^μ. But this comes

(a)   (b)
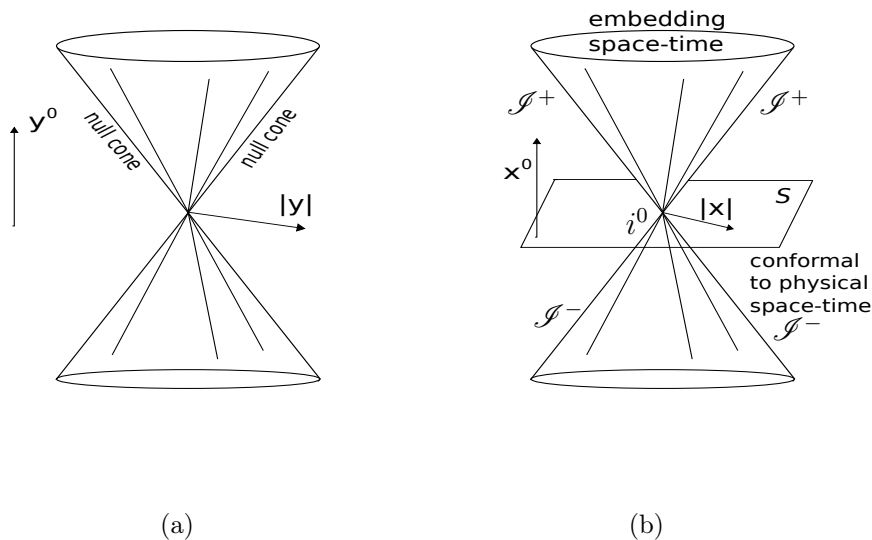
Figure 2.1: (a) The usual causal structure of Minkowski space-time as a light cone. (b) The conformally compactified Minkowski space-time near space-like infinity resulting from the inversion (2.2) and the conformal rescaling (2.5). Points close to the origin $x^\mu = 0$ represent points lying at infinity in the original y^μ coordinates.

at a price: the metric (2.3) is singular at the origin, i.e. at the point representing

infinity. Introducing the conformal factor

$$\Omega = -\mathrm{x}_\lambda\,\mathrm{x}^\lambda, \tag{2.4}$$

one can define the regular conformally compactified metric

$$g = \Omega^2\tilde{g} = \eta_{\mu\nu}\,\mathbf{dx}^\mu\,\mathbf{dx}^\nu, \tag{2.5}$$

which, obviously, extends smoothly to the origin $\mathrm{x}^\mu = 0$. The conformal factor (2.4) vanishes there, indicating that the point i^0, located at the origin $\mathrm{x}^\mu = 0$, represents space-like infinity for the physical metric (2.1). In the conformally compactified picture of Minkowski space-time near space-like infinity, illustrated by Fig. 2.1(b), the region outside the cones is conformal to Minkowski space-time, while the interior of the cones consists the embedding space-time.

2.1.2 The cylinder at space-like infinity

Although the metric (2.5) extends smoothly to space-like infinity, reconstructing the Minkowski space-time described by it, from initial data that satisfy the conformal constraints, is not trivial at all as, see sec. 1.6.4, on S some of the initial data exhibit a singular behaviour at the point i that represents space-like infinity. Following the discussion in sec. 1.7, one can render the initial data regular by performing the rescaling (1.106). In this new picture space-like infinity i^0 has a finite representation as a cylinder, see Fig. 2.2.

In accordance with (1.106) the space-time metric (2.5) rescales to

$$\bar{g} = \kappa^{-2}\,g = \kappa^{-2}\,\eta_{\mu\nu}\,\mathbf{dx}^\mu\,\mathbf{dx}^\nu, \tag{2.6}$$

where κ is defined in (1.107). In spherical coordinates (2.6) can be expressed in the form

$$\bar{g} = \kappa^{-2}\left((\mathrm{dx}^0)^2 - \mathrm{d}r^2 - r^2(\mathrm{d}\theta^2 + \sin^2\theta\,\mathrm{d}\phi^2)\right),$$

where $r = \sqrt{\sum_{a=1}^3 (\mathrm{x}^a)^2}$. The introduction of a new time coordinate t through the transformation $\mathrm{x}^0 = \kappa(r)\,t$ brings the above metric into its final spherically symmetric form

$$\bar{g} = \kappa^{-2}\left(\kappa^2 \mathrm{d}t^2 + 2\,t\,\kappa\,\kappa'\mathrm{d}t\,\mathrm{d}r - (1 - t^2\,\kappa'^2)\mathrm{d}r^2 - r^2(\mathrm{d}\theta^2 + \sin^2\theta\,\mathrm{d}\phi^2)\right), \tag{2.7}$$

where with $'$ we denote differentiation with respect to the radial coordinate r. It is noteworthy that the introduction of the rescaling (2.6) while is successfully addressing issues related to the singular behaviour of the initial data, forces us to work with the slightly more complicated spherical symmetric metric (2.7). Of course, as one would expect, in the limit $\kappa = 1$ one recovers the usual Minkowski metric.
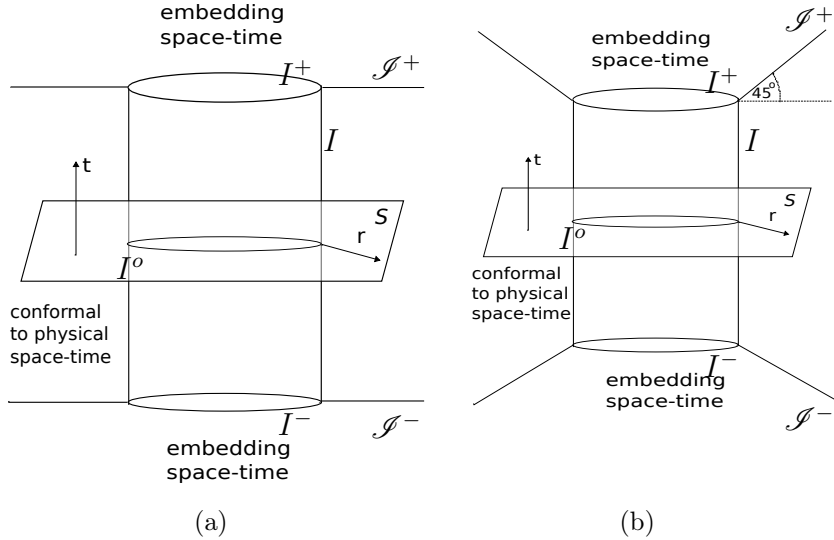

Figure 2.2: The two main finite representations of space-like infinity that are going to be used in the present work. (a) The simplest possible choice $\mu = 1$ leads to a representation where the two branches of null infinity are parallel to each other. (b) For the next simplest choice $\mu = \frac{1}{1+r}$, null infinity forms a 45° "angle" with the horizontal.

Notice that (2.5) and (2.6) imply the relation $\bar{g} = \kappa^{-2} \Omega^2 \tilde{g}$. Thus, by employing the conformal factor

$$\Theta = \kappa^{-1} \Omega,$$

one can conformally compactify (2.1) and, at the same time, introduce the finite representation of space-like infinity. Observing (2.4), the conformal factor Θ can be expressed in terms of the coordinates (t, r) introduced above, i.e.

$$\Theta(t) = \frac{r^2 - \kappa^2 t^2}{\kappa} = \frac{r}{\mu} \left(1 - t^2 \mu^2\right). \tag{2.8}$$

58

This result follows also directly from (1.111), where $\omega = r$ for a conformal factor $\Omega|_{t=0}$ given by (2.4). According to **Definition 1** the conformal factor Θ must vanish at null infinity $\mathscr{I}^\pm$. Thus, the vanishing of (2.8) locates the points lying at null infinity, namely

$$\mathscr{I}^\pm = \{r > 0, \, t = \pm \frac{1}{\mu(r)}\}. \qquad (2.9)$$

In addition, Θ vanishes at the origin $r = 0$ where space-like infinity is situated. Interestingly, at the limit $r \to 0$ future and past null infinity do not meet at the same point as in the conventional picture, see Fig. 2.1(b). They are separated by a finite distance along the time coordinate t. According to (2.9) (or following directly from (1.114)) this distance in our case is $H_{cyl} = 2$. Thus, the finite picture of space-like infinity, which now is represented by the set $I = \{r = 0, -1 < t < 1\}$, follows naturally (see Fig. 2.2). Null-like and space-like infinity meet at the 2-spheres $I^\pm = \{r = 0, t = \pm 1\}$ representing the bases of the cylinder, while the intersection of the initial hypersurface S with I will be denoted as $I^0 = \{r = 0, t = 0\}$.

Obviously, the function μ dictates the shape of the cylindrical structure representing space-like infinity. Thus, through the choice of μ one gains control of the height of the cylinder, of the position of $I^\pm$, of the shape of $\mathscr{I}^\pm$, and even of the "angle" at which null and space-like infinity meet at $I^\pm$. For example, the simplest choice $\mu = 1$ corresponds to the cylinder depicted in Fig. 2.2(a), where I and $\mathscr{I}^\pm$ form a right "angle". Fig. 2.2(b) illustrates the cylindrical structure corresponding to the choice $\mu = (1 + r)^{-1}$. In this representation the location of the points lying at null infinity has a linear dependence on the radial coordinate r, i.e. $t = r + 1$. (Notice that both branches of null infinity form a 45° "angle" with the horizontal.) In general, choosing $\mu = (n\,r + h)^{-1}$ leads to structures with "linear" $\mathscr{I}^\pm$, which meet with I at $I^\pm = \{r = 0, t = \pm h\}$ and form an "angle" $\phi = \arctan n$ with the horizontal. Of course μ can be any function that is regular at the limit $r \to 0$. Hence, we can attach to null infinity almost any shape we want, e.g. the choice $\mu = r^2 + 1$ leads to a null infinity which is "quadratic" in r!

2.2 Spin-2 equation

In this section, and in the rest of this work, the 2-spinor formalism will be employed as it simplifies our arguments and makes the manipulation of the quantities relevant

to our study—which also emerge more naturally in this formalism—easier. In the following the notation and the conventions of the monumental work [65], [66] will be adopted.

2.2.1   Metric, connection, and spin-coefficients

We will start by defining a basis and a connection compatible with (2.7), in the 2-spinor formalism, which will allow us to study, in the subsequent section, the spin-2 equation in the space-time defined by (2.7).

As a first manifestation of the computational power of the 2-spinor formulation, we will begin our treatment of the problem from the most general spherically symmetric metric

$$g = a(t,r)^2 \mathrm{d}t^2 - 2\,c(t,r)\mathrm{d}t\,\mathrm{d}r - b(t,r)^2\mathrm{d}r^2 - g(t,r)^2\,r^2(\mathrm{d}\theta^2 + \sin^2\theta\,\mathrm{d}\phi^2). \quad (2.10)$$

The transition to the specific case (2.7) considered in [36] will be done, subsequently, by taking the appropriate limiting case. (From now on the bar ¯ used to denote quantities living on the rescaled space-time (2.7) will be dropped. Thus, quantities related to the rescaled conformally compactified space-time (2.7) will be denoted without a bar.)

Introducing the spin-frame o^A, ι^A with the usual normalization condition $o_A \iota^A = 1$, one can form a coordinate basis by defining the non-orthonormal null tetrad $(l^\mu, n^\mu, m^\mu, \bar{m}^\mu)$. The metric (2.10) can be always expressed in terms of the null tetrad through the relation

$$g^{\mu\nu} = n^\mu\,l^\nu + l^\mu\,n^\nu - m^\mu\,\bar{m}^\nu - \bar{m}^\mu\,m^\nu.$$

One possible choice, in standard spherical coordinates (t, r, θ, ϕ), that satisfies the above system reads

$$
\begin{aligned}
l^\mu &= \frac{1}{\sqrt{2}}(A, B, 0, 0), \\
n^\mu &= \frac{1}{\sqrt{2}}(C, -B, 0, 0), \\
m^\mu &= \frac{1}{\sqrt{2}\,g\,r}\left(0, 0, 1, -\frac{\mathrm{i}}{\sin\theta}\right), \\
\bar{m}^\mu &= \frac{1}{\sqrt{2}\,g\,r}\left(0, 0, 1, \frac{\mathrm{i}}{\sin\theta}\right),
\end{aligned}
\qquad (2.11)
$$

where the functions $A(t,r), B(t,r)$ and $C(t,r)$ are uniquely defined in terms of the metric coefficients a, b and c, i.e.

$$
\begin{aligned}
A &= \frac{1}{a}\left(1 + \frac{c}{\sqrt{a^2 b^2 + c^2}}\right), \\
B &= \frac{a}{\sqrt{a^2 b^2 + c^2}}, \\
C &= \frac{1}{a}\left(1 - \frac{c}{\sqrt{a^2 b^2 + c^2}}\right).
\end{aligned}
$$

It can be readily confirmed that the null vectors (2.11) satisfy the orthonormality conditions $l^\mu n_\mu = -m^\mu \bar{m}_\mu = 1$—the other scalar products of (2.11) vanish.

The *intrinsic derivatives* follow naturally from (2.11)

$$
\begin{aligned}
D &= l^\mu \partial_\mu = \frac{1}{\sqrt{2}}\left(A\,\partial_t + B\,\partial_r\right), \\
D' &= n^\mu \partial_\mu = \frac{1}{\sqrt{2}}\left(C\,\partial_t - B\,\partial_r\right), \\
\delta &= m^\mu \partial_\mu = \frac{1}{\sqrt{2}\,g\,r}\left(\partial_\theta - \frac{i}{\sin\theta}\,\partial_\phi\right), \\
\delta' &= \bar{m}^\mu \partial_\mu = \frac{1}{\sqrt{2}\,g\,r}\left(\partial_\theta + \frac{i}{\sin\theta}\,\partial_\phi\right).
\end{aligned}
\tag{2.12}
$$

The derivative operators (2.12) are directional derivatives along the null vectors l^μ, n^μ, m^μ, and $\bar{m}^\mu$, respectively. Applying the commutation relations between the intrinsic derivatives (2.12)

$$
\begin{aligned}
[D', D] &= (\gamma + \bar{\gamma})D + (\epsilon + \bar{\epsilon})D' - (\tau - \bar{\tau}')\delta' + (\tau' - \bar{\tau})\delta, \\
[\delta, D] &= (\beta + \bar{\alpha} + \bar{\tau}')D + \kappa D' - \sigma\delta' - (\epsilon - \bar{\epsilon} + \bar{\rho})\delta, \\
[\delta, D'] &= \bar{\kappa}'D - (\bar{\alpha} + \beta - \tau)D' - \bar{\sigma}'\delta' - (\gamma - \bar{\gamma} + \rho')\delta, \\
[\delta', \delta] &= (\rho' - \bar{\rho}')D - (\rho - \bar{\rho})D' - (\bar{\alpha} - \beta)\delta' + (\alpha - \bar{\beta})\delta,
\end{aligned}
$$

successively on our spherical coordinates (t, r, θ, ϕ), one can compute—after a tedious but straightforward calculation—the *spin-coefficients* corresponding to (2.10) and

61

the specific choice of (2.11), namely

$$\alpha = -\beta = \frac{1}{2\sqrt{2}\,g\,r}\cot\theta,$$

$$\gamma = \frac{D'A - DC}{2(A+C)} + \frac{C}{2\sqrt{2}}\frac{\dot{B}}{B},$$

$$\epsilon = \frac{D'A - DC}{2(A+C)} - \frac{A}{2\sqrt{2}}\frac{\dot{B}}{B}, \tag{2.13}$$

$$\rho = -\frac{D(g\,r)}{g\,r}, \quad \rho' = -\frac{D'(g\,r)}{g\,r},$$

$$\sigma = \tau = \kappa = 0, \quad \sigma' = \tau' = \kappa' = 0.$$

2.2.2 The equation

Having defined a basis, a connection, and spin-coefficients compatible with our spherical symmetric metric (2.10), one can proceed further and decompose the linear 2-spinor counterpart of the Bianchi equation (1.73) in terms of them. Here, as a first step in the study of (1.73) on backgrounds of the form (2.10), we will consider only its linearised form. This choice simplifies our endeavour and at the same time retains most of the more important aspects—like the degeneracy at $I^{\pm}$, see below and also [36], [88]—of the full system (1.73).

Recall [65] that in empty space the linearised rescaled conformal Weyl tensor K_{abcd} can be described in the 2-spinor formalism by a totally symmetric *spin-2 zero-rest-mass* spinor field ϕ_{ABCD}.[2] (Because of its totally symmetric nature the spin-2 zero-rest-mass can be completely specified by its five independent components ϕ_k, where $k = 0, \ldots, 4$.) By definition K_{abcd} shares the same symmetries with the Riemann tensor. Therefore, it satisfies a Bianchi identity of the from (1.6), which in the absence of sources is equivalent to $\nabla_{A'}{}^{A}\phi_{ABCD} = 0$.

Hence, in the 2-spinor formalism, the linearised form of the Bianchi equation (1.73) looks like [65]

$$\nabla_{A'}{}^{A}\phi_{ABCD} = 0, \tag{2.14}$$

where $\nabla_{AA'}$ is the spinor covariant derivative related to (2.10). In the following, we will refer to (2.14) as the *spin-2 equation*. In its component form comprises a system

---

[2]Actually, they are related by the expression $K_{AA'BB'CC'DD'} = \phi_{ABCD}\epsilon_{A'B'}\epsilon_{C'D'} + \bar{\phi}_{A'B'C'D'}\epsilon_{AB}\epsilon_{CD}$.

of eight equations. In order to recover them we have, somehow, to decompose (2.14) in its components. One possible way to do that is by expressing $\nabla_{AA'}$ in terms of the weighted differential operators $\eth$ and $\thorn$ of the GHP (Geroch-Held-Penrose) formalism. For this we will employ, as in [65], the $\{0,0\}$-operator[3]

$$\Theta_{AA'} \equiv \nabla_{AA'} - p\,\iota^B\,\nabla_{AA'}o_B - q\,\iota^{B'}\,\nabla_{AA'}o_{B'}, \tag{2.15}$$

where as usual

$$D \equiv \nabla_{00'}, \quad D' \equiv \nabla_{11'}, \quad \delta \equiv \nabla_{01'}, \quad \delta' \equiv \nabla_{10'}$$

are the intrinsic (directional) derivatives (2.12). Transvecting consecutively (2.15) with $o^A o^{A'}$, $\iota^A \iota^{A'}$, $o^A \iota^{A'}$, and $\iota^A o^{A'}$ one gets

$$\thorn \equiv \Theta_{00'}, \quad \thorn' \equiv \Theta_{11'}, \quad \eth \equiv \Theta_{01'}, \quad \eth' \equiv \Theta_{10'},$$

with

$$\begin{aligned}
\thorn\,\eta &\equiv (D + p\,\gamma' + q\,\bar{\gamma}')\eta, \quad \thorn'\eta \equiv (D' - p\,\gamma - q\,\bar{\gamma})\eta, \\
\eth\,\eta &\equiv (\delta - p\,\beta + q\,\bar{\beta}')\eta, \quad \eth'\eta \equiv (\delta' + p\,\beta' - q\,\bar{\beta})\eta
\end{aligned} \tag{2.16}$$

when acting on $\{p,q\}$-scalar quantities η. Now, the $\{0,0\}$-operator $\Theta_{AA'}$ can be decomposed in terms of its components as follows

$$\Theta_{AA'} \equiv \iota_A\,\iota_{A'}\thorn + o_A\,o_{A'}\thorn' - \iota_A\,o_{A'}\eth - o_A\,\iota_{A'}\eth'.$$

It is apparent from (2.15) that for $\{0,0\}$-quantities (like the spin-2 field ϕ_{ABCD}) the covariant derivative and the operator $\Theta_{AA'}$ coincide. Thus, one is allowed to write

$$\nabla_{AA'} \equiv \iota_A\,\iota_{A'}\thorn + o_A\,o_{A'}\thorn' - \iota_A\,o_{A'}\eth - o_A\,\iota_{A'}\eth'. \tag{2.17}$$

Acting with (2.17) on ϕ_{ABCD} one, obviously, gets

$$0 = \iota^A\,\iota_{A'}\thorn\,\phi_{ABCD} + o^A\,o_{A'}\thorn'\phi_{ABCD} - \iota^A\,o_{A'}\eth\,\phi_{ABCD} - o^A\,\iota_{A'}\eth'\phi_{ABCD}. \tag{2.18}$$

Expanding the spin-2 field in (2.18) in terms of its components

$$\begin{aligned}
\phi_{ABCD} &\equiv \iota_{(A}\iota_B\iota_C\iota_{D)}\phi_0 - 4\,\iota_{(A}\iota_B\iota_C o_{D)}\phi_1 + \\
&\quad + 6\,\iota_{(A}\iota_B o_C o_{D)}\phi_2 - 4\,\iota_{(A}o_B o_C o_{D)}\phi_3 + o_{(A}o_B o_C o_{D)}\phi_4,
\end{aligned}$$

---

[3]The real integers p and q describe how scalar quantities transform under spin-boost transformations—for more details consult [65], [60]. To any $\{p,q\}$-scalar quantity we can assign a spin-weight $s = \frac{p-q}{2}$ and a boost-weight $w = \frac{p+q}{2}$.

where the usual definition for spin-2 field's components has been employed

$$\phi_0 \equiv o^A o^B o^C o^D \phi_{ABCD}, \quad \phi_1 \equiv \iota^A o^B o^C o^D \phi_{ABCD}, \quad \phi_2 \equiv \iota^A \iota^B o^C o^D \phi_{ABCD},$$
$$\phi_3 \equiv \iota^A \iota^B \iota^C o^D \phi_{ABCD}, \quad \phi_4 \equiv \iota^A \iota^B \iota^C \iota^D \phi_{ABCD},$$

and taking the components of the resulting expression, we end up with a system of eight equations for the five independent components of the spin-2 zero-rest-mass field ϕ_{ABCD}. Thus, we get[4]

$$\flat \phi_1 - \eth' \phi_0 = -\tau' \phi_0 - 3\kappa \phi_2 + 4\rho \phi_1,$$
$$\flat \phi_2 - \eth' \phi_1 = -2\tau' \phi_1 - 2\kappa \phi_3 + \sigma' \phi_0 + 3\rho \phi_2,$$
$$\flat \phi_3 - \eth' \phi_2 = -3\tau' \phi_2 - \kappa \phi_4 + 2\sigma' \phi_1 + 2\rho \phi_3,$$
$$\flat \phi_4 - \eth' \phi_3 = -4\tau' \phi_3 + 3\sigma' \phi_2 + \rho \phi_4,$$

and their primed versions

$$\flat' \phi_3 - \eth \phi_4 = -\tau \phi_4 - 3\kappa' \phi_2 + 4\rho' \phi_3,$$
$$\flat' \phi_2 - \eth \phi_3 = -2\tau \phi_3 - 2\kappa' \phi_1 + \sigma \phi_4 + 3\rho' \phi_2,$$
$$\flat' \phi_1 - \eth \phi_2 = -3\tau \phi_2 - \kappa' \phi_0 + 2\sigma \phi_3 + 2\rho' \phi_1,$$
$$\flat' \phi_0 - \eth \phi_1 = -4\tau \phi_1 + 3\sigma \phi_2 + \rho' \phi_0.$$

Observing (2.13) most of the spin-coefficients in the above equations drop out; thus, their expression simplifies considerably

$$
\begin{aligned}
&\flat \phi_1 - \eth' \phi_0 = 4\rho \phi_1, && \flat' \phi_3 - \eth \phi_4 = 4\rho' \phi_3,\\
&\flat \phi_2 - \eth' \phi_1 = 3\rho \phi_2, && \flat' \phi_2 - \eth \phi_3 = 3\rho' \phi_2,\\
&\flat \phi_3 - \eth' \phi_2 = 2\rho \phi_3, && \flat' \phi_1 - \eth \phi_2 = 2\rho' \phi_1,\\
&\flat \phi_4 - \eth' \phi_3 = \rho \phi_4, && \flat' \phi_0 - \eth \phi_1 = \rho' \phi_0.
\end{aligned}
\tag{2.19}
$$

In order to obtain a coordinate representation of (2.19), we have, firstly, to express the weighted derivatives appearing therein in terms of the coordinate derivatives defined by (2.11). The expressions (2.16) relating the weighted with the in-

---

[4]The action of the weighted derivatives $\eth$ and $\flat$ on the spin dyad o^A, ι^A was also extensively used in the derivation of the subsequent equations. The explicit formulae can be found in p. 257 of [65].

trinsic derivatives together with (2.12) can be used to establish a coordinate representation of the action of the weighted derivatives on $\{p, q\}$-scalars η

$$\text{þ}\,\eta = \frac{1}{\sqrt{2}}\left(A\,\partial_t + B\,\partial_r - 2\sqrt{2}\,w\,\epsilon\right)\eta,$$

$$\text{þ}'\eta = \frac{1}{\sqrt{2}}\left(C\,\partial_t - B\,\partial_r - 2\sqrt{2}\,w\,\gamma\right)\eta, \tag{2.20}$$

$$\text{ð}\,\eta = \frac{1}{\sqrt{2}\,g\,r}\,\text{ð}_{ang}\,\eta, \quad \text{ð}'\eta = \frac{1}{\sqrt{2}\,g\,r}\,\text{ð}'_{ang}\,\eta,$$

where the purely angular dependent part of ð and $\text{ð}'$ is denoted

$$\text{ð}_{ang} \equiv \partial_\theta - \frac{\mathrm{i}}{\sin\theta}\,\partial_\phi - s\cot\theta, \quad \text{ð}'_{ang} \equiv \partial_\theta + \frac{\mathrm{i}}{\sin\theta}\,\partial_\phi + w\cot\theta \tag{2.21}$$

and $s = \frac{p-q}{2}$, $w = \frac{p+q}{2}$. Keeping in mind that the components ϕ_k of the spin-2 zero-rest-mass field are

$$\{4 - 2k, 0\}\text{-scalars}, \tag{2.22}$$

one can, with the help of (2.20), bring the system (2.19) into the form

$$A\,\partial_t\phi_1 + B\,\partial_r\phi_1 - 2\sqrt{2}\,\epsilon\,\phi_1 - 4\sqrt{2}\,\rho\,\phi_1 = \text{ð}'\phi_0,$$
$$A\,\partial_t\phi_2 + B\,\partial_r\phi_2 - 3\sqrt{2}\,\rho\,\phi_2 = \text{ð}'\phi_1,$$
$$A\,\partial_t\phi_3 + B\,\partial_r\phi_3 + 2\sqrt{2}\,\epsilon\,\phi_3 - 2\sqrt{2}\,\rho\,\phi_3 = \text{ð}'\phi_2,$$
$$A\,\partial_t\phi_4 + B\,\partial_r\phi_4 + 4\sqrt{2}\,\epsilon\,\phi_4 - \sqrt{2}\,\rho\,\phi_4 = \text{ð}'\phi_3,$$
$$C\,\partial_t\phi_3 - B\,\partial_r\phi_3 + 2\sqrt{2}\,\gamma\,\phi_3 - 4\sqrt{2}\,\rho'\phi_3 = \text{ð}\,\phi_4, \tag{2.23}$$
$$C\,\partial_t\phi_2 - B\,\partial_r\phi_2 - 3\sqrt{2}\,\rho'\phi_2 = \text{ð}\,\phi_3,$$
$$C\,\partial_t\phi_1 - B\,\partial_r\phi_1 - 2\sqrt{2}\,\gamma\,\phi_1 - 2\sqrt{2}\,\rho'\phi_1 = \text{ð}\,\phi_2,$$
$$C\,\partial_t\phi_0 - B\,\partial_r\phi_0 - 4\sqrt{2}\,\gamma\,\phi_0 - \sqrt{2}\,\rho'\phi_0 = \text{ð}\,\phi_1.$$

The above system is the component decomposition of (2.14) in a spherical symmetric space-time described by (2.10).

2.2.3 Expansion in spin-weighted spherical harmonics

We can further simplify the equations by making use of the fact that spin-weighted functions, like ϕ_k, can be expanded on the unit sphere as a sum of spin-weighted

spherical harmonics. But, before doing that, we have to express the $\eth$ and $\eth'$ operators in terms of their counterparts on the unit sphere. Observing (2.20), this can be done through the transition

$$\eth \mapsto \frac{1}{\sqrt{2}\,g\,r}\,\eth_{ang}, \quad \eth' \mapsto \frac{1}{\sqrt{2}\,g\,r}\,\eth'_{ang},$$

where, for the sake of simplicity, we will, from now on, denote $\eth_{ang} \equiv \eth$ and $\eth'_{ang} \equiv \eth'$. Now, we can take advantage of the spherical symmetric nature of the background metric (2.10) and expand the components of the spin-2 zero-rest-mass field ϕ_k as a sum of spin-weighted spherical harmonics $_s\Upsilon_{lm}$ in the following way

$$\phi_k(t,r,\theta,\phi) = \sum_{lm} \phi_k^{lm}(t,r)\,_{2-k}\Upsilon_{lm}(\theta,\phi), \tag{2.24}$$

where $s = 2 - k$ is the spin-weight and the quantities s, l, m satisfy the inequalities $|s| \leq l$ and $|m| \leq l$. The "new" unit sphere operators $\eth$ and $\eth'$ defined above can be removed from the system (2.23) as their action on the spin-weighted spherical harmonics $_s\Upsilon_{lm}$ raises or lowers, respectively, the spin-weight [85]

$$\begin{aligned}
\eth(_s\Upsilon_{lm}) &= -\sqrt{l(l+1) - s(s+1)}\,_{s+1}\Upsilon_{lm}, \\
\eth'(_s\Upsilon_{lm}) &= \sqrt{l(l+1) - s(s-1)}\,_{s-1}\Upsilon_{lm}.
\end{aligned} \tag{2.25}$$

Implementing (2.25) into (2.23), we obtain a system of 1+1 dimensional PDEs for any admissible pair (l,m):

$$\begin{aligned}
A\,\partial_t\phi_1^{lm} + B\,\partial_r\phi_1^{lm} - 2\sqrt{2}\,\epsilon\,\phi_1^{lm} - 4\sqrt{2}\,\rho\,\phi_1^{lm} &= \frac{\alpha_2}{rg}\,\phi_0^{lm}, \\
A\,\partial_t\phi_2^{lm} + B\,\partial_r\phi_2^{lm} - 3\sqrt{2}\,\rho\,\phi_2^{lm} &= \frac{\alpha_0}{rg}\,\phi_1^{lm}, \\
A\,\partial_t\phi_3^{lm} + B\,\partial_r\phi_3^{lm} + 2\sqrt{2}\,\epsilon\,\phi_3^{lm} - 2\sqrt{2}\,\rho\,\phi_3^{lm} &= \frac{\alpha_0}{rg}\,\phi_2^{lm}, \\
A\,\partial_t\phi_4^{lm} + B\,\partial_r\phi_4^{lm} + 4\sqrt{2}\,\epsilon\,\phi_4^{lm} - \sqrt{2}\,\rho\,\phi_4^{lm} &= \frac{\alpha_2}{rg}\,\phi_3^{lm}, \\
C\,\partial_t\phi_3^{lm} - B\,\partial_r\phi_3^{lm} + 2\sqrt{2}\,\gamma\,\phi_3^{lm} - 4\sqrt{2}\,\rho'\phi_3^{lm} &= -\frac{\alpha_2}{rg}\,\phi_4^{lm}, \\
C\,\partial_t\phi_2^{lm} - B\,\partial_r\phi_2^{lm} - 3\sqrt{2}\,\rho'\phi_2^{lm} &= -\frac{\alpha_0}{rg}\,\phi_3^{lm}, \\
C\,\partial_t\phi_1^{lm} - B\,\partial_r\phi_1^{lm} - 2\sqrt{2}\,\gamma\,\phi_1^{lm} - 2\sqrt{2}\,\rho'\phi_1^{lm} &= -\frac{\alpha_0}{rg}\,\phi_2^{lm}, \\
C\,\partial_t\phi_0^{lm} - B\,\partial_r\phi_0^{lm} - 4\sqrt{2}\,\gamma\,\phi_0^{lm} - \sqrt{2}\,\rho'\phi_0^{lm} &= -\frac{\alpha_2}{rg}\,\phi_1^{lm},
\end{aligned} \tag{2.26}$$

where we denote $\alpha_x = \sqrt{l(l+1) - x}$. In the following, when we refer to (2.26), the indices l, m will be dropped from the displayed expressions, namely we will denote $\phi_k^{lm} \equiv \phi_k$.

2.3 The spin-2 equation in the F-gauge

The reduction of our results in the preceding section to the F(riedrich)-gauge described by (2.7) readily follows from the identification

$$A = 1 - t\kappa', \qquad B = \kappa, \qquad C = 1 + t\kappa', \qquad g = \frac{1}{\kappa}. \tag{2.27}$$

A direct comparison of (2.7) with (2.10) naturally leads to the above reduction formulae. For the specific choice (2.27) the non-vanishing spin-coefficients (2.13) become

$$
\begin{aligned}
\alpha &= -\beta = \frac{\mu}{2\sqrt{2}} \cot\theta, \\
\gamma &= \epsilon = -\frac{1}{2\sqrt{2}} \kappa', \\
\rho &= -\rho' = \frac{1}{\sqrt{2}} r\mu'.
\end{aligned}
\tag{2.28}
$$

Therefore, inserting (2.27) and (2.28) into the system (2.26), we recover a component decomposition of the spin-2 equation (2.14) on a spherical symmetric background (2.7), i.e.

$$
\begin{aligned}
(1 - t\,\kappa')\,\partial_t\phi_1 + \kappa\,\partial_r\phi_1 &= (3\kappa' - 4\mu)\,\phi_1 + \mu\,\alpha_2\,\phi_0, \\
(1 - t\,\kappa')\,\partial_t\phi_2 + \kappa\,\partial_r\phi_2 &= (3\kappa' - 3\mu)\,\phi_2 + \mu\,\alpha_0\,\phi_1, \\
(1 - t\,\kappa')\,\partial_t\phi_3 + \kappa\,\partial_r\phi_3 &= (3\kappa' - 2\mu)\,\phi_3 + \mu\,\alpha_0\,\phi_2, \\
(1 - t\,\kappa')\,\partial_t\phi_4 + \kappa\,\partial_r\phi_4 &= (3\kappa' - \mu)\,\phi_4 + \mu\,\alpha_2\,\phi_3, \\
(1 + t\,\kappa')\,\partial_t\phi_3 - \kappa\,\partial_r\phi_3 &= -(3\kappa' - 4\mu)\,\phi_3 - \mu\,\alpha_2\,\phi_4, \\
(1 + t\,\kappa')\,\partial_t\phi_2 - \kappa\,\partial_r\phi_2 &= -(3\kappa' - 3\mu)\,\phi_2 - \mu\,\alpha_0\,\phi_3, \\
(1 + t\,\kappa')\,\partial_t\phi_1 - \kappa\,\partial_r\phi_1 &= -(3\kappa' - 2\mu)\,\phi_1 - \mu\,\alpha_0\,\phi_2, \\
(1 + t\,\kappa')\,\partial_t\phi_0 - \kappa\,\partial_r\phi_0 &= -(3\kappa' - \mu)\,\phi_0 - \mu\,\alpha_2\,\phi_1.
\end{aligned}
\tag{2.29}
$$

The system (2.29) of advection equations can be split into five *evolution equations*

$$(1 + t\kappa') \partial_t \phi_0 = \kappa \partial_r \phi_0 - (3\kappa' - \mu) \phi_0 - \alpha_2 \mu \phi_1,$$

$$\partial_t \phi_1 = \frac{1}{2} \alpha_2 \mu \phi_0 - \frac{1}{2} \alpha_0 \mu \phi_2 - \mu \phi_1,$$

$$\partial_t \phi_2 = \frac{1}{2} \alpha_0 \mu \phi_1 - \frac{1}{2} \alpha_0 \mu \phi_3, \qquad (2.30)$$

$$\partial_t \phi_3 = \frac{1}{2} \alpha_0 \mu \phi_2 - \frac{1}{2} \alpha_2 \mu \phi_4 + \mu \phi_3,$$

$$(1 - t\kappa') \partial_t \phi_4 = -\kappa \partial_r \phi_4 + (3\kappa' - \mu) \phi_4 + \alpha_2 \mu \phi_3$$

governing the dynamical evolution and three *constraint equations*

$$2\kappa \partial_r \phi_1 = 6 r\mu' \phi_1 - 2 t \kappa' \mu \phi_1 + \alpha_0 \mu (1 - t\kappa') \phi_2 + \alpha_2 \mu (1 + t\kappa') \phi_0,$$

$$2\kappa \partial_r \phi_2 = 6 r\mu' \phi_2 + \alpha_0 \mu (1 - t\kappa') \phi_3 + \alpha_0 \mu (1 + t\kappa') \phi_1, \qquad (2.31)$$

$$2\kappa \partial_r \phi_3 = 6 r\mu' \phi_3 + 2 t \kappa' \mu \phi_3 + \alpha_0 \mu (1 + t\kappa') \phi_2 + \alpha_2 \mu (1 - t\kappa') \phi_4$$

specifying the constraints. Thus, our initial data must satisfy (2.31) and will be evolved with (2.30). Notice that the evolution system (2.30) acquires a very simple form on the cylinder I (i.e. at $r = 0$). The radial derivatives drop out from the equations controlling the dynamics of the components ϕ_0, ϕ_4 and, thus, the cylinder becomes a total characteristic of the system (2.30). Analytically [33], Friedrich predicted that the resulting intrinsic system will generate logarithmic singularities at the interface of the cylinder with null infinity, i.e. at $I^{\pm}$, where the hyperbolicity of the equations break down (see next paragraph below). In sec. 3.6, the numerical behaviour of the intrinsic evolution system will be intensively studied and our finding will be compared to the analytical results in [33].

As it has been already mentioned in sec. 1.5, the evolution equations can be written in the form of a boundary adapted evolution system

$$(I + A^0) \partial_t \phi + A^1 \partial_r \phi = B \phi,$$

where $\phi \equiv (\phi_0, \phi_1, \phi_2, \phi_3, \phi_4)^T$, I is the 5×5 identity matrix and

$$A^0 = \mathrm{diag}(t\kappa', 0, 0, 0, -t\kappa'),$$
$$A^1 = \mathrm{diag}(-\kappa, 0, 0, 0, \kappa),$$
$$B = \begin{pmatrix} -3\kappa' + \mu & -\alpha_2\,\mu & 0 & 0 & 0 \\ \frac{1}{2}\,\alpha_2\,\mu & -\mu & -\frac{1}{2}\,\alpha_0\,\mu & 0 & 0 \\ 0 & \frac{1}{2}\,\alpha_0\,\mu & 0 & -\frac{1}{2}\,\alpha_0\,\mu & 0 \\ 0 & 0 & \frac{1}{2}\,\alpha_0\,\mu & \mu & -\frac{1}{2}\,\alpha_2\,\mu \\ 0 & 0 & 0 & \alpha_2\,\mu & 3\kappa' - \mu \end{pmatrix}.$$

The matrices A^0, A^1 are obviously Hermitian. Hence, the evolution system (2.30) is symmetric hyperbolic in the range $|t| < \kappa'^{-1}$, i.e. when $I + A^0$ is positive definite.

2.4   Subsidiary system

The constraints (2.31) are preserved when Cauchy data are evolved by the evolution system (2.30). To prove this assertion, the system (2.31) must be brought in the most convenient form

$$C_1 = 2\,\kappa\,\partial_r\phi_1 - 6\,r\mu'\phi_1 + 2\,t\,\kappa'\mu\,\phi_1 - \alpha_0\,\mu\,(1 - t\kappa')\,\phi_2 - \alpha_2\,\mu\,(1 + t\kappa')\,\phi_0 = 0,$$
$$C_2 = 2\,\kappa\,\partial_r\phi_2 - 6\,r\mu'\phi_2 - \alpha_0\,\mu\,(1 - t\kappa')\,\phi_3 - \alpha_0\,\mu\,(1 + t\kappa')\,\phi_1 = 0,$$
$$C_3 = 2\,\kappa\,\partial_r\phi_3 - 6\,r\mu'\phi_3 - 2\,t\,\kappa'\mu\,\phi_3 - \alpha_0\,\mu\,(1 + t\kappa')\,\phi_2 - \alpha_2\,\mu\,(1 - t\kappa')\,\phi_4 = 0.$$
$$(2.32)$$

It can be straightforwardly shown that by taking the temporal derivative of the zero valued quantities (2.32) and using (2.30), (2.31) to replace the resulting time and spatial derivatives of the components ϕ_k appearing therein, one obtains the so-called *subsidiary system* for the propagation of the constraints

$$\partial_t C_1 = -\mu\,C_1 - \frac{1}{2}\,\alpha_0\,\mu\,C_2,$$
$$\partial_t C_2 = \frac{1}{2}\,\alpha_0\,\mu\,(C_1 - C_3), \qquad\qquad (2.33)$$
$$\partial_t C_3 = \mu\,C_3 + \frac{1}{2}\,\alpha_0\,\mu\,C_2.$$

The above system can be written in a more compact form that reveals its symmetric hyperbolic nature, i.e.

$$\partial_t C = A\,C,$$

where $C = (C_1, C_2, C_3)^T$ and

$$A = \mu \begin{pmatrix} -1 & -\frac{\alpha_0}{2} & 0 \\ \frac{\alpha_0}{2} & 0 & -\frac{\alpha_0}{2} \\ 0 & \frac{\alpha_0}{2} & 1 \end{pmatrix}.$$

In addition, the eigenvalues

$$\lambda_1 = 0, \quad \lambda_2 = \frac{\mathrm{i}\,\alpha_2\,\mu}{\sqrt{2}}, \quad \lambda_3 = -\frac{\mathrm{i}\,\alpha_2\,\mu}{\sqrt{2}}$$

of the matrix A entail that even when the initial data do not satisfy exactly the constraints (2.31)—a quite common feature of any numerical simulation—the values of the constraint quantities C_1, C_2, C_3 exhibit an oscillatory behaviour, i.e. they do not diverge during their evolution.

2.5 Characteristic curves

It will be extremely useful in the following to study the behaviour of the characteristic curves of the evolution system (2.30). The hyperbolic system (2.30) has three kinds of characteristic curves. Obviously, the simplest one is the one related to the dynamics of ϕ_1, ϕ_2, and ϕ_3, i.e. the trivial characteristic curve $r = \text{const}$. The form of the characteristic curves for the other two equations governing the temporal evolution of the fields ϕ_0, ϕ_4 can be deduced solely from the coefficients of their principal parts [45].[5] Thus, the slope of the characteristics for the field ϕ_0 and ϕ_4 is given by

$$\frac{dt}{dr} = -\frac{1 + t\kappa'}{\kappa} \quad \text{and} \quad \frac{dt}{dr} = \frac{1 - t\kappa'}{\kappa},$$

respectively. As expected—see the discussion in sec 2.1.2—the behaviour of the above characteristics depends entirely on the choice of the function μ. Recall that the choice $\mu = 1$ leads to the representation depicted in Fig. 2.2(a); the corresponding characteristic curves can be found in Fig. 2.3. In Fig. 2.2(b) future and past null infinity $\mathscr{I}^\pm$ form an 45° "angle" with the cylinder I representing space-like infinity. In this representation μ is chosen as $\mu = (1 + r)^{-1}$; Fig. 2.4 depicts the resulting

---

[5]For first order PDEs with principal part of the form $a(t, r)\,\partial_t u(t, r) + b(t, r)\,\partial_r u(t, r)$, the slope of the characteristic curves is given by $dt/dr = a/b$.
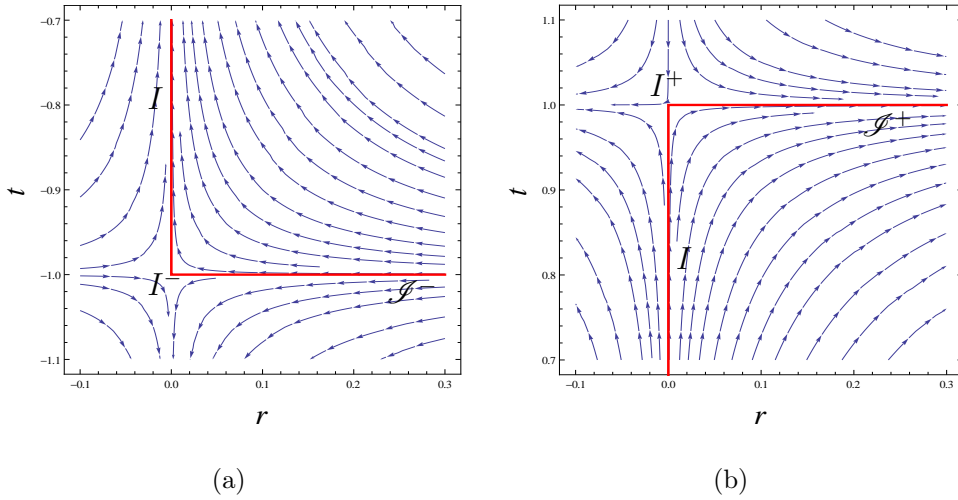
(a)   (b)

Figure 2.3: Characteristic curves of the evolution equations, where μ has been chosen $\mu = 1$. The red line denotes the cylinder, future and past null infinity $\mathscr{I}^{\pm}$. (a) Characteristic curves of the field ϕ_0 with slope $\dfrac{dt}{dr} = -\dfrac{1+t}{r}$ in a neighbourhood of I^-. (b) Characteristic curves of the field ϕ_4 with slope $\dfrac{dt}{dr} = \dfrac{1-t}{r}$ in a neighbourhood of I^+.

characteristic curves. Notice that in both representations the situation is not symmetric around the r-axis. In the neighbourhoods of space-like infinity that are not depicted in the Figs. 2.3 and 2.4, the characteristic curves behave in more or less the same way: they tend to become parallel to the cylinder, i.e. vertical.

The shape of the characteristic curves, for both representations considered above, shows clearly that the cylinder I is a *total characteristic* of our system. This information is extremely useful as we do not have to worry about prescribing boundary conditions for the points lying at the origin ($r = 0$) of our computational domain. It is also apparent that the domain of hyperbolicity of our system coincides with the physically interesting parts of the finite representation of space-like infinity, i.e. those parts that are conformal to the physical space-time. Hence, if we restrict ourselves to the region where $r > 0$, the hyperbolicity is guaranteed. If the left boundary of the computational domain is on the cylinder ($r = 0$) we can proceed until I^+, but not beyond as we will cross through the region of non-hyperbolicity. Setting an initial boundary value problem in the region $r < 0$, although our sys-

71
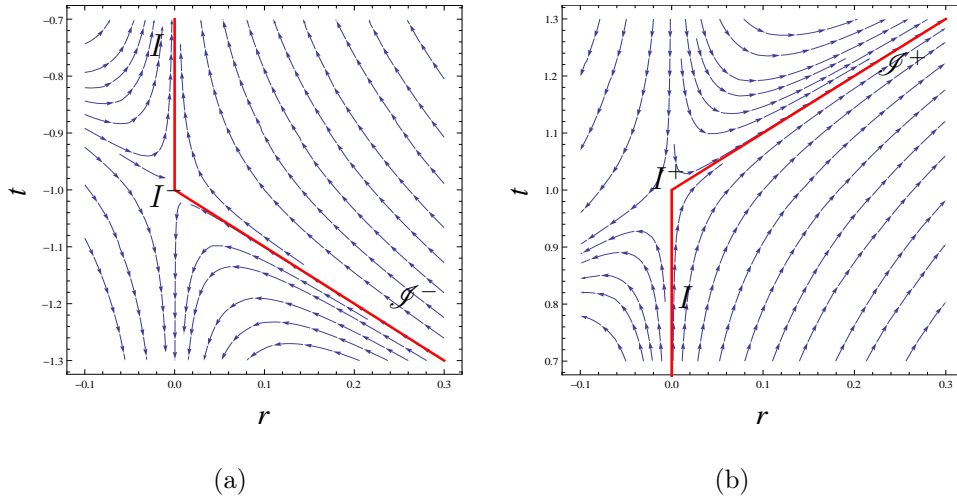
Figure 2.4: Characteristic curves for $\mu = (1 + r)^{-1}$. The red line denotes the cylinder and $\mathscr{I}^{\pm}$. (a) Characteristic curves of the field ϕ_0 with slope $\dfrac{dt}{dr} = -\dfrac{1 + tk'}{k}$ in a neighbourhood of I^-. (b) Characteristic curves of the field ϕ_4 with slope $\dfrac{dt}{dr} = \dfrac{1 - tk'}{k}$ in a neighbourhood of I^+.

tem is piecewise hyperbolic there, is an extremely complicated procedure, which, in one sense, does not worth the effort as the resulting behaviour would not have any physical interest—recall that the inside of the cylinder is part of the embedding space-time and, thus, is not conformally related to the physical space-time we want to study.

Chapter 3

Numerical analysis of the spin-2 system

3.1 Numerical preliminaries

Our objective in the present chapter is the numerical simulation of the Cauchy problem posed by the spin-2 system (2.30)-(2.31). Thus, on a given initial hypersurface, we have to prescribe data that respect the constraints (2.31) and, subsequently, evolve them with (2.30) in such a way that the constraints are preserved during the evolution. Obviously, (2.30)-(2.31) is a $1 + 1$ system (one time and one spatial dimension) of partial differential equations. Therefore, the hypersurfaces of constant time are one dimensional.

One possible way to proceed in the discretization of the aforementioned system is in terms of the so-called *method of lines*. Accordingly, the system (2.30)-(2.31) will be reduced to a system of ordinary differential equations by discretizing the spatial coordinate r. There are several ways to perform this reduction [2]. In this work, *finite difference* techniques will be employed to extract a system of ordinary differential equations from (2.30)-(2.31).

The temporal integration of the resulting semi-discrete system will be in general performed with *explicit fourth order Runge-Kutta* schemes. When higher accuracy is required, especially in studies near the problematic region I^+, time step adaptive Runge-Kutta schemes will be employed. These routines adapt the time step to the speed of the characteristic curves. Specifically, in regions where the characteristic

speed is high, e.g. close to I^+ (see Fig. 2.3), the time step is refined, and vice versa.

To begin with, the hypersurfaces of constant time, used to foliate our 1+1 computational space-time, must be discretized. Consider the computational domain $D = [0, 1]$ on each such hypersurface. A finite representation of D can be obtain through the introduction of an equidistant grid $r_i = r_0 + ih$ with $i = 0, \ldots, N$ on D, where $r_0 = 0$ and $r_N = 1$. As usual, the grid is refined when the grid spacing h is reduced; in the limit $h \to 0$ the continuous case is recovered. The components of the spin-2 zero-rest-mass field will be discretized in a similar way, namely $(\phi_k)_i = \phi_k(r_i)$.

Now, after discretizing the computational domain, we have to approximate the spatial derivatives operators appearing in (2.30)-(2.31) with appropriate finite difference operators. There are numerous ways to do that. Here, we will use the so-called *summation by parts* (SBP) operators originally introduced in [50], [51]. This specific type of widely used in numerical relativity, see for example [52], [53], [80], [48], [61], finite difference operators take advantage of the fact that in the continuous case an appropriate use of the integration by parts property leads to energy estimates that guarantee the well-posedness of the continuous problem [42]. The SBP operators provide a discrete version of these continuous energy estimates. On the discrete level, summation by parts, which is the discrete analogue of integration by parts, is used to obtain discrete energy estimates that guarantee the numerical stability of the discrete schemes. In other words, the SBP operators fully mimic the "energy" behaviour of their continuous counterparts. Another very appealing feature of the SBP operators is that although their accuracy near the boundaries is, depending on the details of their construction, one or two orders smaller than the one in the interior of the grid, their overall accuracy is of the same order with the accuracy in the interior!

A point that needs also special attention is the imposition of the boundary condition on the "right" boundary, i.e. $r_N = 1$, of our computational domain—recall that we do not have to impose boundary conditions on the boundary point on the cylinder as the cylinder is a total characteristic of our system. A wrong imposition of the boundary condition would destroy the designed accuracy of the SBP operators and lead to instabilities [9]. A very simple, but highly efficient, *penalty* method—the so-called *simultaneous approximation term* (SAT) method introduced in [9]—preserves the designed accuracy of the SBP operators and guarantees the numerical stability of our schemes. The combination of the SBP operators with the

SAT method seems quite successful [9], [10], [53], [80], [16], [41]. In addition, the imposed boundary function, say $f(t)$, must be compatible with the prescribed initial conditions, say $g(0, r)$, at the "corner" point $(t, r) = (0, 1)$, namely the condition $f(0) = g(0, 1)$ must be satisfied.

Finally, a comment concerning the computation of the convergence rates. In the following, the formula

$$\text{CR} = \frac{\ln\left(\frac{E_0}{E_1}\right)}{\ln\left(\frac{h_0}{h_1}\right)} \tag{3.1}$$

will be used to compute the convergence rates of our numerical simulations. Where E_0 and E_1 are normalised l^2 error norms for simulations of resolution h_0 and h_1, respectively. (Notice that $h_0 < h_1$.) The errors E will be computed against an exact solution or, in case an exact solution is not available, against the numerical simulation with the highest resolution.

3.2   First derivative SBP operators

Here, we will define SBP finite difference operators that can be used to approximate the first spatial derivative appearing in the evolution equations (2.30) of the fields ϕ_0 and ϕ_4. Clearly, they are advection equations with linear source terms. The definition—see **Definition 3** below—of the first derivative SBP operators depends only on the principal part of these equations. Thus, in order to keep our presentation as simple as possible, we will not include source terms in the following derivation of the SBP operators. One can check the validity of the above assertion by just adding in a trivial way a source term to the subsequent derivation.

The equations in question can be sufficiently modeled by the 1-D scalar advection equation

$$u_t = \lambda\, u_r, \quad 0 \le r \le 1, \quad t \ge 0, \tag{3.2}$$

where λ is an arbitrary real number and the subscripts denote differentiation with respect to their argument. (The problem (3.2) will not be supplemented with initial and boundary conditions as they are irrelevant to our purposes in the present section.) Notice that λ is not constant in (2.30), but this again will not affect the requirements of **Definition 3** as similar energy estimates can be obtain in the case

that λ is not constant—see sec. 9.1 of [42]. Therefore, by introducing the notation

$$(u, w) \equiv \int_0^1 u\,w\,\mathrm{d}r,$$

the energy estimate for (3.2) reads

$$\frac{d}{dt}||u||^2 = (u_t, u) + (u, u_t) = \lambda[u(t,1)^2 - u(t,0)^2], \qquad (3.3)$$

where $||u||^2 \equiv (u, u)$ and at the last step (3.2) and integration by parts was used.

In order to acquire a discrete version of (3.3), we have to introduce firstly, in a similar way with above, the discrete notation

$$(v, \mathrm{v})_H \equiv v^T H \mathrm{v},$$

and then define the discrete counterpart of the first derivative appearing in (3.2), i.e.

$$H\frac{du}{dr} = Qu \Rightarrow \frac{du}{dr} = H^{-1}Q\,u.$$

Thus, we can define

$$D_1 = H^{-1}Q. \qquad (3.4)$$

Now, one can write (3.2) in its semi-discrete form

$$v_t = \lambda D_1\,v = \lambda H^{-1}Q\,v, \qquad (3.5)$$

where $v = (v_0, v_1, \ldots, v_{N-1}, v_N)^T$ and H, Q are $N \times N$ matrices. Having in mind that $||v||^2 \equiv (v, v)_H$, one can obtain the discrete version of the continuous energy estimate (3.3):

$$\frac{d}{dt}||v||^2 = \frac{d}{dt}\left(v^T H v\right) = \lambda\,v^T\left(Q^T(H^{-1})^T H + Q\right)v.$$

To mimic the behaviour of the continuous case (3.3), we have to choose H symmetric and $Q^T + Q = \mathrm{diag}(-1, 0, \ldots, 0, 1)$ in the above expression. Hence, the energy estimate becomes

$$\frac{d}{dt}||v||^2 = \lambda(v_N^2 - v_0^2), \qquad (3.6)$$

which obviously replicates (3.3). The last result leads to the definition of a first derivative SBP operator.

Definition 3 *The first order finite difference operator D_1 defined in* (3.4) *is an SBP operator iff*

  i) H is symmetric, i.e. $H = H^T > 0$,

  ii) $Q^T + Q = diag(-1, 0, \ldots, 0, 1)$.

Any difference operator approximating ∂/∂_r and satisfying the requirements of **Definition 3** is a SBP operator that leads to energy estimates (3.6) that guarantee the numerical stability of our scheme. Such kind of operators were originally constructed in [50], [51], and subsequently enriched and refined in [83], [10], [16].

The requirements of **Definition 3** are the minimum requirements that a SBP operator must satisfy. Obviously, the generality of **Definition 3** leaves a lot of freedom in their construction. To restrict this freedom and define them uniquely several optimization criteria were introduced [83], [16]. In the literature, there is a plethora of SBP operators that satisfy different such criteria, which are related either to the form of the norm matrix H, i.e. diagonal, full, restricted full, or to the minimization of the bandwidth, of the spectral radius, of the truncation error on the boundary points, or to combination of these—see [16] for the definition of the various notions.

Unless otherwise stated, in the following we will be using the minimum bandwidth, restricted full norm, fourth order in the interior and third order near the boundaries SBP operator given in [83]. Several other SBP operators from the aforementioned papers have been tried, but our results showed that the above choice has the most stable behaviour and gives the smallest error.

3.3 The SAT method

In order to complete the study of the advection equation (3.2), we have to appropriately prescribe to it boundary and initial conditions. Having in mind that the cylinder is a total characteristic of (2.30), then boundary conditions have to be imposed only on the "right" boundary point at $r_N = 1$. But this means that boundary conditions have to be imposed only on the equation governing the dynamics of ϕ_0, which can be adequately modeled, for our purposes here, by equation (3.2) with a positive λ. Thus, under the assumption $\lambda > 0$, (3.2) will be supplemented by the

Dirichlet boundary condition

$$u(t, 1) = g_N(t) \tag{3.7}$$

and the initial condition $u(0, r) = f(r)$.

There are several ways, more or less successful, to impose the above boundary condition [55]. In this work, the very successful simultaneous approximation term (SAT) penalty method introduced in [9] will be used. With this method the boundary conditions are imposed in such a way that the requirements of **Definition 3** are satisfied—something not as trivial as it sounds, see [9] and [55]—and an energy estimates can be obtained. The SAT method imposes indirectly the boundary condition (3.7) by adding to the SBP derivative operator a term that is proportional to the difference between the actual value v_N at the boundary and the boundary condition (3.7) we want to impose.

Let's see how the SAT method works. In the rest of the present section, we will try to impose the boundary condition (3.7) to (3.2) using the SAT method. With the inclusion of (3.7), the continuous energy estimate (3.3), which we will try to mimic, now reads

$$\frac{d}{dt}||u||^2 = \lambda[g_N(t)^2 - u(t, 0)^2], \tag{3.8}$$

where $\lambda > 0$. In the discrete case, according to [9], [56], we have to add a boundary term to (3.5) in the following fashion

$$v_t = \lambda H^{-1} Q \, v - \tau \lambda H^{-1}(E_N \, v - e_N \, g_N(t)), \tag{3.9}$$

where $E_N = \mathrm{diag}(0, \ldots, 0, 1)$ is a $N \times N$ matrix, $e_N = (0, \ldots, 0, 1)$, and τ is the so-called penalty parameter. Choosing $\tau = 1$, the energy estimate (3.6) now becomes

$$\frac{d}{dt}||v||^2 = \lambda[g_N(t)^2 - v_0^2 - (v_N - g_N(t))^2], \tag{3.10}$$

which, except of the last term, fully mimics (3.8). The extra term in (3.10) is a remnant of the SAT method; it does not affect the energy estimate though as it is always non-positive. Notice that for compactly supported data, i.e. $g_N(t) = 0$, the energy estimate (3.10) holds trivially as the remaining terms are always non-positive.

3.4   The exact solution

In this section our numerical setting together with the performance of the SBP operators and the SAT method will be checked in realistic numerical simulations.

Specifically, we will first try to reproduce the exact solution derived in Appendix A and, subsequently, check if the constraints for this numerical simulation are preserved in time.

3.4.1 Convergence and stability

Here, we will reproduce numerically the exact solution (A.12) of the system (2.30)-(2.31) obtained in Appendix A. For this we have to prescribe on the initial hypersurface (t=0) Cauchy data that respect the constraints (2.31) and subsequently evolve it with (2.30). Recall that the exact solution (A.12) corresponds to the representation of Fig. 2.2(b), where null infinity meets I at an "angle" of 45° degrees.

(a)   (b)
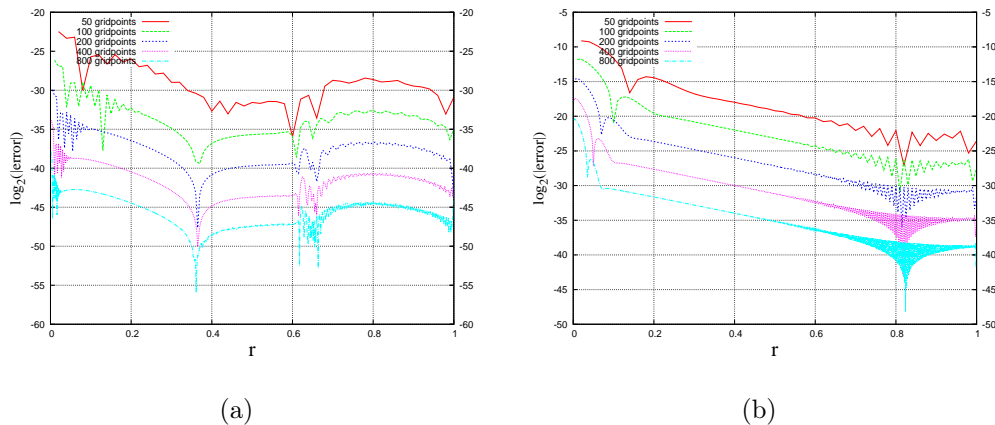
Figure 3.1: The convergence plots of (a) ϕ_0 and (b) ϕ_4 for the evolution of the initial data (3.11) at time $t = 1$. Notice that the maximum of the absolute error between the numerical and the exact solution starts at an order of 10^{-7} and 10^{-3}, respectively, and reduces with fourth order.

The solution (A.12) by its construction satisfies the constraints (2.31). Thus, by setting $t = 0$ in (A.12) one gets appropriate initial data that satisfy initially the constraints, i.e.

$$\phi_0 = \phi_4 = \frac{r^2}{(1+r)^3}, \quad \phi_1 = \phi_3 = \frac{2\,r^2}{(1+r)^3}, \quad \phi_2 = \frac{\sqrt{6}\,r^2}{(1+r)^3}. \tag{3.11}$$

As it has been already mentioned, because of the fact that the cylinder is a total characteristic of our system, see Fig. 2.4, only the right boundary $(r = 1)$ needs

special treatment. Observing (2.30), the inflow boundaries of ϕ_0 and ϕ_4 are at $r = 1$ and $r = 0$, respectively. Thus, we have to impose, implicitly, a boundary condition only on ϕ_0. Therefore, by setting $r = 1$ in (A.12), we obtain the boundary condition

$$g_N(t) = \phi_0(t, 1) = \frac{(2 - t)^4}{128},$$

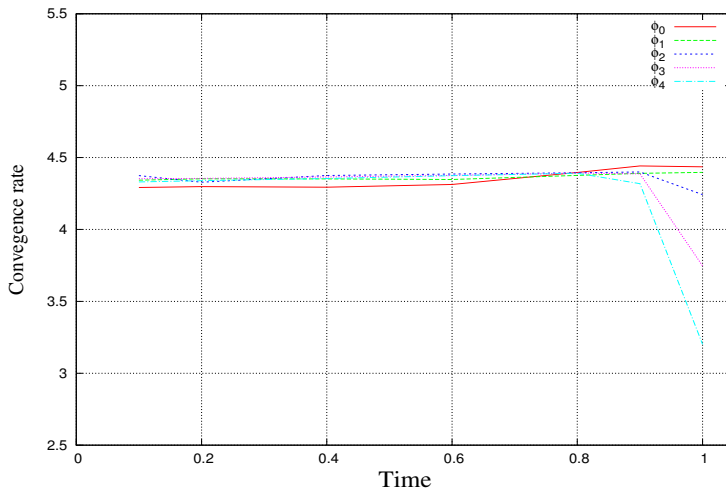which will be imposed through the SAT method. Notice that the above boundary condition is consistent with the choice (3.11) of the initial data at the "corner" point $(t, r) = (0, 1)$.

Figure 3.2: The convergence rates of all the components of the spin-2 zero-rest-mass field for the evolution of the exact initial data (3.11).

Evolving the initial data (3.11) with (2.30), we get the convergence plots for the components ϕ_0 and ϕ_4 at time, say, $t = 1$ depicted in Fig. 3.1. The rest of spin-2 field's components behave in a similar way. From these plots one can safely conclude that our code reproduces the exact solution (A.12)—for a grid of only 50 points (first line on each plot) the maximum of the absolute error between the numerical and the exact data are roughly of the order 10^{-3} or less—and converges. In addition, the behaviour of the actual convergence rates with time is illustrated in Fig. 3.2. It is apparent that during the evolution the convergence rates for all the components of the spin-2 zero-rest-mass field vary between 4 and 4.5. A result that fits quite happily with the fact that the time integration is performed with a fourth order Runge-Kutta method. Notice though that while approaching I^+ the

convergence rates slightly decrease. This most probably happens because of the rapid increase of the characteristic speed in this region, see Fig. 2.4. The high frequency features that appear in Fig. 3.1—the rest of spin-2 field's components exhibit similar behaviour—are most probably numerical artifacts, indicating that the modes hitting the boundaries from inside the grid are reflected due to numerical inaccuracies [5].

From the above results we can safely conclude that i) our code converges with fourth order and reproduces the exact solution (A.12) from the evolution of the initial data (3.11), ii) the SBP operator we chose behaves according to its designed accuracy, iii) the implementation of the SAT method has been done correctly, and iv) imposing the boundary condition with the SAT method indeed preserves the accuracy of the SBP operator.

3.4.2 Conservation of the constraints

Another way to test our code is by checking if the vanishing of the constraint quantities (2.32) is satisfied during the evolution of our system. According to Appendix A the initial data (3.11) satisfy (2.32) analytically. Numerically though is almost im-
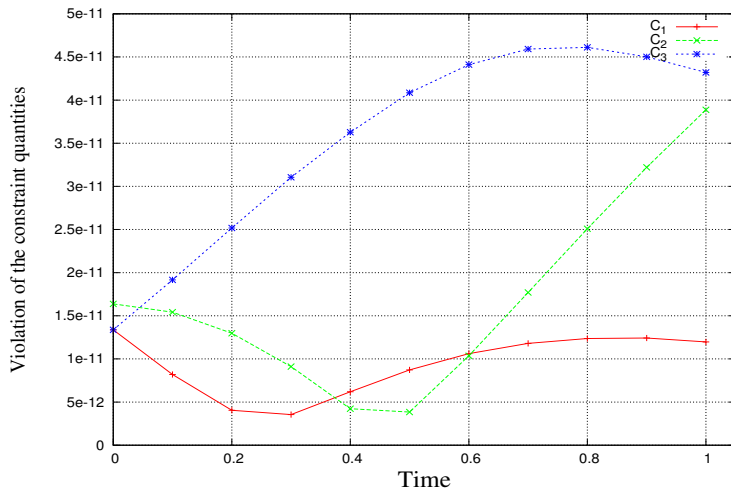
Figure 3.3: Violation of the vanishing of the constraint quantities (2.32) during the evolution of the exact initial data (3.11) for the simulation with 800 grid points. The normalised l^2 is shown.

possible not to violate (2.32) to some order when prescribing the data (3.11) on

the initial hypersurface. We cannot avoid introducing initially some error into our system, thus we have to learn to live with it. What we can do though is to keep it during the evolution at its original levels. In the particular example of sec. 3.4.1, the initial violation of the constraints is of the order of 10^{-11}; thus if it is maintained at these levels during the evolution, then we can say that our code is successfully evolving the constraint quantities C_k. Fig. 3.3 depicts the violation associated with each one of the constraints during the evolution of the initial data (3.11). The violation is still of the same order, i.e. 10^{-11}, thus we can safely conclude that the constraints are preserved during the evolution.

3.5   General Cauchy data

With the confidence of reproducing the exact solution (A.12), we can proceed further in the numerical study of the spin-2 system and evolve initial data that are not exact solutions of the system (2.30)-(2.31). Specifically, we will prescribe on the initial hypersurface data that have to satisfy the conformal constraints (2.31), but not necessarily the evolution equations (2.30). In other words, we will produce numerical solutions of the system (2.30)-(2.31) that cannot be obtain analytically.

In order to do that we have, firstly, to bring the constraints (2.31) in a more manageable form. One way of proceeding is by introducing the transformation $X_i = \mu^{-3}\,\phi_i$ and using the definition $\kappa = r\,\mu(r)$ to obtain the system

$$2\,r\,\partial_r X_1 = -2\,t\,\kappa' X_1 + \alpha_0\,(1 - t\,\kappa')X_2 + \alpha_2\,(1 + t\,\kappa')X_0,$$
$$2\,r\,\partial_r X_2 = \alpha_0\,(1 - t\,\kappa')X_3 + \alpha_0\,(1 + t\,\kappa')X_1,$$
$$2\,r\,\partial_r X_3 = 2\,t\,\kappa' X_3 + \alpha_0\,(1 + t\,\kappa')X_2 + \alpha_2\,(1 - t\,\kappa')X_4,$$

which on the initial hypersurface $t = 0$ reduces to

$$2\,r\,\partial_r X_1 = \alpha_0\,X_2 + \alpha_2\,X_0,$$
$$2\,r\,\partial_r X_2 = \alpha_0\,X_3 + \alpha_0\,X_1, \qquad\qquad (3.12)$$
$$2\,r\,\partial_r X_3 = \alpha_0\,X_2 + \alpha_2\,X_4.$$

Taking advantage of the symmetries of the above system, we will now construct a particular family of solutions of (3.12) in terms of the field X_2 alone. Obviously, (3.12) is a system of three equations with five unknowns, thus one more field must be

explicitly specified in order X_2 to be the only free function in (3.12). Here, inspired by the symmetries of (3.12), it will be assumed that $X_1 = X_3$ and, consequently, $X_0 = X_4$. These choices bring the above system into the form

$$X_0 = X_4 = \frac{-\alpha_0^2 X_2 + 2\, r\, \partial_r X_2 + 2\, r^2\, \partial_{rr} X_2}{\alpha_0\, \alpha_2}, \quad X_1 = X_3 = \frac{r\, \partial_r X_2}{\alpha_0}, \qquad (3.13)$$

where $\alpha_x = \sqrt{l(l+1) - x}$. The field X_2—and consequently ϕ_2—in the above expressions is completely arbitrary and to our disposal. Hence, after specifying explicitly the field X_2, the system (3.13) allows us to compute algebraically the rest of X's components. Then, by choosing the form of μ, i.e. the representation of the cylinder one would like to work with, the actual form of the components of the spin-2 zero-rest-mass field can be recovered through the transformation $X_i = \mu^{-3}\, \phi_i$.

(a)   (b)
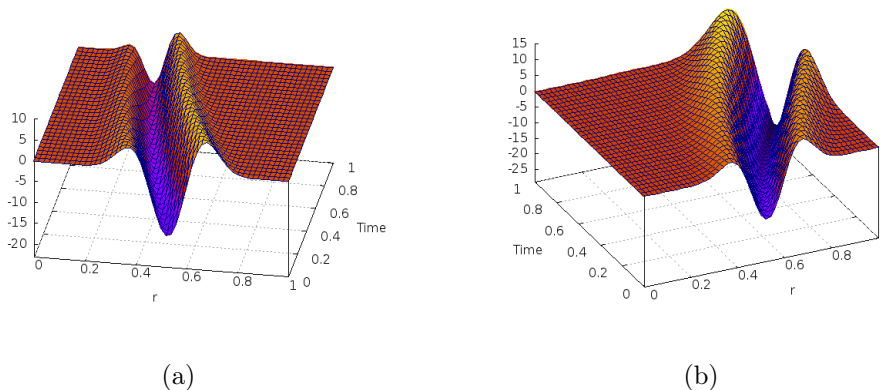
Figure 3.4: The numerical solutions of (a) ϕ_0 and (b) ϕ_4 for the evolution of the initial data (3.14)-(3.13)—centered around $r = 0.5$—in the representation of Fig. 2.2(b)

Let's assume that the initial data for ϕ_2 has the form of a bump function

$$\phi_2(r) = \begin{cases} (4\, r\, b^{-2})^{16}(r-b)^{16}, & 0 \le r \le b \\ 0, & b \le r \le 1 \end{cases}. \qquad (3.14)$$

centered at $r = b/2$. (Recall that the transformation $X_2 = \mu^{-3}\, \phi_2$ relates the fields ϕ_2 and X_2.) So, through b, one controls the proximity of the initial data to the cylinder I. The simplest non-trivial case $l = 2$ will be considered here; thus (3.14) and (3.13), with $l = 2$, will be our initial data. (The numerical analysis of a higher

83

mode, e.g. $l = 10$, in presented in Appendix B.) From their construction our initial data is compactly supported. This choice together with the fact that the initial data for ϕ_0 travel towards the cylinder at $r = 0$, clearly suggest the kind of boundary condition that must be imposed on the "right" boundary point at $r = 1$. Therefore, using the SAT method, the boundary condition

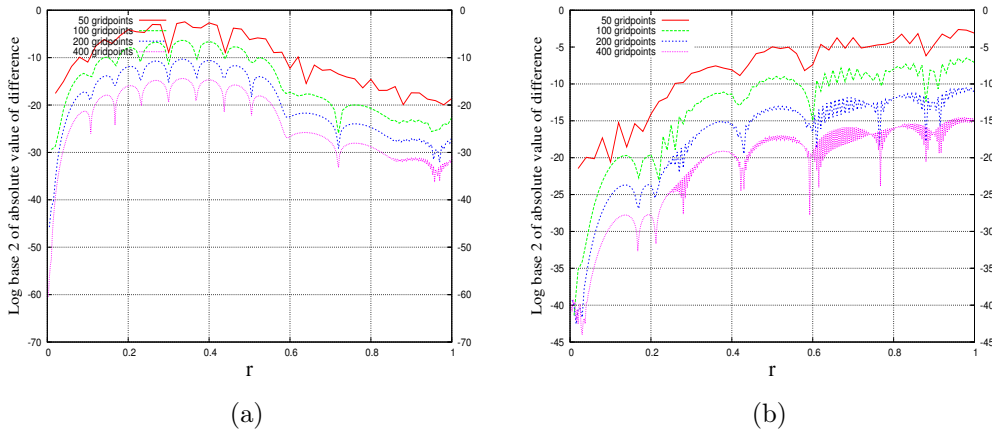$$\phi_0(t, 1) = 0$$

will be imposed on the "right" boundary.

(a)

(b)

Figure 3.5: The convergence plots of (a) ϕ_0 and (b) ϕ_4 for the evolution of the initial data (3.14)-(3.13)—centered around $r = 0.5$—at time $t = 1$. The representation of Fig. 2.2(b) is used, i.e. we choose $\mu = (r + 1)^{-1}$. The maximum of the absolute error of our simulations starts from an order of 10^{-1} and decreases with fourth order.

The convergence plots, e.g., of ϕ_0 and ϕ_4 for the evolution of the initial data (3.14)-(3.13) in the representation of Fig. 2.2(b) at time $t = 1$ can be found in Fig. 3.5. (Notice again the occurrence of the high frequency features.) The corresponding numerical solutions are illustrated in Fig. 3.4. The rest of the components have similar behaviour. The data are initially centered around the middle of the grid, i.e. $r = 0.5$. It must be noted here that, because there is no exact solution to compare with, the plots of Fig. 3.5 depict the absolute error with respect to the numerical solution with the highest resolution, which in our case is 800 grid points. Again, it is apparent that the code is converging and produces a maximum absolute
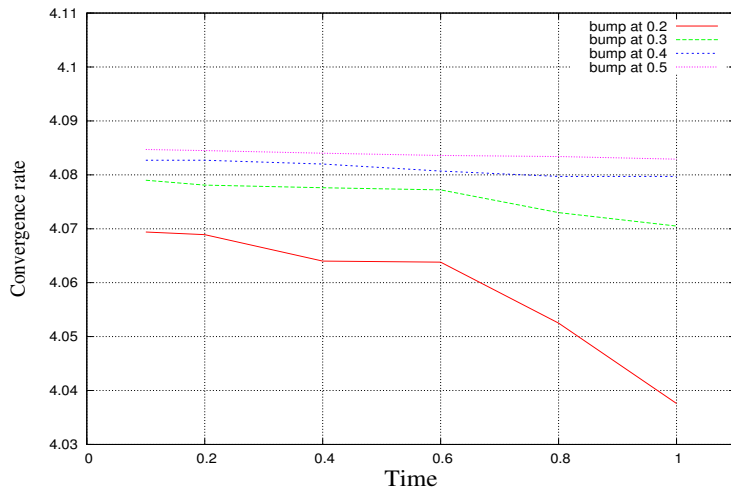
84

Figure 3.6: The convergence rates of ϕ_0 during the evolution of the system for initial data placed in different distances from I.

error of roughly the order of 10^{-1} that decreases with fourth order. Changing the place of the initial data on the computational grid leads to a, more or less, similar convergence behaviour. Placing the initial data closer to the cylinder actually means that the data is squeezed in an increasingly smaller and smaller area of the computational domain. Intuitively, one would expect that the closer one gets to the cylinder the more computational resources will be needed to study the evolution of the system. As higher and higher resolution will be required to evolve the more and more compressed data. The results of Fig. 3.6 point to that direction. There, using the same resolution, the initial data are moved consecutively closer to the cylinder I. The results of this procedure for ϕ_0 are presented in Fig. 3.6—the rest of spin-2 field's components exhibit similar behaviour. Although the convergence rates during the evolution for different placements of the initial data are well above four, the convergence rates are slightly decreasing while approaching the cylinder. If one pushes the initial data even closer to the cylinder, then the convergence rates vary widely. Estimating their values from such kind of data is highly unreliable. Therefore, in order to prescribe initial data so close to the cylinder, and subsequently study their evolution, we have to increase substantially the resolution of our grid.

Fortunately, the behaviour of our system does not depend on the proximity of the initial data to I. Thus, we do not have to place the initial data too close to

the cylinder to read off its behaviour. The initial data moving towards the cylinder, mainly the components ϕ_0 and ϕ_1, never reaches the cylinder independently of how close we place it to I. The amplitude of this data decreases with time. In addition, the data slows down while approaching the cylinder. On the other hand, data that are moving away from the cylinder, mainly the components ϕ_3 and ϕ_4, exhibit the exactly opposite behaviour. Namely, the data speeds up and its amplitude increases. This behaviour is in agreement with Penrose's conformally compactified picture [62]. According to which, although infinity is brought (through a conformal transformation) into a finite distance, data travelling towards it will never reach it.

Let's see now if the vanishing of the constraint quantities (2.32) is preserved during the evolution. Initially, the violation associated with each one of the constraint quantities C_k is roughly of the order of 10^{-7} or less. Fig. 3.7 depicts the violation of the constraints during the evolution of data that are initially centered around $r = 0.5$. Clearly, the violation of the vanishing of the constraint quantities remains at the initial levels, i.e. 10^{-7}; hence, we can safely conclude that they are preserved during the evolution.
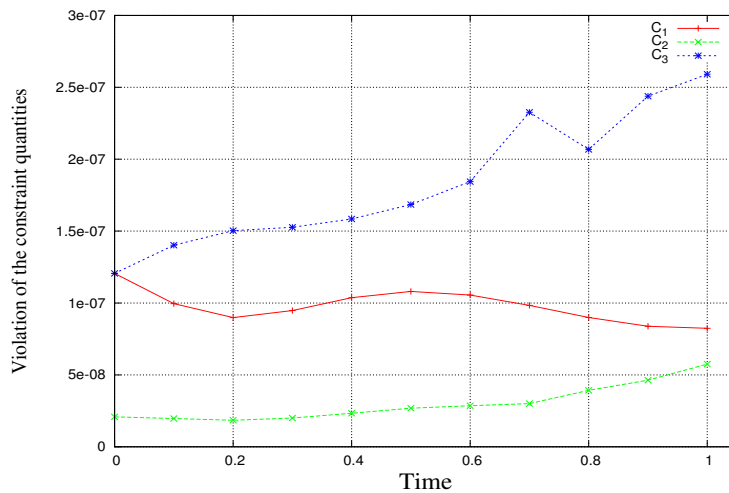
Figure 3.7: The behaviour of the constraint quantities (2.32) during the evolution of the initial data (3.14) with the bump function centered at $r = 0.5$.

So far, we are working in the finite representation of space-like infinity where $\mathscr{I}^{\pm}$ meet I at an 45° "angle", see Fig. 2.2(b). All our results hold in this representation. What will happen if one changes representation and uses for example the

representation of Fig. 2.2(a)? Are there any advantages or disadvantages concerning our numerical studies? Analytically, it does not make any difference though as always one can translate the results from one to another representation through an appropriate transformation.[1] For example, the two representations of Fig. 2.2 are related by the simple transformation

$$\phi_i^{\mu=(1+r)^{-1}} = \frac{1}{(1+r)^3} \, \phi_i^{\mu=1}.$$

Observing the form of the characteristic curves depicted in Figs. 2.3 and 2.4, one would expect that the former representation is numerically more challenging as its characteristics in their effort to change abruptly direction, while approaching I^+, and align with the horizontal $\mathscr{I}^+$ get more and more squeezed. This observation strongly indicates that numerical studies in the vicinity of I^+, in the representation of Fig. 2.2(a), demand more computational resources and/or more elaborated time integration techniques—e.g. with adaptive time step. The results of Fig. 3.8 confirm
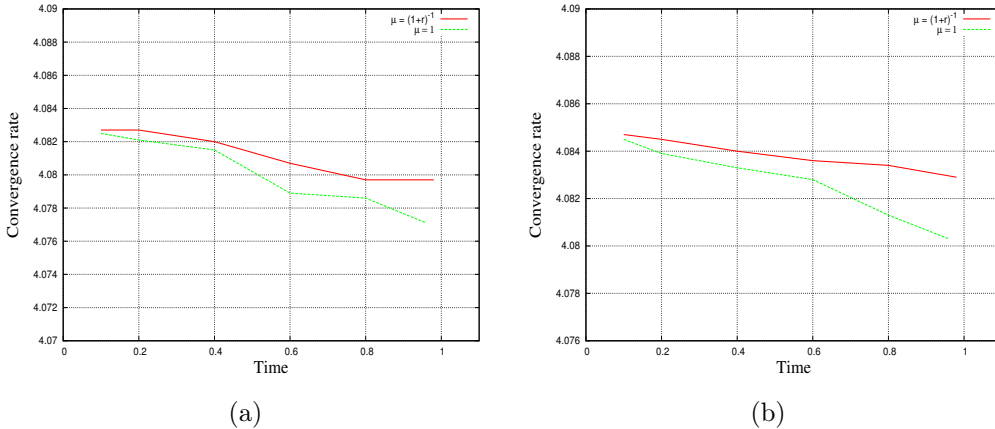
Figure 3.8: The convergence rates of the evolution of the initial data (3.14)-(3.13) centered around (a) $r = 0.4$ and (b) $r = 0.5$ for the two representation of Fig. 2.2.

these expectations. There, while keeping the same resolution, i.e. 800 grid points, the initial data (3.14)-(3.13) was evolved for the two representation of Fig. 2.2. The same procedure was carried out twice for different positions of the initial data. The

[1]In analytical calculations, the representation $\mu = 1$ is usually preferred because the system (2.30)-(2.31) simplifies considerably.

graphs of Fig. 3.8 depict the behaviour of the convergence rates during the evolution for the two different representations. The relative behaviour of the convergence rates seems not to depend on the position of the initial data. It is apparent that the convergence rates for the different representations deviate from each other the closer one gets to I^+. As expected the convergence rates for $\mu = 1$ decrease faster than the corresponding ones for $\mu = (1 + r)^{-1}$. In addition, the code for the former representation becomes unstable earlier than the one for the latter. Therefore, in the representation of Fig. 2.2(b) one, for the same resources and techniques, cannot only get closer to I^+ but also can have more accurate results. Of course, at the expense of higher resolution and more complicated time integration techniques, the behaviour of our system can be studied solely in the representation of Fig. 2.2(a).

3.6 Transport equations

Now, one is in position to reproduce Friedrich's analytical results [33] on the cylinder ($r = 0$). Specifically, we will try to reproduce the singular behaviour of some components of the spin-2 field at I^+. Observing (2.30), the equation governing the dynamics of ϕ_4 is clearly degenerating at I^+, i.e. $t = 1$; a fact that leads to the appearance of logarithmic singularities in its solutions. In the following, we will work in the representation of Fig. 2.2(a), i.e. we set $\mu(r) = 1$—this choice is made solely because it simplifies considerably the system (2.30)-(2.31).

It was proven in [33] that, under the assumption of analyticity of the rescaled "unphysical" metric g, near space-like infinity the components of the spin-2 zero-rest-mass field can be expanded in terms of the spatial component r as

$$\phi_n(t, r, \theta, \varphi) = \sum_{p=|2-n|}^{\infty} \Phi_n^p(t, \theta, \varphi)\, r^p, \tag{3.15}$$

with

$$\Phi_n^p(t, \theta, \varphi) = \sum_{q=|2-n|}^{p} \sum_{k=0}^{2q} a(t)_{n,p;q,k}\, T_{2q}{}^k{}_{q-2+n}, \tag{3.16}$$

where $\Phi_n^p = \partial_r^{(p)} \phi_n|_{r=0}$. Friedrich's angular dependent functions T that appear in the above expansion are related to the spin-weighted spherical harmonics ${}_s\Upsilon_{lm}$, used

in (2.24) to perform a similar angular expansion, in the following way [89]

$$_s\Upsilon_{lm} = (-\mathrm{i})^{s+2\,l+m} \sqrt{\frac{2\,l+1}{4\,\pi}}\, T_{2l}{}^{l-m}{}_{l-s}.^2$$

Therefore, the expansion coefficients of the two approaches will differ by a factor that depends on the specific value of the triple (s, l, m).

The expansion coefficients Φ_n^p, and subsequently the time dependent functions $a(t)_{n,p;q,k}$, can be derived by appropriately differentiating the system (2.30)-(2.31) and evaluating the resulting equations on the cylinder, i.e. taking the limit $r \to 0$. Following the procedure described in [33], one can compute the exact form of the first coefficients that exhibit a singular behaviour, namely the one with $p = q = 2$:

$$\begin{aligned}
a_{0,2;2,k} &= h(t)(1-t)^4 + \frac{c_2}{48}\left(16 - 19\,t + 12\,t^2 - 3\,t^3\right), \\
a_{1,2;2,k} &= 2\left[h(t)(1-t)^3(1+t) + \frac{c_2}{48}\left(4 + t - 6t^2 + 3t^3\right)\right], \\
a_{2,2;2,k} &= \sqrt{6}\left[h(t)(1-t^2)^2 + \frac{c_2}{48}\left(5\,t - 3\,t^3\right)\right], \qquad (3.17) \\
a_{3,2;2,k} &= 2\left[h(t)(1-t)(1+t)^3 + \frac{c_2}{48}\left(-4 + t + 6\,t^2 + 3\,t^3\right)\right], \\
a_{4,2;2,k} &= h(t)(1+t)^4 - \frac{c_2}{48}\left(16 + 19\,t + 12\,t^2 + 3\,t^3\right),
\end{aligned}$$

where $h(t) \equiv c_1 - \frac{\mathrm{i}\,\pi\,c_2}{32} + \frac{c_2}{16}\operatorname{arctanh}(t)$. Notice that at the C^0 level only ϕ_4 develops logarithmic singularities at $t = 1$; in the rest of the components the singular terms are always multiplied by a polynomial that is vanishing at $t = 1$. In some stage though one of their derivatives will develop a logarithmic behaviour. Specifically, it will appears at the level C^{4-n}, where $n = 0, \ldots, 4$ are the components of the spin-2 field.

To reproduce numerically (3.17), one has to prescribe initial data that behave approximately as r^2 near the cylinder, a possible choice is

$$\phi_0 = 100\, r^2 (r-1)^{36}, \quad \phi_4 = -100\, r^2 (r-1)^{36}. \qquad (3.18)$$

These initial conditions violate in first order the regularity conditions introduced in [33] to prevent the occurrence of logarithmic singularities. In order to relate the solutions (3.17) with the initial conditions (3.18), one has to specify the constants

---

[2]Notice that $l = q$, $k = l - m$ and, as one would expect, the spin-weight $s = 2 - n$.

c_1, c_2 by evaluating (3.17) at $t = 0$ and then equating it with (3.18); thus, we get $c_1 = \frac{75i\pi}{8}$, $c_2 = 300$ and the time dependent coefficients (3.17) take the form

$$a_{0,2;2,k} = \frac{25}{4} \left[16 - 19\,t + 12\,t^2 - 3\,t^3 + 3\,(1-t)^4 \operatorname{arctanh}(t) \right],$$

$$a_{1,2;2,k} = \frac{25}{2} \left[4 + t - 6\,t^2 + 3\,t^3 + 3\,(1-t)^3(1+t) \operatorname{arctanh}(t) \right],$$

$$a_{2,2;2,k} = \frac{25}{2} \sqrt{\frac{3}{2}} \left[5\,t - 3\,t^3 + 3\,\left(1-t^2\right)^2 \operatorname{arctanh}(t) \right], \qquad (3.19)$$

$$a_{3,2;2,k} = \frac{25}{2} \left(-4 + t + 6\,t^2 + 3\,t^3 + 3\,(1-t)(1+t)^3 \operatorname{arctanh}(t) \right),$$

$$a_{4,2;2,k} = \frac{25}{4} \left(-16 - 19\,t - 12\,t^2 - 3\,t^3 + 3\,(1+t)^4 \operatorname{arctanh}(t) \right).$$

The initial data for the fields ϕ_0 and ϕ_4 has been specified in (3.18); to prescribe initial data, that is consistent with the above choice (3.18), for the rest of the components of the spin-2 field, we will numerically integrate the constraints (2.31) using an eighth order adaptive Dormand-Prince Runge-Kutta method, see [43]. In accordance with the choice (3.18), the required initial conditions at $r = 0$ will be chosen $\phi_1(0,0) = \phi_2(0,0) = \phi_3(0,0) = 0$.

Choosing a boundary condition for the "right" boundary point of ϕ_0 is here far more complicated than in our previous simulations. For there is no way to predict the form of $\phi_0(t,1)$. An exact solution is lacking and the initial data do not have some specific feature that would allow us to guess the temporal evolution of the boundary point at $r = 1$. Fortunately, there is a way to estimate the form of the required boundary condition. One has first to express it, through a Taylor expansion, as a polynomial in t:

$$\phi_0(t,r) = \phi_0(0,r) + \dot{\phi}_0(0,r)\,t + \ddot{\phi}_0(0,r)\,\frac{t^2}{2!} + \dddot{\phi}_0(0,r)\,\frac{t^3}{3!} + \ddddot{\phi}_0(0,r)\,\frac{t^4}{4!} + \mathcal{O}(t^5).$$

Then, using the system (2.30)-(2.31), one can express the expansion coefficients in terms of the components ϕ_n of the spin-2 field and of spatial derivatives of ϕ_0 only. The numerically computed values of the field ϕ_0 near the cylinder can be used to approximate its spatial derivatives—we used fourth order accurate finite difference operators taken from [21]. Finally, evaluating the resulting expressions at $r = 1$, one can compute the numerical values of above expansion coefficients at $(t,r) = (0,1)$. Hence, a boundary condition consistent with the choice (3.18) looks like

$$\phi_0(t,1) = 0 - 0.1422\,t + 0.2845\,t^2 - 0.2845\,t^3 + 0.2845\,t^4,$$

which will be imposed through the SAT method.

The convergence rates for the evolution of the initial data (3.18) are presented in Fig. 3.9. The results therein clearly indicate that our simulation is stable and converges with roughly fourth order.
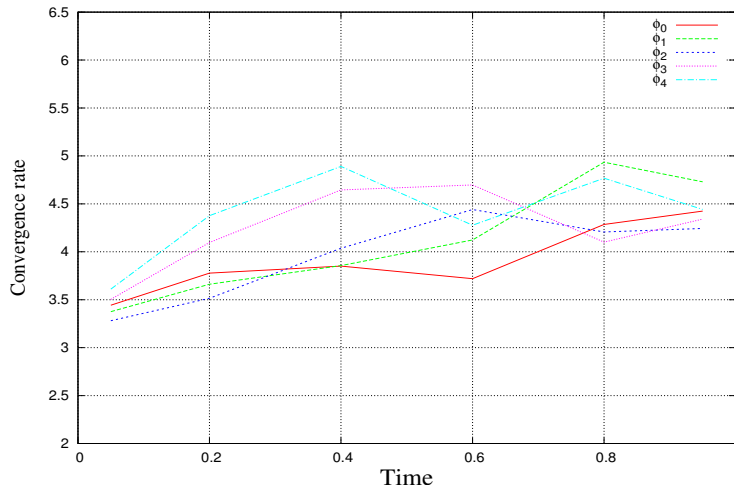

Figure 3.9: The convergence rates for the evolution of the initial data (3.18).

Now, based on the results of the above simulation, we have somehow to reproduce numerically the analytic results (3.19). Observe that by their definition, see (3.15) and (3.16), the coefficients $a_{n,2;2,k}$ are nothing else than the second spatial derivative of the spin-2 field's components on the cylinder ($r = 0$). Thus, they can be approximated by

$$(a_{n,2;2,k})_{num} = \frac{1}{2} \frac{\partial^2 \phi_n}{\partial r^2}|_{r=0}. \tag{3.20}$$

The second derivative operator appearing in (3.20) will be approximated by one sided fourth order accurate finite difference operators that can be found in [21]. As it was mentioned in the preceding section, the study of the behaviour of (3.20) close to I^+ requires a more accurate time integration method. Thus, for the temporal integration of the initial data (3.18) now a time step adaptive Runge-Kutta scheme will be employed. The results of the above procedure, for a numerical grid that consists of 400 points, and the comparison with the expected exact behaviour (3.19) of the coefficient $a_{4,2;2,k}$ are illustrated in Fig. 3.10. The numerical reproduction of the rest of the expansion coefficients (3.19) leads to results of similar accuracy. The agreement between our numerical results and Friedrich's analytic solutions is quite

apparent. It is worth mentioning that the numerical data of Fig. 3.10 is a product of two consecutive numerical approximations. A fact that makes the accuracy of the results depicted in Fig. 3.10 even more impressive. Firstly, the initial data (3.18) was evolved and the temporal behaviour of the fields ϕ_k was computed; afterwards, their values on the cylinder ($r = 0$) were used to approximate the expansion coefficients (3.20).
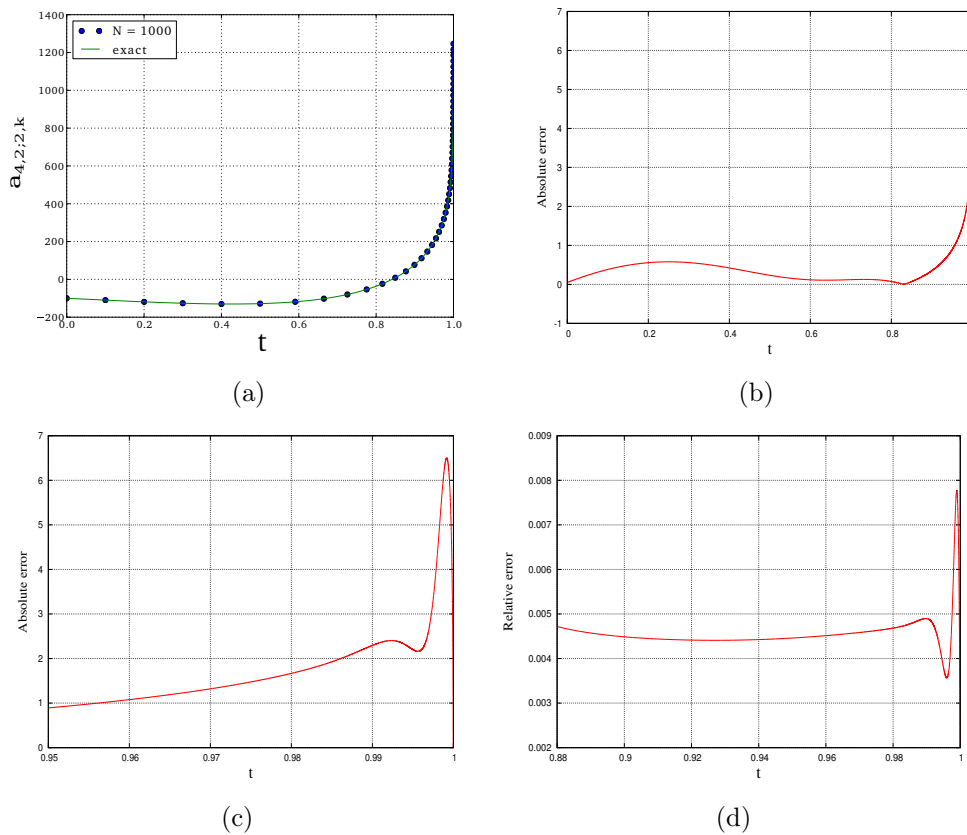

Figure 3.10: (a) A direct comparison of the numerically computed expansion coefficient $a_{4,2;2,k}$, see (3.20), with its corresponding exact expression in (3.19). (b) The absolute error between the exact and numerical data. (c) The absolute error close to $t = 1$—a detail of (b). (d) The relative error near $t = 1$ is of the order of 10^{-3}.

Chapter 4

The spin-2 wave system on Minkowski space-time

4.1 Spin-2 wave equation

Our objectives in the present chapter are to derive a second order system from the first order system described by the spin-2 equation (2.14) and establish a correspondence between them. Our main motivation for this is the claim by several numerical analysts, e.g. [49], that the numerical solutions of second order wave equations have better properties than those for the corresponding first order systems. Specifically, according to [49], numerical approximations based on second order equations lead to better accuracy than the ones based on first order equations. In addition, in the second order case, spurious high-frequency waves travelling against the characteristics disappear. We investigate these claims in the following chapter. In the present chapter, we provide a more detailed account of the presentation of the same topic in [17].

4.1.1 Derivation

The setting described in sec. 2.1 and the results and notation of sec. 2.2 will be repeatedly used throughout this section. We will be again working on the more general spherically symmetric background described by (2.10) and then will specialise our results to the F-gauge (2.7) in sec. 4.2.

Our starting point will be the spin-2 equation (2.14) in the slightly different notation

$$\nabla_F{}^{A'}\phi^F{}_{BCD} = 0.$$

Acting on it with the spinorial covariant derivative, one constructs a second order equation of the form

$$\nabla_{A'A}\nabla_F{}^{A'}\phi^F{}_{BCD} = 0.$$

Splitting the above differential operator into its symmetric and skew symmetric parts in AF

$$\nabla_{A'A}\nabla_F{}^{A'} = \nabla_{A'(A}\nabla_{F)}{}^{A'} - \frac{1}{2}\epsilon_{AF}\nabla_{A'}{}^X\nabla_X{}^{A'},$$

and introducing the abbreviations $\Box_{AF} \equiv \nabla_{A'(A}\nabla_{F)}{}^{A'}$ and $\Box \equiv \nabla_{A'}{}^X\nabla_X{}^{A'}$, the above equation splits into

$$\Box_{AF}\,\phi^F{}_{BCD} - \frac{1}{2}\Box\,\phi_{ABCD} = 0.$$

Following [65], namely using the identities $\Box_{AB}\kappa^C = \Psi_{ABE}{}^C\kappa^E$ and $\Box_{AB}\kappa_C = -\Psi_{ABC}{}^E\kappa_E$ derived therein for an arbitrary spinor κ_E,[1] the action of $\Box_{AF}$ on the spin-2 zero-rest-mass field simplifies considerably

$$6\,\Psi_{FQ(AB}\phi_{CD)}{}^{FQ} - \Box\,\phi_{ABCD} = 0.$$

Since here we are concerned only with the study of the linearised case, the first term on the l.h.s drops out. Thus, the remaining term constitutes the so-called *spin-2 wave equation*

$$\Box\,\phi_{ABCD} = 0, \tag{4.1}$$

which will be used to describe the second order system. Because of the symmetries involved, in its component form (4.1) comprises a system of five equations. Following the same line of thought with sec. 2.2.2, the spinor covariant derivative $\nabla_{FF'}$ will be expressed, as in (2.17), in terms of the weighted differential operators of the GHP formalism, i.e.

$$\nabla_{FF'} \equiv \iota_F\,\iota_{F'}\text{þ} + o_F\,o_{F'}\text{þ}' - \iota_F\,o_{F'}\text{ð} - o_F\,\iota_{F'}\text{ð}'.$$

---

[1] The spinor Ψ_{ABCD} is the Weyl spinor.

Acting with the above operator on the spin-2 zero-rest-mass field one, in accordance with (2.18), gets

$$\nabla^{FF'}\phi_{ABCD} = \iota^F\,\iota^{F'}\,\text{þ}\,\phi_{ABCD} + o^F\,o^{F'}\,\text{þ}'\,\phi_{ABCD} - \iota^F\,o^{F'}\,\eth'\,\phi_{ABCD} - o^F\,\iota^{F'}\,\eth\,\phi_{ABCD}.$$

Using the normalization conditions $o_{A'}\iota^{A'} = 1 = o_A\iota^A$, the action of the weighted derivatives on the spin dyad [65]

$$\eth'\,o^A = -\rho\,\iota^A, \quad \eth\,\iota^A = -\rho'\,o^A, \quad \eth\,o^{A'} = -\rho\,\iota^{A'}, \quad \eth'\,\iota^{A'} = -\rho'\,o^{A'},$$

where the rest vanish for spherically symmetric space-times (2.10), and the specific values of the spherically symmetric spin-coefficients (2.13), one can act another time with (2.17) on the spin-2 zero-rest-mass field and bring (4.1) into the form

$$\begin{aligned}\nabla_{FF'}\nabla^{FF'}\phi_{ABCD} = \Box\,\phi_{ABCD} = 2\,\rho\,(\text{þ}\phi_{ABCD} + \text{þ}'\phi_{ABCD}) + \\ + \text{þ}\text{þ}'\phi_{ABCD} + \text{þ}'\text{þ}\phi_{ABCD} - \eth\eth'\phi_{ABCD} - \eth'\eth\phi_{ABCD}.\end{aligned} \tag{4.2}$$

Observe that by employing the commutation relation for the weighted derivative operators a further simplification of (4.2) can be achieved.

In order to derive these relations we have to express the spinorial covariant derivative in term of its components, i.e. $\nabla_{\mathbf{AA'}} = \varepsilon_{\mathbf{A}}{}^A\varepsilon_{\mathbf{A'}}{}^{A'}\nabla_{AA'}$, while keeping the abstract index notation for the spin-2 field:

$$\begin{aligned}\varepsilon_{\mathbf{A}}{}^A\varepsilon_{\mathbf{B'}}{}^{B'}\varepsilon_{\mathbf{C}}{}^C\varepsilon_{\mathbf{D'}}{}^{D'}\nabla_{AB'}\nabla_{CD'}\phi_{KLMN} = \\ = \varepsilon_{\mathbf{C}}{}^C\varepsilon_{\mathbf{D'}}{}^{D'}\nabla_{\mathbf{AB'}}(\varepsilon_C{}^{\mathbf{Q}}\varepsilon_{D'}{}^{\mathbf{Q'}}\nabla_{\mathbf{QQ'}}\phi_{KLMN}) = \\ = \nabla_{\mathbf{AB'}}\nabla_{\mathbf{CD'}}\phi_{KLMN} - \bar{\gamma}_{\mathbf{AB'D'}}{}^{\mathbf{Q'}}\nabla_{\mathbf{CQ'}}\phi_{KLMN} - \gamma_{\mathbf{AB'C}}{}^{\mathbf{Q}}\nabla_{\mathbf{QD'}}\phi_{KLMN}.\end{aligned}$$

Reversing the order in which the covariant derivatives act on the spin-2 field one gets

$$\begin{aligned}\varepsilon_{\mathbf{A}}{}^A\varepsilon_{\mathbf{B'}}{}^{B'}\varepsilon_{\mathbf{C}}{}^C\varepsilon_{\mathbf{D'}}{}^{D'}\nabla_{CD'}\nabla_{AB'}\phi_{KLMN} = \\ = \nabla_{\mathbf{CD'}}\nabla_{\mathbf{AB'}}\phi_{KLMN} - \bar{\gamma}_{\mathbf{CD'B'}}{}^{\mathbf{Q'}}\nabla_{\mathbf{AQ'}}\phi_{KLMN} - \gamma_{\mathbf{CD'A}}{}^{\mathbf{Q}}\nabla_{\mathbf{QB'}}\phi_{KLMN}.\end{aligned}$$

The l.h.s of the last two expressions are symmetric in the indices A, C and B', D', thus by subtracting them, their l.h.s cancel out, namely

$$\begin{aligned}[\nabla_{\mathbf{AB'}}, \nabla_{\mathbf{CD'}}]\phi_{KLMN} = \bar{\gamma}_{\mathbf{AB'D'}}{}^{\mathbf{Q'}}\nabla_{\mathbf{CQ'}}\phi_{KLMN} + \gamma_{\mathbf{AB'C}}{}^{\mathbf{Q}}\nabla_{\mathbf{QD'}}\phi_{KLMN} - \\ - \bar{\gamma}_{\mathbf{CD'B'}}{}^{\mathbf{Q'}}\nabla_{\mathbf{AQ'}}\phi_{KLMN} - \gamma_{\mathbf{CD'A}}{}^{\mathbf{Q}}\nabla_{\mathbf{QB'}}\phi_{KLMN}.\end{aligned}$$

By taking the components of the above expression one can derive the commutation relations between the intrinsic derivative operators for the spherical symmetric metric (2.10):

$$(D'D - DD')\phi_{KLMN} = (\gamma + \bar{\gamma})D\phi_{KLMN} + (\varepsilon + \bar{\varepsilon})D'\phi_{KLMN},$$
$$(\delta D - D\delta)\phi_{KLMN} = -\rho\,\delta\phi_{KLMN},$$
$$(\delta D' - D'\delta)\phi_{KLMN} = \rho\,\delta\phi_{KLMN},$$
$$(\delta'\delta - \delta\delta')\phi_{KLMN} = 2\,\beta\,\delta'\phi_{KLMN} + 2\,\alpha\,\delta\phi_{KLMN}.$$

(4.3)

To extract the commutators between the weighted derivatives from (4.3), one has to be a little bit careful when substituting the intrinsic derivatives with their weighted counterparts through (2.16). Replacing the intrinsic derivatives that act directly on the spin-2 field is trivial: $D \mapsto \text{þ}$, $D' \mapsto \text{þ}'$, $\delta \mapsto \eth$, $\delta' \mapsto \eth'$, as Φ_{ABCD} is a $\{0, 0\}$-quantity. The resulting quantities have non-zero weights though, namely

$$\text{þ}\,\phi_{ABCD} : \{1, 1\}\text{-quantity}, \quad \text{þ}'\phi_{ABCD} : \{-1, -1\}\text{-quantity},$$
$$\eth\,\phi_{ABCD} : \{1, -1\}\text{-quantity}, \quad \eth'\phi_{ABCD} : \{-1, 1\}\text{-quantity}.$$

Thus, in order to replace the intrinsic derivatives that act on the above quantities with weighted derivatives, the full expressions (2.16) must be used, where p, q take values according to the scheme above. The commutators (4.3) then become

$$(\text{þ}'\text{þ} - \text{þ}\text{þ}')\phi_{KLMN} = 0,$$
$$(\eth\text{þ} - \text{þ}\eth)\phi_{KLMN} = -\rho\,\eth\phi_{KLMN},$$
$$(\eth\text{þ}' - \text{þ}'\eth)\phi_{KLMN} = \rho\,\eth\phi_{KLMN},$$
$$(\eth'\eth - \eth\eth')\phi_{KLMN} = 0.$$

(4.4)

Now, by inserting (4.4) into (4.2), we get the quite simple expression

$$\Box\,\phi_{ABCD} = 2\,(\text{þ}\text{þ}' - \eth\eth' + \rho\,(\text{þ} - \text{þ}'))\,\phi_{ABCD}.$$

Finally, expanding the spin-2 field in terms of its components in the familiar way

$$\phi_{ABCD} \equiv \iota_{(A}\iota_B\iota_C\iota_{D)}\phi_0 - 4\,\iota_{(A}\iota_B\iota_C o_{D)}\phi_1 +$$
$$+ 6\,\iota_{(A}\iota_B o_C o_{D)}\phi_2 - 4\,\iota_{(A}o_B o_C o_{D)}\phi_3 + o_{(A}o_B o_C o_{D)}\phi_4,$$

and taking the components of the resulting expression, one obtains five equations of the form

$$\text{þ}\text{þ}'\phi_\lambda + \rho\,\text{þ}\phi_\lambda - \rho\,\text{þ}'\phi_\lambda + \lambda(5 - \lambda)\,\rho^2\,\phi_\lambda = \eth\eth'\phi_\lambda + (4 - \lambda)\,\rho\,\eth\phi_{\lambda+1} - \lambda\,\rho\,\eth'\phi_{\lambda-1} \quad (4.5)$$

with $\lambda = 0, 1, 2, 3, 4$. Notice that (2.20) and (2.21) allows us to obtain a coordinate representation of (4.5). But we will leave that for later.

4.1.2 Expansion in spin-weighted spherical harmonics

In a similar fashion with sec. 2.2.3, the system (4.5) can be further simplified by expanding spin-2 field's components as a sum of spin-weighted spherical harmonics on the unit sphere. Thus, by firstly expressing the $\eth$ and $\eth'$ operators on the unit sphere

$$\eth \mapsto \frac{1}{\sqrt{2}\,g\,r}\,\eth, \quad \eth' \mapsto \frac{1}{\sqrt{2}\,g\,r}\,\eth',$$

and then expanding, as in (2.24), the $\{p,q\}$-scalars ϕ_λ as a sum of spin-weighted spherical harmonics

$$\phi_k(t, r, \theta, \phi) = \sum_{lm} \phi_k^{lm}(t, r)\,{}_{2-k}\Upsilon_{lm}(\theta, \phi),$$

the operators defined above can be removed from the system (4.5) as their action on the spin-weighted spherical harmonics ${}_s\Upsilon_{lm}$ yields

$$\begin{aligned}
\eth({}_s\Upsilon_{lm}) &= -\sqrt{l(l+1) - s(s+1)}\,{}_{s+1}\Upsilon_{lm}, \\
\eth'({}_s\Upsilon_{lm}) &= \sqrt{l(l+1) - s(s-1)}\,{}_{s-1}\Upsilon_{lm}, \\
\eth\eth'({}_s\Upsilon_{lm}) &= -[l(l+1) - s(s-1)]\,{}_s\Upsilon_{lm}.
\end{aligned} \tag{4.6}$$

Therefore, the implementation of the aforementioned operations into (4.5) forces the angular related weighted derivatives to drop out, i.e.

$$\begin{aligned}
\text{\thorn}\text{\thorn}'\phi_\lambda^{lm} &+ \rho\,\text{\thorn}\phi_\lambda^{lm} - \rho\,\text{\thorn}'\phi_\lambda^{lm} + \lambda(5-\lambda)\,\rho^2\,\phi_\lambda^{lm} = \\
&= -\frac{\alpha_{(2-\lambda)(1-\lambda)}^2}{2\,g^2 r^2}\,\phi_\lambda^{lm} - \frac{(4-\lambda)\,\alpha_{(2-\lambda)(1-\lambda)}\,\rho}{\sqrt{2}\,g\,r}\,\phi_{\lambda+1}^{lm} - \frac{\lambda\,\alpha_{(2-\lambda)(3-\lambda)}\,\rho}{\sqrt{2}\,g\,r}\,\phi_{\lambda-1}^{lm},
\end{aligned} \tag{4.7}$$

where $\alpha_x = \sqrt{l(l+1) - x}$ and as before we will introduce the notation $\phi_\lambda^{lm} = \phi_\lambda$.

4.2 Spin-2 wave equation in the F-gauge

Now, in order to obtain a coordinate representation of (4.7) in the F-gauge, we have to replace the weighted derivative operators $\text{\thorn}, \text{\thorn}'$ with coordinate derivatives related

to the metric (2.7). As before, using the coordinate expression of the weighted derivatives[2]

$$\text{þ}\,\eta = \frac{1}{\sqrt{2}}\left(A\,\partial_t + B\,\partial_r - 2\sqrt{2}\,w\,\epsilon\right)\eta,$$

$$\text{þ}'\,\eta = \frac{1}{\sqrt{2}}\left(C\,\partial_t - B\,\partial_r - 2\sqrt{2}\,w\,\gamma\right)\eta,$$

the reduction formulae

$$A = 1 - t\kappa', \qquad B = \kappa, \qquad C = 1 + t\kappa', \qquad g = \frac{1}{\kappa},$$

and the related spin-coefficients

$$\gamma = \varepsilon = -\frac{\kappa'}{2\sqrt{2}}, \quad \rho = \frac{r\,\mu'}{\sqrt{2}},$$

a coordinate representation of (4.7) in the F-gauge (2.7) can be obtained

$$
\begin{aligned}
&(1 - t^2\kappa'^2)\partial_{tt}\phi_\lambda - \kappa^2\partial_{rr}\phi_\lambda + 2\,t\kappa\kappa'\partial_{tr}\phi_\lambda + 2\,[(2-\lambda)\kappa' - t(\kappa'^2 + r\,\mu'\kappa' - \\
&- \frac{1}{2}\kappa\,\kappa'')]\partial_t\phi_\lambda + 2\,r\kappa\mu'\partial_r\phi_\lambda + [(2-\lambda)(\kappa\kappa'' + (1-\lambda)\kappa'^2) + \\
&+ \lambda(5-\lambda)r^2\mu'^2]\phi_\lambda = -\mu^2\,\alpha^2_{(2-\lambda)(1-\lambda)}\phi_\lambda - \alpha_{(2-\lambda)(1-\lambda)}(4-\lambda)\,r\,\mu\,\mu'\,\phi_{\lambda+1} - \\
&- \alpha_{(2-\lambda)(3-\lambda)}\,\lambda\,r\,\mu\,\mu'\,\phi_{\lambda-1}.
\end{aligned}
\tag{4.8}
$$

The above system of five equations is the component decomposition of the spin-2 wave equation (4.1) on a spherically symmetric background (2.7). It can be readily confirmed that the exact solution (A.12) derived in Appendix A is also satisfying the system (4.8). Notice that, as in the case of the first order evolution system (2.30), the radial derivatives drop out from the above system when the equations are restricted to the cylinder I at $r = 0$. Therefore, on I, (4.8) reduces to the following intrinsic system

$$(1 - t^2\mu^2)\partial_{tt}\phi_\lambda + 2\mu\,(2-\lambda - t\mu)\partial_t\phi_\lambda + (2-\lambda)(1-\lambda)\mu^2\phi_\lambda = -\mu^2\,\alpha^2_{(2-\lambda)(1-\lambda)}\phi_\lambda.$$

The cylinder is again a total characteristic and as expected the intrinsic system above generates logarithmic singularities at $t = \pm k'^{-1}$, i.e. at the interface $I^\pm$ of the cylinder with null infinity, where the hyperbolicity of the equations break down.

---

[2]Recall that $w = \frac{p+q}{2}$ is the boost-weight of $\{p, q\}$-scalar quantities.

To prove the latter, we have to look at the principal part of the symbol of (4.8). Following [73] we can write down the associated symmetric matrix of (4.8):

$$\begin{pmatrix} -(1 - t^2 \kappa'^2) & -t\kappa\kappa' \\ -t\kappa\kappa' & \kappa^2 \end{pmatrix}.$$

The eigenvalues of the above matrix at $t = \pm \kappa'^{-1}$ read $\lambda_{1,2} = \frac{1}{2}\kappa(\kappa \pm \sqrt{4 + \kappa^2})$.[3] It is apparent that for $r > 0$ the system (4.8) is hyperbolic as the eigenvalues λ_1, λ_2 are of opposite sign. At $r = 0$ though both eigenvalues vanish and the hyperbolicity of (4.8) breaks down.

The system (4.8) of five wave-like equations is clearly coupled because of the last two terms on the r.h.s. Interestingly, if one chooses $\mu = $ const., then these two terms drop out and the system decouples

$$\begin{aligned} (1 - t^2\mu^2)\partial_{tt}\phi_\lambda - r^2\mu^2\partial_{rr}\phi_\lambda + 2\,t\,r\mu^2\,\partial_{tr}\phi_\lambda + 2\,\mu\,(2 - \lambda - t\,\mu)\partial_t\phi_\lambda = \\ = -(2 - \lambda)(1 - \lambda)\,\mu^2\phi_\lambda - \mu^2\,\alpha^2_{(2-\lambda)(1-\lambda)}\phi_\lambda. \end{aligned} \tag{4.9}$$

(Notice that also the first spatial derivative drops out.) Recall that this choice for μ (specifically $\mu = 1$) corresponds to the representation of space-like infinity depicted in Fig. 2.2(a), where future and past null infinity $\mathscr{I}^\pm$ are horizontal, namely they are perpendicular to the cylinder I representing space-like infinity. Although, in this representation, the system is easier to handle analytically, as it simplifies significantly, its numerical implementation is considerably harder—mainly because of the form of its characteristic curves.

There is another possible way to decouple the system (4.8) without restricting ourselves to a specific representation of space-like infinity. This can be done by implementing the spin-2 equation (2.14) in the system (4.8). The spin-2 equation in its component form (2.29) reads

$$\begin{aligned} \lambda = 0, \ldots, 3: \quad (1 + t\kappa')\partial_t\phi_\lambda - \kappa\,\partial_r\phi_\lambda + \kappa'(2 - \lambda)\phi_\lambda + r\mu'(\lambda + 1)\phi_\lambda = \\ = -\mu\,\alpha_{(\lambda-1)(\lambda-2)}\phi_{\lambda+1}, \\ \lambda = 1, \ldots, 4: \quad (1 - t\kappa')\partial_t\phi_\lambda + \kappa\,\partial_r\phi_\lambda + \kappa'(2 - \lambda)\phi_\lambda + r\mu'(\lambda - 5)\phi_\lambda = \\ = \mu\,\alpha_{(\lambda-2)(\lambda-3)}\phi_{\lambda-1}. \end{aligned}$$

---

[3]Reminder: $\kappa = r\,\mu(r)$ with $\mu(0) = 1$.

Inserting the above expression into (4.8) one can eliminate the coupling terms $\phi_{\lambda+1}, \phi_{\lambda-1}$ in the following way

$$(1 - t^2\kappa'^2)\partial_{tt}\Phi_\lambda - \kappa^2\partial_{rr}\Phi_\lambda + 2\,t\kappa\kappa'\partial_{tr}\Phi_\lambda + 2[(2-\lambda)\mu - t(3\,r\,\mu'\kappa' + \kappa'^2 -$$

$$-\frac{1}{2}t\kappa'')]\partial_t\Phi_\lambda + 6\,r\kappa\mu'\partial_r\Phi_\lambda + [(2-\lambda)(\kappa\kappa'' + (1-\lambda)\kappa'^2) - 2(\lambda-2)^2r\kappa'\mu' +$$

$$(\lambda+1)(\lambda-4)r^2\mu'^2]\Phi_\lambda = -\mu^2\,\alpha^2_{(2-\lambda)(1-\lambda)}\Phi_\lambda.$$

4.3 Characteristic curves

The hyperbolic nature of the system (4.8) entails that it has *two* real characteristic curves. As in the first order system, the study of their behaviour will be very useful in the subsequent numerical studies of the spin-2 wave equation. Again, the form of the characteristic curves of second order partial differential equations like (4.8) depends only on their principal part. Following [45], the slope of the characteristic curves of second order partial differential equations of the form

$$a(t,r)\,\partial_{tt}u(t,r) + b(t,r)\,\partial_{tr}u(t,r) + c(t,r)\,\partial_{rr}u(t,r) + \ldots$$

is given by

$$\frac{dt}{dr} = \frac{b \pm \sqrt{b^2 - 4\,a\,c}}{2\,a}. \tag{4.10}$$

Thus, as expected, (4.8) has two real characteristic curves. Observing (4.8), in our case we have $a = 1 - t^2\kappa'^2$, $b = 2\,t\kappa\kappa'$ and $c = -\kappa^2$. The quantity under the square root is always positive, i.e. $b^2 - 4\,a\,c = 2\,\kappa^2 > 0$, which guaranties the hyperbolic nature of (4.8). Substituting $a, b,$ and c in the above expression and evaluating, one gets

$$\frac{dt}{dr} = -\frac{1 + t\kappa'}{\kappa}, \qquad \frac{dt}{dr} = \frac{1 - t\kappa'}{\kappa}.$$

Interestingly, the characteristic curves of the spin-2 wave equation are identical to those of the spin-2 equation. Fig. (4.1) depicts the characteristic curves of (4.8) near a neighbourhood of I^+. There is a slight difference with the first order case though. Now, the behaviour of the characteristic curves is more universal, in the sense that the characteristics of all the components of the spin-2 field, and not only of specific components, behave in the way depicted in Fig. (4.1). This observation follows naturally from (4.8), where the evolution equations for all the fields degenerate at $I^\pm$. In addition, the situation is now symmetric around the r-axis. (Remember that in
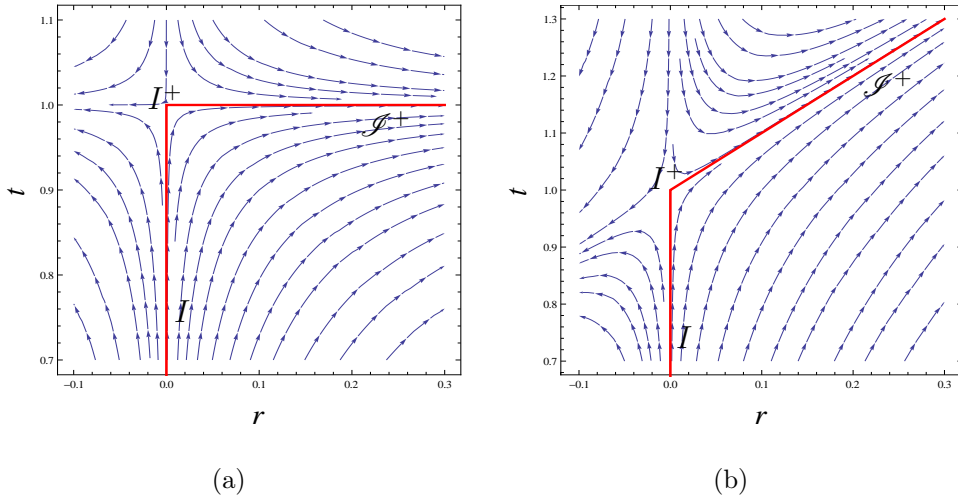
Figure 4.1: Characteristic curves of all the fields ϕ_λ in a neighbourhood of I^+. The red line denotes the cylinder, future and past null infinity $\mathscr{I}^\pm$. The situation close to I^- is obtained by a reflection in the r-axis. (a) Characteristic curves of slope $\dfrac{dt}{dr} = \dfrac{1-t}{r}$ in the case $\mu = 1$. (b) Characteristic curves of slope $\dfrac{dt}{dr} = \dfrac{1 - t\kappa'}{\kappa}$ in the case $\mu = (1+r)^{-1}$.

the first order case, the behaviour of the characteristic curves in the neighbourhoods of I^+ and I^- where different.) Again, the cylinder is a total characteristic of our system, thus we do not have to worry about prescribing boundary conditions on the cylinder. In addition, the domain of hyperbolicity still coincides with the parts of Friedrich's representation that are conformally related to the physical space-time.

4.4 Relating the first and the second order systems

In this section, we will try to correlate the first (2.14) with the second (4.1) order system. Establishing this correspondence will help us to compare the numerical behaviour of the two systems and study their similarities and differences.

We will start with the definition of the spinor

$$\Sigma^{A'}{}_{BCD} \equiv \nabla_F{}^{A'} \phi^F{}_{BCD} \tag{4.11}$$

101

and then differentiate it

$$\nabla_{A'A}\Sigma^{A'}{}_{BCD} = \nabla_{A'A}\nabla_F{}^{A'}\phi^F{}_{BCD}$$

Following the procedure described at the beginning of sec. 4.1.1, the r.h.s of the last expression takes the form

$$\nabla_{A'A}\Sigma^{A'}{}_{BCD} = -\frac{1}{2}\Box\,\phi_{ABCD}.$$

Obviously, if the spin-2 field ϕ_{ABCD} satisfies the spin-2 wave equation (4.1), then the r.h.s of the last expression vanishes

$$\nabla_{A'A}\Sigma^{A'}{}_{BCD} = 0. \tag{4.12}$$

Notice that the vanishing of the spinor (4.11) is nothing else than the spin-2 equation (2.14). Thus, if it holds initially, i.e. $\Sigma^{A'}{}_{BCD}|_S = 0$, and the above system is well-posed, then it also holds throughout the evolution. In summary, if the spin-2 field is a solution of the spin-2 wave equation (4.1) and, in addition, satisfies on the initial hypersurface S the spin-2 equation (2.14), then it is also a solution of the latter in a neighbourhood of S. We will take advantage of this result in the subsequent chapter; there the initial data and the boundary conditions for the second order system will be specified from the first order system in the aforementioned way and subsequently evolved with the second order system.

In the following we will prove that (4.12) is a symmetric hyperbolic system in the F-gauge. From its definition (4.11) the spinor $\Sigma^{A'}{}_{BCD}$ is a $\{0,0\}$-quantity, thus, according to (2.17), the action of the covariant derivative $\nabla^{A'}{}_A$ on $\Sigma_{A'BCD}$ looks like

$$\nabla^{A'}{}_A\Sigma_{A'BCD} = (\iota_A\,\iota^{A'}\text{þ} + o_A\,o^{A'}\text{þ}' - \iota_A\,o^{A'}\eth - o_A\,\iota^{A'}\eth')\Sigma_{A'BCD}.$$

The eight independent components of the spinor $\Sigma_{A'BCD}$ can be defined in the following way

$$\Sigma_{0'0} \equiv o^{A'}o^Bo^Co^D\,\Sigma_{A'BCD}, \quad \Sigma_{0'1} \equiv o^{A'}\iota^Bo^Co^D\,\Sigma_{A'BCD},$$

$$\Sigma_{0'2} \equiv o^{A'}\iota^B\iota^Co^D\,\Sigma_{A'BCD}, \quad \Sigma_{0'3} \equiv o^{A'}\iota^B\iota^C\iota^D\,\Sigma_{A'BCD},$$

$$\Sigma_{1'0} \equiv \iota^{A'}o^Bo^Co^D\,\Sigma_{A'BCD}, \quad \Sigma_{1'1} \equiv \iota^{A'}\iota^Bo^Co^D\,\Sigma_{A'BCD},$$

$$\Sigma_{1'2} \equiv \iota^{A'}\iota^B\iota^Co^D\,\Sigma_{A'BCD}, \quad \Sigma_{1'3} \equiv \iota^{A'}\iota^B\iota^C\iota^D\,\Sigma_{A'BCD}.$$

Now, expanding $\Sigma_{A'BCD}$ into the above expression in terms of its components, i.e.

$$\Sigma_{A'BCD} \equiv \iota_{A'}\iota_{(B}\iota_C\iota_{D)}\Sigma_{0'0} - 3\,\iota_{A'}\iota_{(B}\iota_C o_{D)}\Sigma_{0'1} + 3\,\iota_{A'}\iota_{(B}o_C o_{D)}\Sigma_{0'2}-$$
$$- \iota_{A'}o_{(B}o_C o_{D)}\Sigma_{0'3} - o_{A'}\iota_{(B}\iota_C\iota_{D)}\Sigma_{1'0} + 3\,o_{A'}o_{(B}\iota_C\iota_{D)}\Sigma_{1'1}-$$
$$- 3\,o_{A'}\iota_{(B}o_C o_{D)}\Sigma_{1'2} + o_{A'}o_{(B}o_C o_{D)}\Sigma_{1'3},$$

taking the components of the resulting expression, and observing (2.13), one ends up with the following system of eight equations

$$\begin{aligned}
\text{þ}\,\Sigma_{1'0} - \eth\,\Sigma_{0'0} &= \rho\,\Sigma_{1'0}, & \text{þ}'\Sigma_{0'0} - \eth'\Sigma_{1'0} &= \rho\,(3\,\Sigma_{1'1} - \Sigma_{0'0}), \\
\text{þ}\,\Sigma_{1'1} - \eth\,\Sigma_{0'1} &= \rho\,(\Sigma_{1'1} - \Sigma_{0'0}), & \text{þ}'\Sigma_{0'1} - \eth'\Sigma_{1'1} &= \rho\,(2\,\Sigma_{1'2} - \Sigma_{0'1}), \\
\text{þ}\,\Sigma_{1'2} - \eth\,\Sigma_{0'2} &= \rho\,(\Sigma_{1'2} - 2\,\Sigma_{0'1}), & \text{þ}'\Sigma_{0'2} - \eth'\Sigma_{1'2} &= \rho\,(\Sigma_{1'3} - \Sigma_{0'2}), \\
\text{þ}\,\Sigma_{1'3} - \eth\,\Sigma_{0'3} &= \rho\,(\Sigma_{1'3} - 3\,\Sigma_{0'2}), & \text{þ}'\Sigma_{0'3} - \eth'\Sigma_{1'3} &= -\rho\,\Sigma_{0'3}.
\end{aligned}$$

In the coordinate representation (2.20), the principal parts of the weighted derivatives appearing above acquire the form

$$\text{þ} = \frac{1}{\sqrt{2}}\,(A\,\partial_t + B\,\partial_r), \quad \text{þ}' = \frac{1}{\sqrt{2}}\,(C\,\partial_t - B\,\partial_r).$$

Therefore, introducing the column vector

$$\Sigma \equiv (\Sigma_{0'0}, \Sigma_{0'1}, \Sigma_{0'2}, \Sigma_{0'3}, \Sigma_{1'0}, \Sigma_{1'1}, \Sigma_{1'2}, \Sigma_{1'3})^T$$

and defining the diagonal matrices

$$\Sigma^0 = \frac{1}{\sqrt{2}}\,\mathrm{diag}(C, C, C, C, A, A, A, A),$$
$$\Sigma^1 = \frac{B}{\sqrt{2}}\,\mathrm{diag}(-1, -1, -1, -1, 1, 1, 1, 1),$$

the above set of equations can be expressed into the form

$$\Sigma^0\,\partial_t\Sigma + \Sigma^1\,\partial_r\Sigma + \text{lower order terms} = 0.$$

The matrices Σ^0, Σ^1 are Hermitian. Keeping in mind that in the F-gauge (2.27) the functions A, B, C have the form $A = 1 - t\kappa'$, $B = \kappa$, and $C = 1 + t\kappa'$, then Σ^0 is, in addition, positive definite in the range $|t| < \kappa'^{-1}$, i.e. in the domain of hyperbolicity of our setting, see Fig. 4.1. Thus, the system (4.12) is symmetric hyperbolic in the physically interesting parts of our construction and, consequently, defines there a well-posed problem for (4.11).

Chapter 5

Numerical analysis of the spin-2 wave system

5.1 Preliminaries

In this chapter, we will try to numerically simulate the initial value problem posed by the spin-2 wave equation (4.8) and the findings of sec. 4.4. Specifically, we will prescribe initial data that satisfy the constraints (2.31) of the first order system and subsequently evolve it with (4.8). In addition, the boundary conditions will be also specified from the first order system. The numerical setting described in sec. 3.1, with slight modifications, will be also used here. Namely, an equidistant grid will be introduced to discretise the computational domain; the continuous spatial derivatives in (4.8) will be approximated by appropriate SBP operators; the boundary conditions will be imposed through the SAT method; and the temporal integration will be performed with explicit fourth order Runge-Kutta techniques.

Observing (4.8), one quickly realises that **Definition 3** must be supplemented with a similar definition for the second spatial derivative appearing therein. Of course, one could avoid this by using the first derivative SBP operator twice. In this way, the first derivative SBP operators would be also used to define their second derivative counterparts. Thus, one has to construct a first derivative SBP operator that is stable and minimises the error for both first and second derivatives. A procedure not as simple as it sounds. It turns out, see [10], [56], that this approach restricts the freedom of choosing the second derivative SBP operator and,

consequently, would lead to lower accuracy.

Ideally, one would like to minimize as much as possible the dependence of the definition of the second derivative SBP operators on **Definition 3**. In this way there would be more freedom at hand to construct more accurate second derivative operators. It turns out that such an objective is feasible [10], [56], [57], [58]. Therein, for stability reasons, the construction of the second derivative operators is based on the same norm matrix H as in the case of the SBP operators approximating the first derivative. This is the only restriction that the first derivative SBP operators impose upon their second derivative counterparts.

Now, one has to decide how to solve the system (4.8) numerically: in a first or second order form? Here, we will choose the former representation for a number of reasons. Firstly, the numerical implementation of the system (4.8) in a first order formulation is quite simple and very well studied. The imposition of the boundary conditions with the SAT method is also simpler in the first order case. In addition, when (4.8) is considered in its second order form, the construction of SBP operators introduces an extra stability requirement that limits the operators available to those with diagonal norm, see [56] for the details.

5.2   Second derivative SBP operators

Here, we will show how to construct SBP finite difference operators that approximate the second spatial derivative in (4.8). To begin with, introducing the column vector $\phi \equiv (\phi_0, \phi_1, \phi_2, \phi_3, \phi_4)^T$ the principal part of (4.8) can be expressed in the form

$$\partial_{tt}\phi = C\,\partial_{rr}\phi + \text{lower order terms,}$$

where

$$C = c\,I \quad \text{with} \quad c \equiv \frac{\kappa^2}{1 - t^2\kappa'^2},$$

$\phi \equiv (\phi_0, \phi_1, \phi_2, \phi_3, \phi_4)^T$, and I is the 5×5 identity matrix. For our purposes in the present section, it suffices to keep the first two terms of the principal part of (4.8); the inclusion of lower order terms would not affect the results of the subsequent derivation. Defining the ten dimensional column vector $\mathrm{v} \equiv (\partial_t\phi, \phi)^T$, the above

system can be written in the first order form

$$\partial_t \mathrm{v} = \begin{pmatrix} 0 & C \\ 0 & 0 \end{pmatrix} \partial_{rr}\mathrm{v} + \text{lower order terms},$$

where the entries of the above matrix are 5×5 matrices. Here, we will not work in the above generalised setting. Observing (4.8), one can write a first order system of the above form for each component of the spin-2 field

$$\partial_t \mathrm{v}_\lambda = \bar{C}\,\partial_{rr}\mathrm{v}_\lambda + \text{lower order terms}$$

with

$$\bar{C} \equiv \begin{pmatrix} 0 & c \\ 0 & 0 \end{pmatrix},$$

where c is now just a 1×1 element, v_λ is a two dimensional column vector, and as usual $\lambda = 0, \ldots, 4$.

In order to unveil the constitutive properties of the second derivative SBP operators and exemplify the requirements that lead to their definition, the above first order system will be approximated with its closest scalar counterpart, namely the 1-D heat equation

$$u_t = \Lambda\,u_{rr}, \quad 0 \le r \le 1, \quad t \ge 0, \tag{5.1}$$

where Λ is an arbitrary positive constant. Initial and boundary conditions will be prescribed to (5.1) in the next section, where the SAT method will be discussed. The subsequent results derived for (5.1) can be generalised to systems with non-constant coefficient matrices, see sec. 9.2 of [42]. As in sec. 3.2, using the notation $(u, w) \equiv \int_0^1 u\,w\,dr$, the expression (5.1), and integration by parts, the energy estimate for (5.1) reads

$$\frac{d}{dt}||u||^2 = \Lambda(u, u_{rr}) + (u_{rr}, u) = 2\Lambda(u\,u_r|_0^1 - ||u_r||^2), \tag{5.2}$$

where again $||u||^2 \equiv (u, u)$.

Let's denote the discrete version of the continuous second derivative operator in (5.1) as

$$\frac{d^2 u}{dr^2} \equiv D_2,$$

then the semi-discrete 1-D heat equation looks like

$$v_t = D_2 v, \tag{5.3}$$

107

where again $v = (v_0, v_1, \ldots, v_{N-1}, v_N)^T$ and D_2 is a $N \times N$ matrix. If D_2 is going to be an SBP operator, then it must satisfy a discrete version of the energy estimate (5.2). Using the discrete notation $||v||^2 = (v, v)_H \equiv v^T H v$ and the semi-discrete heat equation (5.3), one can write the discrete version of (5.2) in the form

$$\frac{d}{dt}||v||^2 = \frac{d}{dt}\left(v^T H v\right) = \Lambda\, v^T \left(D_2^T H + H D_2\right) v.$$

Choosing

$$D_2 = H^{-1}(-A + C),$$

this choice will be justified in the following, the above energy estimate becomes

$$\frac{d}{dt}||v||^2 = \Lambda\, v^T \left((-A + C)^T (H^{-1})^T H - A + C\right) v.$$

To continue, we have to use a norm matrix H that is symmetric, i.e. $H = H^T$. Under this assumption, the expression of the energy estimate simplifies to

$$\frac{d}{dt}||v||^2 = -\Lambda\, v^T \left(A^T + A\right) v + \Lambda\, v^T \left(C^T + C\right) v.$$

The first term in the above expression replicates the last term in (5.2) whenever $A^T + A \geq 0$. Hence, in order to fully mimic the continuous estimate, C must be a boundary matrix involving only points at the boundaries. By choosing

$$C = BS,$$

where $B = \mathrm{diag}(-1, 0, \ldots, 0, 1)$ and S is an appropriate approximation of the first derivative operator at the boundary, the discrete energy estimate finally reads

$$\frac{d}{dt}||v||^2 = -\Lambda\, v^T \left(A^T + A\right) v + 2\,\Lambda\left(v_N (Sv)_N - v_0 (Sv)_0\right), \tag{5.4}$$

which obviously mimics the continuous result (5.2) when $A^T + A \geq 0$ holds. Thus, we are led to the definition of a second derivative SBP operator.

Definition 4 *The second order finite difference operator $D_2 = H^{-1}(-A + BS)$ is an SBP operator iff*

   i) H is symmetric, i.e. $H = H^T > 0$,

   ii) $A^T + A \geq 0$,

iii) $B = diag(-1, 0, \ldots, 0, 1)$,

iv) S *is an approximation of the first derivative operator at the boundary.*

Any operator of the form $D_2 = H^{-1}(-A + BS)$ that approximates $\partial^2/\partial r^2$ and satisfies the criteria of **Definition 4** is a second derivative SBP operator that leads to an energy estimate (5.4) and, consequently, guarantees the numerical stability of our code. Such kind of operators were firstly introduced in [10] but did not satisfy the *ii)* requirement of **Definition 4**; later in [56] a wide variety of second derivative SBP operators that satisfy all the requirements of **Definition 4** were constructed.

It can be readily checked that the inclusion of lower order terms like λu_r in the above derivation would lead again to an energy estimate. Their presence would just add terms of the form (3.3) and (3.6) to the continuous (5.2) and discrete (5.4) energy estimates, respectively. Notice that now in the evaluation of the discrete energy estimate (5.4) the same norm matrix H must be used in the derivation of the energy terms related to the first and the second derivative. This essentially is the only additional requirement that is introduced when dealing with systems that involve approximations of both first and second derivatives.

In the following, a variety of different combinations of the first and second derivative SBP operators will be used in our numerical experiments. Specifically, we will combine SBP operators based on a diagonal or full norm that respect the above requirement of approximating both the first and second derivative with SBP operators of the same norm. However, we will also use a combination of SBP operators that violate this requirement. From now on, for the sake of clarity, an SBP operator that is nth-order accurate in the interior and kth-order at the boundary will be denoted by (n, k) and called an (n, k)-operator.

5.3   SAT method

In order to implement boundary conditions to (5.1) with the SAT method, we have to be a little bit more careful and include in our study the lower order terms of (4.8) that involve first spatial derivatives, i.e. terms of the form $\partial_{tr}\phi_\lambda$ and $\partial_r\phi_\lambda$. In contrast to the additive contribution of the first and second derivative terms in the energy estimates derived in the previous section, the penalty terms due to the SAT

method are not contributing additively as a single penalty term accommodates both spatial derivatives.

In the first order formulation $v_\lambda = (\partial_t \phi_\lambda, \phi_\lambda)^T$ introduced in the preceding section we can write (4.8) in the form

$$\partial_t v_\lambda = \begin{pmatrix} 0 & a \\ 0 & 0 \end{pmatrix} \partial_{rr} v_\lambda - \begin{pmatrix} b & c \\ 0 & 0 \end{pmatrix} \partial_r v_\lambda + \text{lower order terms},$$

where $a = \dfrac{\kappa^2}{1 - t^2 \kappa'^2}$, $b = \dfrac{2t\kappa\kappa'}{1 - t^2\kappa'^2}$, and $c = \dfrac{2r\kappa\mu'}{1 - t^2\kappa'^2}$. Again, in order to exemplify the use of the SAT method in the simplest possible way, we will approximate the above system with its closest scalar counterpart. The scalar advection-diffusion equation will serve this purpose

$$u_t = \Lambda\, u_{rr} - \lambda\, u_r, \quad 0 \le r \le 1, \quad t \ge 0, \tag{5.5}$$

where Λ, λ are positive constants, supplemented with Robin boundary conditions

$$\alpha\, u(t,0) + u_r(t,0) = g_0(t), \quad \beta\, u(t,1) + u_r(t,1) = g_N(t) \tag{5.6}$$

and initial conditions $u(0,x) = f(x)$, $u_t(0,x) = h(x)$. (Where α and β are arbitrary constants.)

It must be mentioned here that the choice (5.6) is not unique, there are numerous other possible choices depending on the problem under consideration. To implement boundary conditions for the system (4.8), we can also use other formulations of boundary conditions which are known to lead to well-posed problems for the wave equation like Neumann or Sommerfeld type boundary conditions. Since we need to use informations from the 1st order formulation of the spin-2 equation (as discussed in sec. 4.4), which provides relations for the values of the first derivatives of the components but not for the values of the functions themselves, we cannot impose Dirichlet conditions.

Combining (3.3) and (5.2), one gets the continuous energy estimate for the equation (5.5)

$$\frac{d}{dt}||u||^2 = 2\Lambda(u\, u_r|_0^1 - ||u_r||^2) - \lambda\, u^2|_0^1,$$

which when the boundary conditions (5.6) are taken into account takes the quite complicated form

$$\begin{aligned} \frac{d}{dt}||u||^2 = &-(\lambda + 2\,\Lambda\,\beta)\, u(t,1)^2 + (\lambda + 2\,\Lambda\,\alpha)\, u(t,0)^2 + \\ &+ 2\,\Lambda\, g_N(t)\, u(t,1) - 2\,\Lambda\, g_0(t)\, u(t,0) - 2\,\Lambda\,||u_r||^2, \end{aligned} \tag{5.7}$$

where for the choice $\lambda + 2\Lambda\beta > 0$ and $\lambda + 2\Lambda\alpha < 0$ an energy estimate always exists [56]. Fortunately, the situation simplifies considerably in our case because of the form of the characteristics curves of (4.8), see Fig. 4.1. The cylinder is a total characteristic of our system, thus we do not have to worry about the boundary treatment of the point at the origin $r = 0$ of the computational domain.

We will try now to mimic (5.7) in the semi-discrete case. According to [10], [55], [56] boundary terms can be added to (5.5) by the SAT method in the following way

$$
\begin{aligned}
v_t = \Lambda\,D_2\,v - \lambda\,D_1\,v - \tau_0\,H^{-1}[E_0(\alpha I + S)v - e_0\,g_0(t)] - \\
- \tau_N H^{-1}[E_N(\beta I + S)v - e_N\,g_N(t)],
\end{aligned}
\tag{5.8}
$$

where $E_0 = \mathrm{diag}(-1, 0\ldots, 0)$, $E_N = \mathrm{diag}(0, \ldots, 0, 1)$ are $N \times N$ matrices, $e_0 = (1, 0, \ldots, 0)$, $e_N = (0, \ldots, 0, 1)$, I is the $N \times N$ identity matrix, D_1, D_2, S are as in **Definition 3** and **Definition 4**, and τ_0, τ_N are the so-called penalty parameters. A convenient choice of the penalty parameters is $\tau_N = -\tau_0 = \Lambda$. With this choice the semi-discrete energy estimate (5.4) takes the form

$$
\begin{aligned}
\frac{d}{dt}||v||^2 = -(\lambda + 2\,\Lambda\,\beta)\,v_N^2 + (\lambda + 2\,\Lambda\,\alpha)\,v_0^2 + \\
+ 2\,\Lambda\,g_N(t)\,v_N - 2\,\Lambda\,g_0(t)\,v_0 - \Lambda\,v^T\left(A^T + A\right)v,
\end{aligned}
\tag{5.9}
$$

which for $A^T + A \geq 0$ completely mimics (5.7). Notice that for compact supported data $g_N(t) = 0$, the choice $\lambda + 2\,\Lambda\,\beta > 0$ and $\lambda + 2\,\Lambda\,\alpha < 0$ leads always to an energy estimate. The choice $\tau_N = -\tau_0 = \Lambda$ simplifies also considerably (5.8), i.e.

$$
\begin{aligned}
v_t = -\Lambda\,H^{-1}A\,v - \lambda\,H^{-1}Q\,v + \Lambda\,H^{-1}[\alpha E_0 v - e_0\,g_0(t)] - \\
- \Lambda H^{-1}[\beta E_N v - e_N\,g_N(t)],
\end{aligned}
\tag{5.10}
$$

where the expanded expressions of the first and second derivative SBP operators were taken also into account.

5.4   The exact solution

Again before we start using our code in a general setting, we have to test it against the exact solution derived in Appendix A. Therefore, we will try to reproduce numerically the exact solution (A.12) in the context of the spin-2 wave system described by (4.8). According to the discussion in sec. 4.4, the initial data must

satisfy the constraints (2.31) of the first order system and be subsequently evolved with the second order system (4.8). In a similar way with sec. 3.4.1, the initial data will be derived from the exact solution (A.12).

As before, we set $t = 0$ in (A.12) and get initial data that satisfy initially the constraints:

$$\phi_0 = \phi_4 = \frac{r^2}{(1+r)^3}, \quad \phi_1 = \phi_3 = \frac{2\,r^2}{(1+r)^3}, \quad \phi_2 = \frac{\sqrt{6}\,r^2}{(1+r)^3}. \tag{5.11}$$

In addition, because of the second order nature of (4.8), the values of the first temporal derivative of the spin-2 field's components must be also specified on the initial hypersurface. Differentiating (A.12) with respect to t and evaluating at $t = 0$ one gets

$$\partial_t \phi_0 = \partial_t \phi_1 = -\partial_t \phi_3 = -\partial_t \phi_4 = -\frac{4\,r^2}{(1+r)^4}, \quad \partial_t \phi_2 = 0. \tag{5.12}$$

The cylinder is a total characteristic of (4.8), see Fig. 4.1, thus only boundary conditions at $r = 1$ must be imposed. In contrast to the first order case, here we have to implicitly prescribe boundary conditions to all of the components of the spin-2 zero-rest-mass field. Therefore, again, by differentiating (A.12) with respect to the spatial coordinate r and subsequently evaluating at $r = 1$, Robin boundary condition of the form (5.6) can be obtained for each component of the spin-2 field:

$$g_{0,N}(t) = -\frac{1}{256}\,(-2 + t)^3(6 + t), \quad g_{1,N}(t) = \frac{1}{128}\,(48 - 32t + t^4),$$

$$g_{2,N}(t) = -\frac{1}{128}\,\sqrt{\frac{3}{2}}\,(t^2 - 4)(12 + t^2), \tag{5.13}$$

$$g_{3,N}(t) = \frac{1}{128}\,(48 + 32t + t^4), \quad g_{4,N}(t) = -\frac{1}{256}\,(-6 + t)(2 + t)^3,$$

where we chose $\beta = 1$. The above boundary conditions will be imposed with the SAT techniques described in the preceding section.

Now, the initial data (5.11), (5.12) will be evolved with the second order system (4.8) for three different choices of finite difference SBP operators.

5.4.1 Diagonal norms

Firstly, a minimal width,[1] diagonal norm, second derivative $(4, 2)$-operator, i.e.

---

[1]A second derivative SBP operator of the same width and internal order of accuracy as the corresponding first derivative approximation [56].
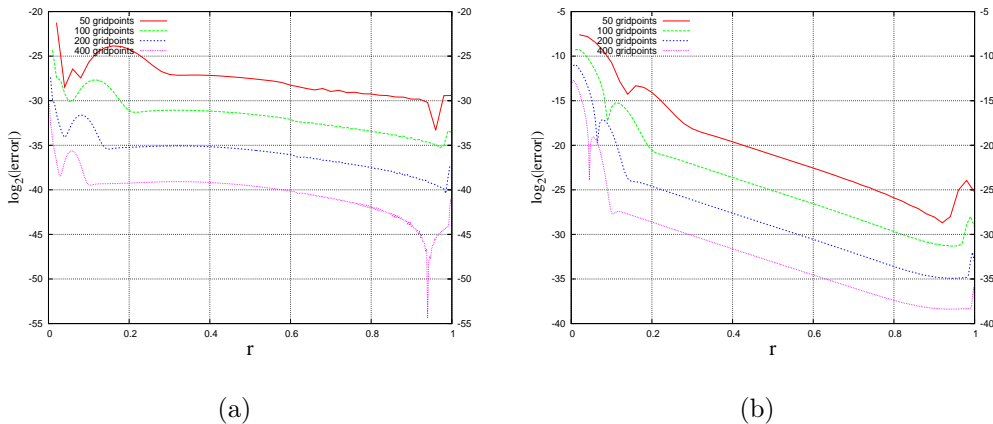
Figure 5.1: The convergence plots of (a) ϕ_0 and (b) ϕ_4 for the evolution of the initial data (5.11), (5.12) at time $t = 1$ when finite difference SBP operators based on a diagonal norm with boundary closure two orders less accurate than the interior are used. The absolute error is computed against the exact solution (A.12).

fourth order accurate in the interior and second order at the boundary, accompanied by a first derivative SBP operator of the same accuracy and norm will be used—both given in [56]. The resulting convergence plots for the components ϕ_0, ϕ_4 at time $t = 1$ are depicted in Fig. 5.1. It is obvious that the numerical results reproduce quite accurately the exact ones as the maximum of the absolute error between them starts at roughly an order of 10^{-2} and decreases with third order. The behaviour of the convergence rates with time for each component of the spin-2 field is illustrated in Fig. 5.2. During the evolution the convergence rates are well above 3. Fourth order convergence could not be achieved with this combination of operators mainly because of the complexity of the boundary conditions (5.13). (We have to keep also in mind that the expected accuracy of the first derivative operator,[2] when used alone in first order hyperbolic problems of the form (3.2), is roughly of 3rd order [56].) In the following section, we will see that for less demanding boundary conditions fourth order accuracy can be achieved even with the above choice of SBP operators. At the last stages of the evolution the convergence rates, as expected, slightly decrease. The reason for this behaviour can be traced back to the fact that

---

[2]Notice that its accuracy at the boundary is two orders less than in the interior.
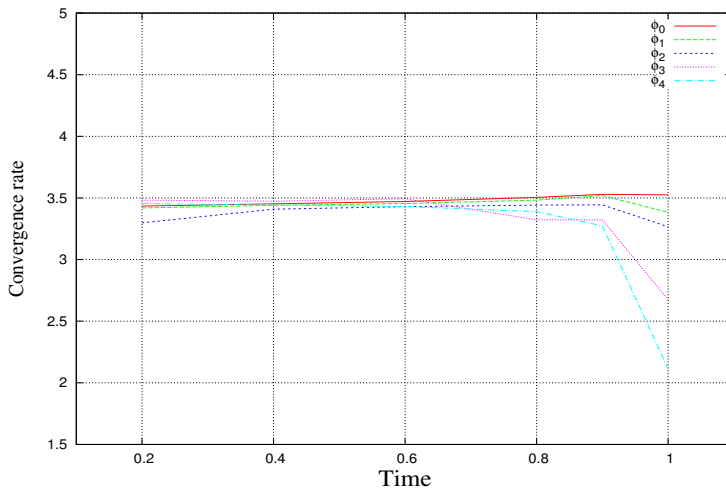
Figure 5.2: The convergence rates for the components of the spin-2 zero-rest-mass field. SBP operators with a diagonal norm and a boundary closure two orders less accurate than the interior are used.

the characteristic speed increases rapidly while approaching the ill-behaved region I^+ where null and space-like infinity meet, see Fig. 4.1. Our results are in complete agreement with the corresponding results in [56].

5.4.2   Full norms

In order to produce even better results, one naturally would try to use more accurate SBP operators near the boundary. For this, we approximate the second order derivatives with the minimal width, full norm $(4, 2)$-operator given in [56]. The first order derivatives are approximated by the corresponding first order $(4, 3)$-operator of the same norm matrix originally constructed in [10]. The time dependence of the convergence rates for the components of the spin-2 field and the convergence plot of the component $\phi_4{}^3$ at $t = 1$ are presented in Fig. 5.3. Qualitatively, the numerical behaviour of our system is roughly similar with the case above where SBP operators based on a diagonal were used. Notice though that the maximum of the absolute error between the numerical and the exact data starts now roughly at an order of 10^{-3} and decreases with fourth order. Thus, by using SBP operators based on a

---

[3]We chose ϕ_4 mainly because we want to get an estimation of the maximum error; notice that ϕ_4 exhibits the lowest accuracy among the components of the spin-2 field.
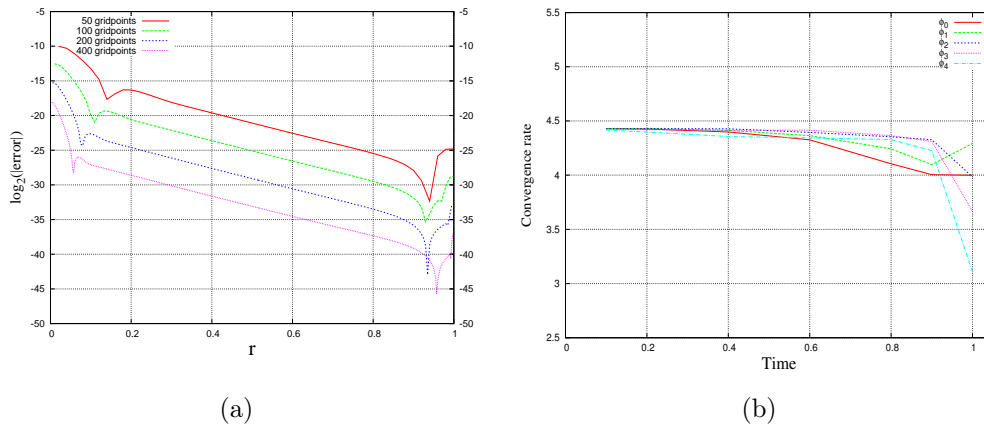
Figure 5.3: (a) The convergence plot of the component ϕ_4 at $t = 1$. (b) The convergence rates for the components of the spin-2 zero-rest-mass field. SBP operators with a full norm and a boundary closure of two and one order less accurate than the interior are used to approximate the second and first derivative, respectively.

full norm the accuracy of our results increased by at least one order of magnitude and the convergence of our code by one order. The fact that the convergence rates and the accuracy are better now is not surprising as the first derivative operator we are using now is one order more accurate at the boundary. Lastly, as expected, due to the increase of the characteristic speed, there is again a small decrease in the convergence rates of the components of the spin-2 field near $t = 1$.

5.4.3 Different norms

Here, we will experiment with the possibility of combining first and second derivative SBP operators based on different norm matrices. Specifically, we combine the second derivative $(4, 2)$-operator used in the previous section with the minimum bandwidth, restricted full norm first derivative $(4, 3)$-operator constructed in [83], the use of which proved quite successful in the numerical implementation of the first order system. Of course, with this choice, we consciously violate the requirement of approximating both first and second derivatives with SBP operators of the same norm [56]. Theoretically though, under certain conditions on the norm matrices of the two operators, energy estimates of the form (5.9) might be still possible to be

115

obtained. With the above choice of SBP operators, the convergence plots for the components ϕ_0, ϕ_4 at $t = 1$ and the time evolution of the convergence rates are depicted in Fig. 5.4. Interestingly, comparing these results with the corresponding ones in sec. 5.4.2, where SBP operators based on the same norm were used, we notice that the accuracy of our results and the behaviour of the convergence rates are very similar—almost identical!
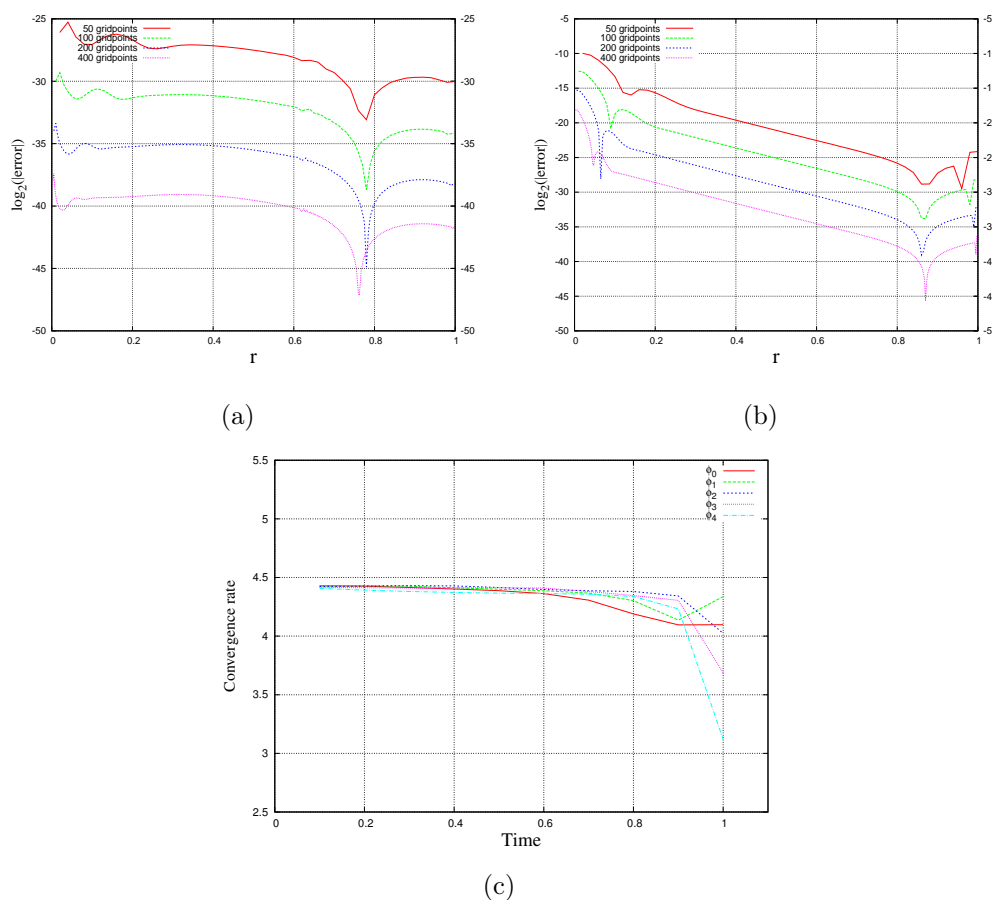

(a)

(b)

(c)

Figure 5.4: The convergence plots of (a) ϕ_0 and (b) ϕ_4 for the evolution of the initial data (5.11), (5.12) at time $t = 1$. First and second finite difference SBP operators based on different norms are used. (c) The time evolution of the corresponding convergence rates.

The results displayed in Fig. 5.4 indicate that the requirement of using (first and second derivative) SBP operators that are based on the same norm does not

116

seem very restrictive in our case. Results of similar accuracy and convergence were obtained with another restricted full norm first derivative $(4, 3)$-operator taken from [16]. It seems that the second derivative full norm operator we are using is performing quite well when combined with first derivative SBP operators based on restricted full norms. From our numerical findings, it appears that requiring the same norm for first and second derivative SBP operators is sufficient but not necessary for stability.

5.4.4 Conservation of the constraints

Finally, we will check the behaviour of the constraint quantities (2.32) during the evolution of our system. The data evaluated for the choice of SBP operators in sec. 5.4.2 will be also used here to obtain the constraint quantities (2.32). Our computational domain consists of 400 grid points. The constraints are initially violated at an order of 10^{-10}. The behaviour with time of the normalised l^2 norm
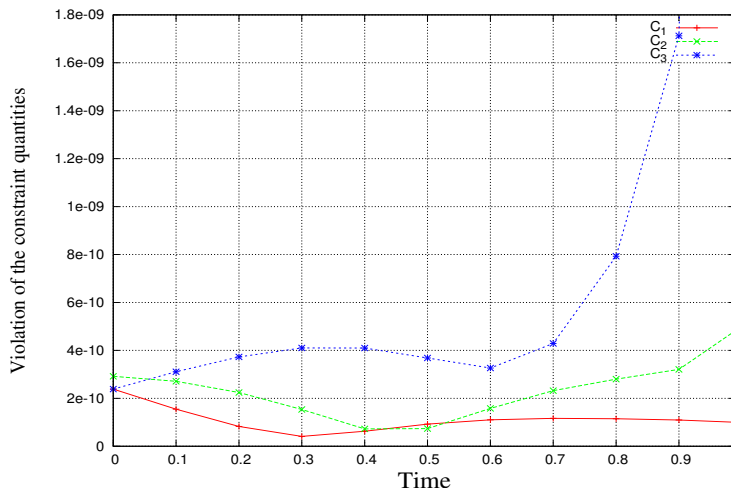

Figure 5.5: Violation of the vanishing of the constraint quantities (2.32) for various time instances. The normalised l^2 norm for each one of the quantities C_k is shown.

for each one of the constraint quantities is illustrated in Fig. 5.5. The magnitude of the constraint violation during the evolution remains roughly the same. A slight increase is observed again as we approach I^+. This increase is mainly picked up by the quantity C_3. Something that can be easily explained by observing the definition (2.32) of C_3 and the results of Fig. 5.3. Namely, the observed increase in the violation

of the quantity C_3 is actually reflecting the loss of convergence of the components ϕ_3, ϕ_4 while approaching I^+, see Fig. 5.3.

5.5 General initial data

In this section, we will attempt to evolve more general data, i.e. data that does not comprise an exact solution of (4.8). First, we have to specify initial conditions. Again, in accordance with sec. 4.4, the initial data must satisfy the conformal constraints (2.31). Here, we will use the constraints in the form (3.13)

$$X_0 = X_4 = \frac{-\alpha_0^2 X_2 + 2\, r\, \partial_r X_2 + 2\, r^2\, \partial_{rr} X_2}{\alpha_0\, \alpha_2}, \quad X_1 = X_3 = \frac{r\, \partial_r X_2}{\alpha_0},$$

a choice that leaves the component ϕ_2—recall that $X_i = \mu^{-3}\, \phi_i$—completely to our disposal and allows us to compute the rest of the components in a simple algebraic way.

Let's assume that the initial data for ϕ_2 has the form of a bump function

$$\phi_2(r) = \begin{cases} (4\, r\, b^{-2})^{16}(r-b)^{16}, & 0 \le r \le b \\ 0, & b \le r \le 1 \end{cases}. \tag{5.14}$$

centered at $r = b/2$, then the initial data for the rest of the components can be easily computed from the aforedisplayed formulas. We also have to specify initially the first temporal derivative of the spin-2 field's components. The evolution equations (2.30) of the first order system will be used for this purpose, i.e.

$$\begin{aligned}
\dot{\phi}_0(r) &= \kappa\, \phi_0'(r) - (3\kappa' - \mu)\, \phi_0(r) - \alpha_2\, \mu\, \phi_1(r), \\
\dot{\phi}_1(r) &= \frac{1}{2}\, \alpha_2\, \mu\, \phi_0(r) - \frac{1}{2}\, \alpha_0\, \mu\, \phi_2(r) - \mu\, \phi_1, \\
\dot{\phi}_2(r) &= \frac{1}{2}\, \alpha_0\, \mu\, \phi_1(r) - \frac{1}{2}\, \alpha_0\, \mu\, \phi_3(r), \\
\dot{\phi}_3(r) &= \frac{1}{2}\, \alpha_0\, \mu\, \phi_2(r) - \frac{1}{2}\, \alpha_2\, \mu\, \phi_4(r) + \mu\, \phi_3(r), \\
\dot{\phi}_4(r) &= -\kappa\, \phi_4'(r) + (3\kappa' - \mu)\, \phi_4(r) + \alpha_2\, \mu\, \phi_3(r),
\end{aligned} \tag{5.15}$$

where the values of the fields on the r.h.s can be evaluated from (5.14) and the spatial derivatives will be approximated by first derivative SBP operators. (The $\dot{\ }$ and $'$ denote differentiation with respect to the temporal and spatial coordinate, respectively.)

Now, we explain how to specify the boundary conditions. As discussed in sec. 4.4 we need to use the available information from the first order system (2.30)-(2.31). In this system there is only one component, namely ϕ_0, which propagates inward from the boundary at $r = 1$. Thus, there is only one free function to be specified on that boundary, which characterizes the solution inside for given initial data. This must be also the case for the second order system after imposing the boundary conditions.
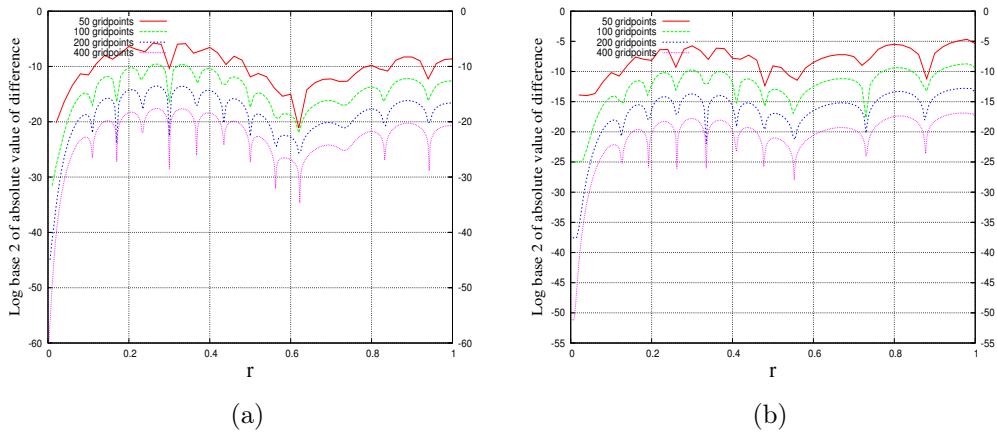

(a) (b)

Figure 5.6: The convergence plots of (a) ϕ_0 and (b) ϕ_4 for the evolution of the initial data (5.14), (5.15), centered around $r = 0.5$, at time $t = 1$ in the "diagonal" representation of Fig. 2.2(b).

The second order wave equations (4.8) require for each component of the spin-2 field a boundary condition at $r = 1$. (Recall that $r = 0$ is a total characteristic so we cannot prescribe any conditions there.) We impose these conditions in the form of a Robin condition (5.6), i.e.

$$g_{i,N}(t) = \phi_i(t, 1) + \phi_i'(t, 1), \quad i = 0, 1, 2, 3, 4, \tag{5.16}$$

where we set $\beta = 1$. The boundary functions $g_{i,N}(t)$ are computed from the first order system in terms of the fields and their time derivatives on each computational time slice from the already available data. Specifically, the values of the spatial derivatives of the fields ϕ_1-ϕ_3 and ϕ_0, ϕ_4 appearing in (5.16) will be approximated by the constraints (2.31) and the evolution equations (2.30) of ϕ_0 and ϕ_4, respectively.

119

Namely, the $\phi'_i(t, 1)$ are given by

$$\phi'_0(t, 1) = \frac{1}{\kappa}((1 + t\kappa')\,\partial_t\phi_0 + (3\kappa' - \mu)\,\phi_0 + \alpha_2\,\mu\,\phi_1)|_{r=1},$$

$$\phi'_1(t, 1) = \frac{1}{2\,\kappa}(6\,r\mu'\phi_1 - 2\,t\,\kappa'\mu\,\phi_1 + \alpha_0\,\mu\,(1 - t\kappa')\,\phi_2 + \alpha_2\,\mu\,(1 + t\kappa')\,\phi_0)|_{r=1},$$

$$\phi'_2(t, 1) = \frac{1}{2\,\kappa}(6\,r\mu'\phi_2 + \alpha_0\,\mu\,(1 - t\kappa')\,\phi_3 + \alpha_0\,\mu\,(1 + t\kappa')\,\phi_1)|_{r=1},$$

$$\phi'_3(t, 1) = \frac{1}{2\,\kappa}(6\,r\mu'\phi_3 + 2\,t\,\kappa'\mu\,\phi_3 + \alpha_0\,\mu\,(1 + t\kappa')\,\phi_2 + \alpha_2\,\mu\,(1 - t\kappa')\,\phi_4)|_{r=1},$$

$$\phi'_4(t, 1) = \frac{1}{\kappa}(-(1 - t\kappa')\,\partial_t\phi_4 + (3\kappa' - \mu)\,\phi_4 + \alpha_2\,\mu\,\phi_3)|_{r=1}.$$

Since ϕ_0 is freely specifiable on the boundary we choose it simply as zero,[4] so that ϕ_0 and its time derivative vanish on the boundary. Wherever ϕ_0 appears in the equations used, we simply drop it. This means that the first two expression displayed above simplify to

$$\phi'_0(t, 1) = \frac{\alpha_2}{r}\,\phi_1|_{r=1},$$

$$\phi'_1(t, 1) = \frac{1}{2\,\kappa}(6\,r\mu'\phi_1 - 2\,t\,\kappa'\mu\,\phi_1 + \alpha_0\,\mu\,(1 - t\kappa')\,\phi_2)|_{r=1}.$$

The boundary conditions (5.16) will be imposed with the SAT techniques discussed in sec. 5.3.

Here, again, the simplest non-trivial case $l = 2$ in the "diagonal" representation of Fig. 2.2(b) will be considered. (The numerical analysis of a higher mode, e.g. $l = 10$, can be found in Appendix B.) The spatial derivatives will be approximated with the combination of the first and second derivative $(4, 2)$-operators of the same norm constructed in [10] and [56], respectively, that proved quite successful in the case of the exact solution, see sec. 5.4.2. The parameter b in (5.14) will be chosen $b = 1$, which suggests that initially our data is centered around $r = 0.5$. The numerical solutions and the convergence plots of ϕ_0, ϕ_4 for the evolution of this data are presented in Figs. 3.4 and 5.6, respectively. The absolute error is computed with respect to the numerical simulation with the highest resolution, which here is 800 grid points. The code is converging with fourth order, see Tab. 5.1, and produces an absolute error, compared to the numerical solution with the highest resolution (800 grid points), that starts at an order of 10^{-1} and decreases with fourth order.

---

[4]That is a very reasonable choice as ϕ_0 is purely "ingoing", i.e. moves towards the cylinder I at $r = 0$.

	ϕ_0		ϕ_4	
Grid	$\log_2(\|\|E\|\|_2)$	Rate	$\log_2(\|\|E\|\|_2)$	Rate
50	-2.5929		-1.2413	
100	-6.4725	3.8796	-5.1716	3.9303
200	-10.4455	3.9730	-9.1489	3.9772
400	-14.5248	4.0793	-13.2228	4.0739

Table 5.1: The normalised l^2 norm of the absolute error E, compared to the numerical simulation with the higher resolution (800 grid points), and the corresponding convergence rates at time $t = 1$ for the evolution of the initial data (5.14), (5.15).

The behaviour of the constraint quantities (2.32) during the evolution of the initial data (5.14), (5.15) is depicted in Fig. 5.7. The results therein are obtained from the numerical data with the highest resolution, i.e. 800 grid points. The initial violation of the constraints is roughly of the order of 10^{-7}, and remains at these levels during the evolution.
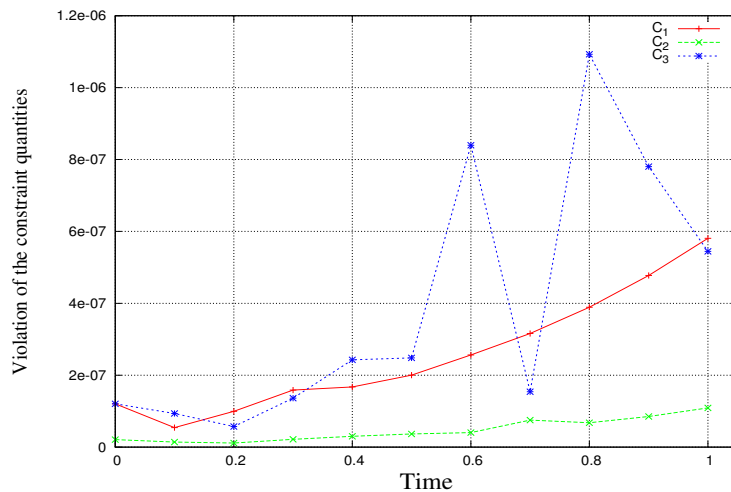

Figure 5.7: Violation of the vanishing of the constraint quantities (2.32) for various time instances. The normalised l^2 norm for each one of the quantities C_k is shown.

Performing the above numerical experiments with the diagonal norm SBP operators given in [56], which were also used in sec. 5.4.1, similar results with the ones

in Fig. 5.6 and Tab. 5.1 could be obtained, i.e. fourth order convergence. But, at the last stages of the evolution, the observed violation of the constraints was one to three orders of magnitude, depending on the component of C_k, higher than the one depicted in Fig. 5.7. This behaviour is most probably due to the lower (by one order) accuracy of the first derivative SBP operator at the boundary.

We also evolved the initial conditions (5.14), (5.15) in the above setting using a combination of operators based on different norms. Specifically, the initial data was evolved with the second derivative $(4, 2)$-operator and the two different first derivative $(4, 3)$-operators, all used in sec. 5.4.3. Results almost identical with the ones depicted in Figs 5.6, 5.7 and Tab. 5.1 were obtained, confirming our previous statement made in sec. 5.4.3 that the specific combination of SBP operators with different norms we are using perform as well as the one based on the same norm.

The dependence of the convergence rates to the proximity of the initial data to the cylinder I was also studied. The same behaviour as in the first order case, see Fig. 3.6, was observed. Namely, for the same resolution, the convergence rates are getting smaller and smaller the closer we place the initial data to the cylinder. In addition, the performance of the code for the two representations of Fig. 2.2 mimics the results obtained in the first order system, see Fig. 3.8. While approaching the region I^+, the convergence rates in the "horizontal" case of Fig 2.2(a) decrease faster than the corresponding ones in the "diagonal" representation of Fig 2.2(b). Moreover, the code becomes again unstable earlier in the "horizontal" representation.

	ϕ_0		ϕ_4	
Grid	$\log_2(||E||_2)$	Rate	$\log_2(||E||_2)$	Rate
50	0.4593		0.5439	
100	-3.4714	3.9307	-3.5608	4.1047
200	-7.4508	3.9794	-7.4986	3.9378
400	-11.4352	3.9844	-11.4859	3.9873

Table 5.2: Convergence of the solutions to the wave equations towards a solution at high resolution (800 grid points) of the first order equations. The table shows the (logarithms of) the normalized l^2 norm of the absolute differences and the corresponding convergence rates at time $t = 1$.

Finally, we reproduce numerically the analytic result of sec. 4.4: we show that if

the initial data satisfy the constraints (3.13) of the first order system and are evolved with the second order system (4.8), then the resulting numerical solutions converge (with increasing resolution) to the one obtained by evolving the same initial data with the evolution equations (2.30) of the first order system. We consider again initial data centered around $r = 0.5$ of the form (5.14), (5.15) and impose boundary conditions as described above. We evolve this data with both evolution systems and compute the absolute error between the numerical solutions of the second order approach and the numerical solution of the highest resolution (800 grid points) in the first order approach. The normalized l^2 norm of the computed absolute error and the corresponding convergence rates at time $t = 1$ for the components ϕ_0, ϕ_4 are listed in Tab. 5.2. We find that the solutions agree within numerical accuracy. This confirms the statement made in sec. 4.4 that the two systems have identical solutions given the same initial data.

5.6 Comparison of the two approaches

In the present section a comparison of the two numerical approaches presented in chapters 3 and 5 will be attempted. They both serve the same purpose of studying numerically the behaviour of gravitational fields near space-like infinity in Friedrich's conformal representation, briefly presented in chapter 1. We will try to investigate any possible advantages and/or disadvantages related to them, and then see if there are any good reasons to prefer the one over the other [49].

The first approach relies on the system of first order partial differential equations (2.30), (2.31), while the second on the system of second order partial differential equations (4.8). They both admit (A.12) as an exact solution. Thus, the first thing one could check is how well the two approaches reproduce (A.12). In Tab. 5.3 the logarithm of the normalised l^2 norm of the absolute error E, i.e. $\log_2(||E||_2)$, of the components ϕ_0, ϕ_4 for the two numerical approaches at time $t = 1$ in the "diagonal" representation is presented. Here, the same first derivative $(4, 3)$-operator developed in [10] is used in both approaches; the second derivatives are approximated by the $(4, 2)$-operator introduced in [56]. A slightly, but noticeable, better accuracy is achieved in the 2nd order approach; a result that confirms the first of the claims made in [49]. However, in the "horizontal" case the accuracy is slightly better in the 1st order approach, most probably because in the second order case the characteristic

	ϕ_0		ϕ_4	
Grid	1st order	2nd order	1st order	2nd order
50	-25.2218	-27.6006	-11.1643	-12.3418
100	-29.3956	-31.5941	-13.9924	-15.1743
200	-33.7109	-35.6075	-16.9978	-18.1782
400	-38.1000	-39.6068	-20.1075	-21.2850

Table 5.3: The logarithm of the normalised l^2 norm of the absolute error E, compared to the exact solution (A.12), at time $t = 1$ for the two numerical approaches in the "diagonal" representation.

curves of all the components, and not only of ϕ_0, of the spin-2 field tend to become horizontal in the limit $t = 1$. In addition, for the same resolution, the violation of the constraint is of the same order in both approaches. The only exception is the violation of the C_3 quantity, which at the last stages of the evolution is slightly more violated in the 2nd order case. The rapid increase of the characteristic speed, and the subsequent loss of accuracy, while approaching I^+ in combination with the fact that we have to impose a boundary condition at $r = 1$ for the purely "outgoing" field ϕ_4—in terms of which C_3 is defined—can be blamed for this behaviour.

Most of the difficulties we face in both numerical approaches are related to the shape of the characteristic curves near the regions $I^\pm$ and the imposition of the boundary conditions. In the 1st order approach the characteristic speed of only one component of the spin-2 field increases rapidly at each region, i.e. ϕ_0 at I^- and ϕ_4 at I^+, while in the 2nd order case the behaviour is more universal, see Fig. 4.1. In addition, only ϕ_0 demands boundary treatment in the 1st order approach, while the second order nature of the system (4.8) entails that all spin-2 field's components must be supplemented with boundary conditions at $r = 1$. As a result working in the 2nd order approach is more challenging.

There is one additional advantage when working in the 2nd order approach. There are no high frequency features in the simulations done with the second order system, compare Fig. 3.1 with Fig. 5.3 and Fig. 3.5 with Fig. 5.6. For a quick reference we included in Fig. 5.8 the results of Figs. 3.5 and 5.6 for the ϕ_4 component. Notice that in the second order case the plots look much cleaner. This behaviour possibly reflects the different nature of the boundary conditions used in each case, i.e.

Dirichlet conditions (3.7) in the 1st order approach and Robin boundary conditions (5.6) in the 2nd order approach. It seems that the Robin boundary conditions are more transparent to the outgoing modes that are hitting the boundaries. This result confirms the prediction of [49] that the spurious waves will disappear in the second order formulation.
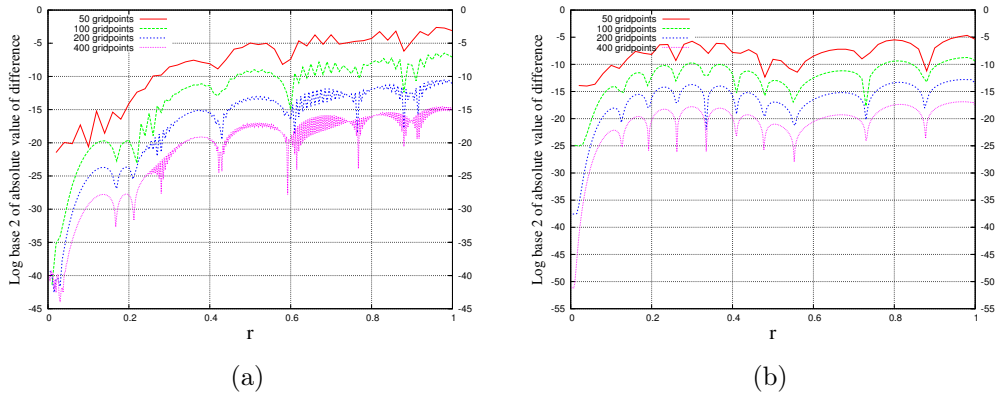

(a)   (b)

Figure 5.8: The convergence plots of ϕ_4 for the evolution of the initial data (5.14), (5.15) in the 'diagonal' representation at time $t = 1$ in (a) the first order approach and (b) the second order approach.

A more technical remark now regarding the time and computational resources needed to produce our numerical data. For the evolution of the same initial data, the CPU time in the second order approach is, as expected, slightly bigger than that in the first order approach. In addition, the system time is roughly the same in both approaches. It is worth mentioning that the RAM memory usage during our numerical simulations appears also roughly the same in both approaches.

Conclusions

In this work, the linearised general conformal field equations were extensively used to evolve several classes of asymptotically Euclidean initial data close to space-like infinity of Minkowski space-time in the settings of Fig. 2.2. The behaviour of the resulting numerical solutions near the cylinder I, which represents space-like infinity i^0 in the F-gauge, in the "horizontal" and "diagonal" conformal representations of Fig. 2.2(a) and 2.2(b), respectively, was studied. In addition, the performance of our code near the ill-behaved region I^+ was tested in various settings of the initial data.

Two distinct approaches to the linearised general conformal field equations were developed and subsequently implemented numerically. The first approach is based on a first order system of five evolution (2.30) and three constraint (2.31) equations, while the second one is described by the second order system of the five wave equations (4.8). Although, from an analytical perspective, they are equivalent, their numerical implementation could very well differ. In sec. 4.4 it was shown how to relate these two approaches in a way that helps us to compare their numerical behaviour and study any potential similarities or differences.

A brief comparison of the two approaches was carried out in sec. 5.6. Quantitatively, both codes exhibit similar behaviour close to the region I^+ where the cylinder I meets null infinity. The performance of the second order system is better regarding issues related to the accuracy of the numerical simulations. Specifically, better accuracy roughly by a factor of 4 was obtained in the second order approach. In addition, the high frequency features clearly visible in the convergence plots of the first order system disappear in the second order one. Both these results confirm the claims made in [49]. On the other hand, the numerical implementation of the second order system is more challenging mainly because of complications related to the imposition of the boundary conditions at $r = 1$.

But, this unpleasant complication can be bypassed by an appropriate coordinate transformation that will lead to a compact conformal representation of Friedrich's construction. Namely, firstly Minkowski space-time will be embedded into Einstein's static universe and then space-like infinity i^0 will be "blown up" to I. In this way, both boundaries of our computational domain will be on the cylinder I. Recall that the cylinder is a total characteristic in both approaches; thus, this setting will allow us to get rid of the artificial boundary at $r = 1$. This possibility is currently under investigation.

Our code and our numerical setting was extensively tested against already known analytical results, namely a specific family of exact solutions that respect a separation by parts ansatz (A.12) and the analytically computed expansion coefficients (3.19). Our numerical results, see secs. 3.4.1, 5.4, and 3.6 reproduce quite well the corresponding analytical results. Specifically, the accuracy involved in the reproduction of the singular logarithmic behaviour of the $a_{4,2;2,k}$ expansion coefficient is quite remarkable considering that the numerically computed data used to approximate it undergo the additional approximation (3.20).

In the "diagonal" representation, both approaches successfully evolve without loss of convergence several different classes of initial data until the region I^+ at $t = 1$. This behaviour is due to the explicit Runge-Kutta method we are using; specifically, we never evaluate the singular equations at $t = 1$ and thus we never see the singular behaviour of their coefficients $1 - \kappa'(0)$ in the first order case and $1 - \kappa(0)'^2$ in the second order case. At $(t, r) = (1, 0)$ the evolution equations degenerate and, as expected, running our code beyond that point leads quickly to numerical instabilities and code crashing.

In the "horizontal" representation though we cannot reach $t = 1$ without loss of convergence because at $t = 1$ the evolution equations become singular not only on the cylinder but on the whole computational domain $(1, r)$, see Fig. 2.2(a). The rapidly increasing characteristic speed near the region I^+ suggests the use of a Runge-Kutta method with adaptive time step, which can cope better with the behaviour of the characteristic curves near the region I^+. But, this just gets us a little bit closer to $t = 1$, again we cannot reach in finite time I^+ without loss of convergence.

However, recently [6] it was shown that in the first order formulation of the spin-2 zero-rest-mass equation it is possible to evolve asymptotically Euclidean initial data beyond I^+ and extract the physically important radiation fields on $\mathscr{I}^+$.

In sec. 5.4 we experimented with the use of the SBP operators. Specifically, we carried out numerical simulations using (first and second derivative) SBP operators of the same (full or diagonal) norm. Our results agree with their designed accuracy as described in [56]. In addition, in order to explore the potentialities of the available SBP operators, we went one step further and combined first and second derivative SBP operators with respect to *different* inner products. Our numerical results indicate that the requirement of using SBP operators with the same norm does not seem to be necessary: the second derivative full norm operator we are using seems to perform quite well even when combined with first derivative SBP operators based on a a different restricted full norm.

Having successfully reached $t = 1$ in the "diagonal" representation, the next objective is to try to go beyond it. The reason for that is the desire to use the resulting numerical solution as initial data on a hyperboloidal hypersurface and evolve it with already existing codes, e.g. [22]-[24], that have managed to evolve successfully such kind of initial data along null infinity. Thus, our code will serve as a "bridging point" between ingoing and outgoing radiation, which is exactly the reason why the cylinder was originally introduced by Friedrich.

In addition, less restrictive symmetry requirements have been considered in the construction of the background space-time on which our conformal equations will be operating. Quite substantial work has already been done in that direction and as was reported in [5] it will be soon published.

Appendix A

An exact solution of the spin-2 equation

In order to find a family of exact solutions for the system (2.30)-(2.31), one has to take a step back and start from a somehow simpler version of it. The ideal starting point for this strenuous effort is in terms of the original Minkowski metric (2.1) in Cartesian coordinates y^μ. In this setting space-like infinity is represented as a point, see Fig. 2.1(a). Our goal is to obtain, in this context, an analytic solution of the considerably simplified spin-2 system and then by transforming it according to the transformations described in sec. 2.1 to arrive at an exact solution for the complete system (2.30)-(2.31).

To acquire the form of (2.30)-(2.31) in terms of the metric $\tilde{g}$, we have first to substitute $\mu(r) = 1/r$ (and consequently $\kappa(r) = 1$) into them and then replace $t \mapsto T, r \mapsto R$, where $T = y^0$, $R^2 = (y^1)^2 + (y^2)^2 + (y^3)^2$. Thus, we end up with the system of evolution

$$
\begin{aligned}
R\,\partial_T \tilde{\phi}_0 - R\,\partial_R \tilde{\phi}_0 - \tilde{\phi}_0 + \alpha_2\,\tilde{\phi}_1 &= 0, \\
2R\,\partial_T \tilde{\phi}_1 + 2\,\tilde{\phi}_1 - \alpha_2\,\tilde{\phi}_0 + \alpha_0\,\tilde{\phi}_2 &= 0, \\
2R\,\partial_T \tilde{\phi}_2 - \alpha_0\,(\tilde{\phi}_1 - \tilde{\phi}_3) &= 0, \\
2R\,\partial_T \tilde{\phi}_3 - 2\tilde{\phi}_3 - \alpha_0\,\tilde{\phi}_2 + \alpha_2\,\tilde{\phi}_4 &= 0, \\
R\,\partial_T \tilde{\phi}_4 + R\,\partial_R \tilde{\phi}_4 + \tilde{\phi}_4 - \alpha_2\,\tilde{\phi}_3 &= 0,
\end{aligned}
\tag{A.1}
$$

and constraint

$$2R\,\partial_R\tilde{\phi}_1 + 6\,\tilde{\phi}_1 - \alpha_0\,\tilde{\phi}_2 - \alpha_2\,\tilde{\phi}_0 = 0,$$
$$2R\,\partial_R\tilde{\phi}_2 + 6\,\tilde{\phi}_2 - \alpha_0\,\tilde{\phi}_3 - \alpha_0\,\tilde{\phi}_1 = 0, \qquad \text{(A.2)}$$
$$2R\,\partial_R\tilde{\phi}_3 + 6\,\tilde{\phi}_3 - \alpha_0\,\tilde{\phi}_2 - \alpha_2\,\tilde{\phi}_4 = 0$$

equations. The first two evolution equations and the first constraint equation of (A.1)-(A.2) can be combined to produce a partial differential equation for the $\tilde{\phi}_0$ component:

$$R^2\,\partial_T^2\tilde{\phi}_0 - R^2\,\partial_R^2\tilde{\phi}_0 + 4\,R\,\partial_T\tilde{\phi}_0 - 6\,R\,\partial_R\tilde{\phi}_0 + (\alpha_2^2 - 4)\tilde{\phi}_0 = 0. \qquad \text{(A.3)}$$

Through the ansatz

$$\tilde{\phi}_0(T,R) \equiv \mathcal{R}(R)\,\mathcal{T}(T)$$

equation (A.3) takes the "almost" separable form

$$R\frac{\ddot{\mathcal{T}}}{\mathcal{T}} + 4\frac{\dot{\mathcal{T}}}{\mathcal{T}} - R\frac{\mathcal{R}''}{\mathcal{R}} - 6\frac{\mathcal{R}'}{\mathcal{R}} + \frac{\alpha_2^2 - 4}{R} = 0,$$

where $\dot{}$ and $'$ denote differentiation with respect to the time and spatial coordinate, respectively. Although the first term in the above expression is multiplied by R, the method of separation of variables can be still applied. One has to make the ansatz

$$R\frac{\mathcal{R}''}{\mathcal{R}} + 6\frac{\mathcal{R}'}{\mathcal{R}} - \frac{\alpha_2^2 - 4}{R} = k\,R + m, \qquad \text{(A.4)}$$

where the quantities appearing on the r.h.s must be constants—real, imaginary or complex. Alternatively, the above ansatz can be interpreted as

$$R\frac{\ddot{\mathcal{T}}}{\mathcal{T}} + 4\frac{\dot{\mathcal{T}}}{\mathcal{T}} = k\,R + m. \qquad \text{(A.5)}$$

Obviously, one can set

$$\frac{\ddot{\mathcal{T}}}{\mathcal{T}} = k, \quad 4\frac{\dot{\mathcal{T}}}{\mathcal{T}} = m,$$

which entails that $k \equiv \frac{m^2}{16}$. Thus, the most general solution of (A.5) is of the form

$$\mathcal{T}(T) = c_3\,e^{\frac{m}{4}\,T}, \qquad \text{(A.6)}$$

where c_3 is a constant of integration. The equation for the spatial part admits also an analytic solution. In order to keep things as simply as possible, we will consider

here only the first non-trivial case $l = 2$. For this choice of l (A.4) admits a solution of the form[1]

$$\mathcal{R}(R) = \frac{c_1 e^{\frac{mR}{4}}\left(384 + mR(-192 + mR(48 + mR(-8 + mR)))\right)}{R^5} - \frac{2c_2 e^{-\frac{mR}{4}}}{m^5 R^5}. \quad \text{(A.7)}$$

Using (A.6), (A.7), the first four evolution equations and making the convenient choice $c_2 \mapsto \frac{384 c_2 m^5}{2}, c_3 = 1$ for the constants appearing in the solutions (A.6), (A.7), it is straightforward to show that

$$\tilde{\phi}_0 = \frac{e^{-\frac{1}{4}m(R-T)}\left(e^{\frac{mR}{2}}\left(384 - 192mR + 48m^2R^2 - 8m^3R^3 + m^4R^4\right)c_1 - 384c_2\right)}{R^5},$$

$$\tilde{\phi}_1 = \frac{4e^{-\frac{1}{4}m(R-T)}\left(e^{\frac{mR}{2}}\left(-192 + 72mR - 12m^2R^2 + m^3R^3\right)c_1 + 24(8 + mR)c_2\right)}{R^5},$$

$$\tilde{\phi}_2 = \frac{8\sqrt{6}e^{-\frac{1}{4}m(R-T)}\left(e^{\frac{mR}{2}}\left(48 - 12mR + m^2R^2\right)c_1 - (48 + 12mR + m^2R^2)c_2\right)}{R^5},$$

$$\tilde{\phi}_3 = \frac{4e^{-\frac{1}{4}m(R-T)}\left(24e^{\frac{mR}{2}}(-8 + mR)c_1 + (192 + 72mR + 12m^2R^2 + m^3R^3)c_2\right)}{R^5},$$

$$\tilde{\phi}_4 = \frac{e^{-\frac{1}{4}m(R-T)}\left(384e^{\frac{mR}{2}}c_1 - (384 + 192mR + 48m^2R^2 + 8m^3R^3 + m^4R^4)c_2\right)}{R^5}.$$

The above relations provide a family of solutions for the system (A.1)-(A.2) that satisfy a separation by parts ansatz. Before we continue to the derivation of the solutions for the complete system (2.30)-(2.31), we will make a specific choice for the constants c_1, c_2, m, namely $c_1 = \frac{1}{384}, c_2 = 0, m = 0$. With this choice the above expressions reduce to the static solution

$$\tilde{\phi}_0 = \frac{1}{R^5}, \quad \tilde{\phi}_1 = -\frac{2}{R^5}, \quad \tilde{\phi}_2 = \frac{\sqrt{6}}{R^5}, \quad \tilde{\phi}_3 = -\frac{2}{R^5}, \quad \tilde{\phi}_4 = \frac{1}{R^5}. \quad \text{(A.8)}$$

Let's concentrate now on the transformations that take us from the metric $\tilde{g}$ to the one providing a cylindrical representation of space-like infinity, i.e. g. First, we have to take care of the transformations of the coordinates T, R. Following sec. 2.1, where a reflection at the origin, a rescaling, and a new time coordinate

---

[1]This solution corresponds to a special case of Teukolsky's family of quadrupole solutions [84] with $F(x) = e^{\omega x}$. In [74], the quadrupole solution of [84] has been generalised for higher multipoles, i.e. $l > 2$.

were introduced, we can establish a correspondence between the original T, R and the final t, r coordinates:

$$T = \frac{t\,k(r)}{r^2 - t^2 k(r)^2}, \quad R = \frac{r}{r^2 - t^2 k(r)^2}. \tag{A.9}$$

Relations (A.9) take care of the transformation behaviour of the r.h.s of the solutions (A.8), but do not provide any information about the behaviour of the l.h.s. That the l.h.s also transforms under (A.9) is apparent if one considers that it serves as an abbreviation for expressions of the form $\tilde{\phi}_0 = \tilde{o}^A \tilde{o}^B \tilde{o}^C \tilde{o}^D \tilde{\phi}_{ABCD}$. According to [65] the spin-2 zero-rest-mass field transforms, under rescalings of the form (2.6), as $\phi_{ABCD} = \Theta^{-1}\tilde{\phi}_{ABCD}$, where Θ is given by (2.8). The spin dyad o, ι also transforms under (A.9). To find out how they transform we have to start from the definition of the null-tetrad (2.11). For the metric $\tilde{g}$ one has $A = B = C = 1$; thus, the intrinsic derivatives (2.12) reduce to

$$\tilde{l}^a \partial_a = \frac{1}{\sqrt{2}}\left(\partial_T + \partial_R\right), \quad \tilde{n}^a \partial_a = \frac{1}{\sqrt{2}}\left(\partial_T - \partial_R\right). \tag{A.10}$$

The transformation rules for the partial derivatives in (A.10) follow easily from (A.9)

$$dT = \frac{r^2 \kappa + t^2 \kappa^3}{\left(r^2 - t^2 \kappa^2\right)^2}\,dt + \frac{-2rt\kappa + r^2 t \kappa' + t^3 \kappa^2 \kappa'}{\left(r^2 - t^2 \kappa^2\right)^2}\,dr,$$

$$dR = \frac{2rt\kappa^2}{\left(r^2 - t^2 \kappa^2\right)^2}\,dt + \frac{-r^2 - t^2 \kappa^2 + 2rt^2 \kappa \kappa'}{\left(r^2 - t^2 \kappa^2\right)^2}\,dr.$$

Plugging them into (A.10) we get the null-tetrad in terms of the t, r coordinates

$$\tilde{l}^a \partial_a = \frac{(r - t\kappa)^2\,(1 + t\kappa')}{\sqrt{2}\kappa}\,\partial_t - \frac{(r - t\kappa)^2}{\sqrt{2}}\,\partial_r$$

$$\tilde{n}^a \partial_a = \frac{(r + t\kappa)^2\,(1 - t\kappa')}{\sqrt{2}\kappa}\,\partial_t + \frac{(r + t\kappa)^2}{\sqrt{2}}\,\partial_r.$$

Finally, observing (2.11) and (2.27), one ends up with

$$\tilde{l}^a = \frac{(r - t\kappa)^2}{\kappa}\,n^a, \quad \tilde{n}^a = \frac{(r + t\kappa)^2}{\kappa}\,l^a.$$

Employing the relations $\tilde{l}^a = \tilde{o}^A \tilde{o}^{A'}, \tilde{n}^a = \tilde{\iota}^A \tilde{\iota}^{A'}, l^a = o^A o^{A'}, n^a = \iota^A \iota^{A'}$, one can establish a relation between the spin dyads o, ι and $\tilde{o}, \tilde{\iota}$:

$$\tilde{o}^A = -\frac{r - t\kappa}{\sqrt{\kappa}}\,\iota^A, \quad \tilde{\iota}^A = \frac{r + t\kappa}{\sqrt{\kappa}}\,o^A.$$

134

Now we are in position to derive the transformation laws for the components of the spin-2 zero-rest-mass field. For the 0-component we have

$$\tilde{\phi}_0 = \tilde{o}^A\tilde{o}^B\tilde{o}^C\tilde{o}^D\tilde{\phi}_{ABCD} = \frac{(r - t\kappa)^4}{\kappa^2}\iota^A\iota^B\iota^C\iota^D\Theta\,\phi_{ABCD} = \frac{(r - t\kappa)^5(r + t\kappa)}{k^3}\phi_4.$$

In a similar fashion we can obtain the transformation laws for the rest components, i.e.

$$\phi_0 = \frac{\kappa^3}{(r - t\kappa)(r + t\kappa)^5}\,\tilde{\phi}_4, \quad \phi_1 = -\frac{\kappa^3}{(r - t\kappa)^2(r + t\kappa)^4}\,\tilde{\phi}_3,$$

$$\phi_2 = \frac{\kappa^3}{(r^2 - t^2\kappa^2)^3}\,\tilde{\phi}_2, \quad \phi_3 = -\frac{\kappa^3}{(r - t\kappa)^4(r + t\kappa)^2}\,\tilde{\phi}_1, \qquad \text{(A.11)}$$

$$\phi_4 = \frac{\kappa^3}{(r - t\kappa)^5(r + t\kappa)}\,\tilde{\phi}_0.$$

Finally, by choosing $\kappa = r/(1 + r)$, i.e. the representation of Fig 2.2(b), and substituting the expressions (A.8) and (A.9) into (A.11), one ends up with an exact solution of the complete system (2.30)-(2.31):

$$\phi_0 = \frac{r^2(1 + r - t)^4}{(1 + r)^7},$$

$$\phi_1 = \frac{2r^2(1 + r - t)^3(1 + r + t)}{(1 + r)^7},$$

$$\phi_2 = \frac{\sqrt{6}r^2(1 + r - t)^2(1 + r + t)^2}{(1 + r)^7}, \qquad \text{(A.12)}$$

$$\phi_3 = \frac{2r^2(1 + r - t)(1 + r + t)^3}{(1 + r)^7},$$

$$\phi_4 = \frac{r^2(1 + r + t)^4}{(1 + r)^7}.$$

Appendix B

Numerical analysis of higher modes

For completeness, we will present here some numerical results concerning the evolution of initial data for higher order modes, i.e. $l > 2$, in the two numerical approaches considered in this work. Only the case $l = 10$ will be studied here.

Spin-2 system

The same initial bump-like data (3.14)

$$\phi_2(r) = \begin{cases} (4\,r\,b^{-2})^{16}(r-b)^{16}, & 0 \le r \le b \\ 0, & b \le r \le 1 \end{cases}$$

will be also considered here. Notice that although the initial data for ϕ_2, and consequently for X_2, coincide with the one in the $l = 2$ case, the initial data for the rest of the components are different because of (3.13). (Recall that $\alpha_x = \sqrt{l(l+1) - x}$.) Hence, our initial data are still compact supported. Which means that the same boundary condition

$$\phi_0(t, 1) = 0$$

can be still imposed on the "right" boundary with the SAT method.

   Evolving the above initial data for $b = 1$, i.e. centered around $r = 0.5$, with the evolution equations (2.30) in the "diagonal" representation $\mu = (1 + r)^{-1}$, one gets the convergence rates for ϕ_0, ϕ_4 at time $t = 1$ depicted in Tab. B.1. (The corresponding numerical solutions can be found in Fig. B.1.) The results therein are computed with respect to the numerical simulation with the higher resolution,
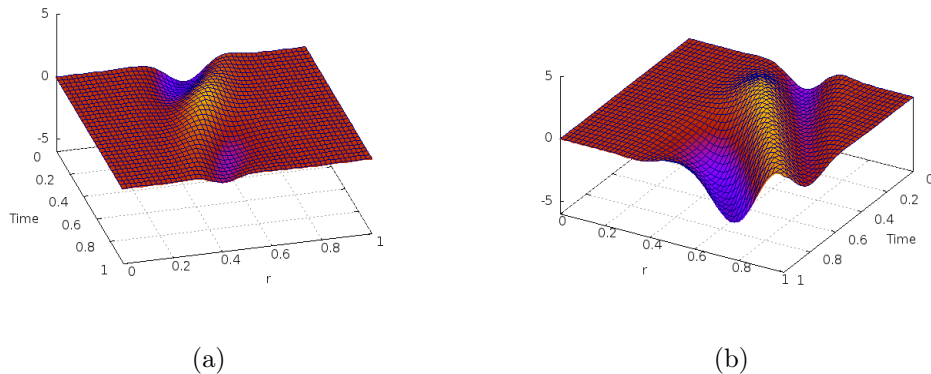
(a)   (b)

Figure B.1: The numerical solutions of (a) ϕ_0 and (b) ϕ_4 for the evolution of the initial data (3.14)—centered around $r = 0.5$—in the representation of Fig. 2.2(b)

i.e. 800 grid points. As expected, we obtain fourth order convergence for both components—similar results hold for the rest of the components. Comparing these results with the corresponding ones in the $l = 2$ case, one observes that although fourth order convergence has been obtain in both cases, the accuracy is slightly better in the $l = 10$ case. This happens because of the form of the prescribed initial data. Specifically, the amplitude of the initial data in the $l = 10$ case is smaller, see (3.13), and therefore the data are more smooth. Thus, the code is performing a little bit worse in the $l = 2$ case, as it always happens when dealing with more complicated and less smooth data.

	ϕ_0		ϕ_4	
Grid	$\log_2(||E||_2)$	Rate	$\log_2(||E||_2)$	Rate
50	-4.8375		-3.1898	
100	-8.7699	3.9325	-7.0604	3.8706
200	-12.7578	3.9879	-11.1014	4.0410
400	-16.8407	4.0829	-15.2079	4.1065

Table B.1: The normalised l^2 norm of the absolute error E and the corresponding convergence rates at time $t = 1$ for the evolution of the initial data (3.14) in the "diagonal" representation with $l = 10$.

138

Let's see now how well the constraints are preserved during the evolution of the initial data. The behaviour of the quantities (2.32) with time is illustrated in Fig. B.2. The simulation with 800 grid points was used in the derivation of the data
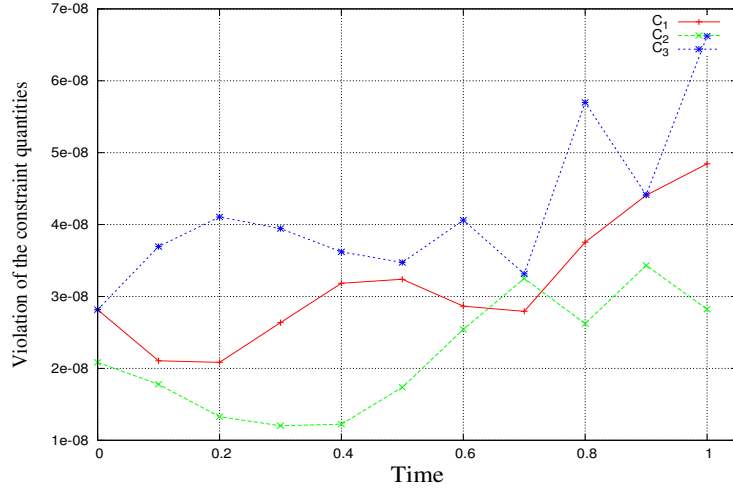

Figure B.2: The behaviour of the constraint quantities (2.32) during the evolution of the initial data (3.14) with the bump function centered at $r = 0.5$ and $l = 10$.

presented therein. Clearly, the violation of the vanishing of the constraint quantities remains at the initial labels of the order of 10^{-8}. The violation is one order smaller than the $l = 2$ case, but this again follows from the fact that in the $l = 10$ the initial data are more smooth.

Spin-2 wave system

As above, we will assume that our initial data satisfy the constraints (2.31) in the form (3.13). Therefore, we will choose again

$$\phi_2(r) = \begin{cases} (4\,r\,b^{-2})^{16}(r - b)^{16}, & 0 \le r \le b \\ 0, & b \le r \le 1 \end{cases}$$

with the first time derivatives given by (5.15), i.e.

$$\dot{\phi}_0(r) = \kappa\, \phi_0'(r) - (3\kappa' - \mu)\, \phi_0(r) - \alpha_2\, \mu\, \phi_1(r),$$
$$\dot{\phi}_1(r) = \frac{1}{2}\, \alpha_2\, \mu\, \phi_0(r) - \frac{1}{2}\, \alpha_0\, \mu\, \phi_2(r) - \mu\, \phi_1,$$
$$\dot{\phi}_2(r) = \frac{1}{2}\, \alpha_0\, \mu\, \phi_1(r) - \frac{1}{2}\, \alpha_0\, \mu\, \phi_3(r),$$
$$\dot{\phi}_3(r) = \frac{1}{2}\, \alpha_0\, \mu\, \phi_2(r) - \frac{1}{2}\, \alpha_2\, \mu\, \phi_4(r) + \mu\, \phi_3(r),$$
$$\dot{\phi}_4(r) = -\kappa\, \phi_4'(r) + (3\kappa' - \mu)\, \phi_4(r) + \alpha_2\, \mu\, \phi_3(r).$$

The Robin boundary conditions (5.6) in the from

$$g_{i,N}(t) = \phi_i(t, 1) + \phi_i'(t, 1), \quad i = 0, 1, 2, 3, 4$$

will be imposed with the SAT method, where the spatial derivatives $\phi_i'(t, 1)$ will be computed from (2.30) and (2.31) in the way described in sec. 5.5.

	ϕ_0		ϕ_4	
Grid	$\log_2(||E||_2)$	Rate	$\log_2(||E||_2)$	Rate
50	-7.4454		-4.5253	
100	-11.3557	3.9104	-8.6100	4.0847
200	-15.3389	3.9831	-12.6113	4.0013
400	-19.4204	4.0815	-16.7020	4.0907

Table B.2: The convergence rates at time $t = 1$ for the evolution of initial data centered around $r = 0.5$ in the "diagonal" representation with $l = 10$.

The numerical solutions and the convergence rates for the evolution of the above initial data with the spin-2 wave system (4.8) in the "diagonal" representation are given in Fig. B.1 and Tab. B.2, respectively. Fourth order convergence has been achieved. In addition, the violation of the constraints during the evolution is maintained at the levels of 10^{-7}, see Fig. B.3. Again, our results are slightly better than the $l = 2$ case because of the smoother initial data we are dealing with.
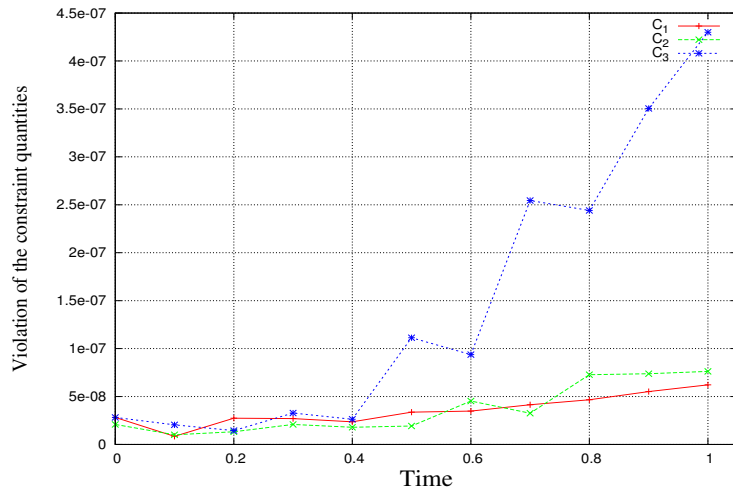
Figure B.3: The behaviour of the constraint quantities (2.32) during the evolution of initial data (5.14), (5.15) centered at $r = 0.5$ in the "diagonal" representation.

References

[1] M. A. Akivis and V. V. Goldberg, *Conformal Differential Geometry and its Generalizations*, John Wiley & Sons (1996).

[2] W. F. Ames, *Numerical Methods for Partial Differential Equations*, Academic Press (1992).

[3] A. Ashtekar and R. O. Hansen, *A Unified Treatment of Null and Spatial Infinity in General Relativity. I. Universal Structure, Asymptotic Symmetries, and Conserved Quantities at Spatial Infinity*, J. Math. Phys. 19 (1978), pp. 1542-1566.

[4] A. Ashtekar and J. D. Romano, *Spatial Infinity as a Boundary of Space-Time*, Class. Quantum Grav. 9 (1992), pp. 1069-1100.

[5] F. Beyer, G. Doulis, J. Frauendiener, and B. Whale, *Numerical Space-Times Near Space-Like and Null Infinity. The Spin-2 System on Minkowski Space*, Class. Quantum Grav. 29 (2012) 245013.

[6] F. Beyer, G. Doulis, J. Frauendiener, and B. Whale, *Linearized Gravitational Waves Near Space-Like and Null Infinity* , arXiv:1302.0043 (2013).

[7] H. Bondi, F. A. E. Pirani, and I. Robinson, *Gravitational Waves in General Relativity. III. Exact Plane Waves*, Proc. R. Soc. Lond. A 251 (1959), pp. 519-533.

[8] H. Bondi, M. G. J. van der Burg, and A. W. K. Metzner, *Gravitational Waves in General Relativity. VII. Waves from Axi-Symmetric Isolated Systems*, Proc. R. Soc. Lond. A 269 (1962), pp. 21-52.

[9] M. H. Carpenter, D. Gottlieb, and S. Abarbanel, *Time-Stable Boundary Conditions for Finite-Difference Schemes Solving Hyperbolic Systems: Methodology and Applications to High-Order Compact Schemes*, J. Comput. Phys. 111 (1994), pp. 220-236.

[10] M. H. Carpenter, J. Nordström, and D. Gottlieb, *A Stable and Conservative Interface Treatment of Arbitrary Spatial Accuracy*, J. Comput. Phys. 148 (1998), pp. 341-365.

[11] S. S. Chern, W. H. Chen, and K. S. Lam, *Lectures on Differential Geometry*, World Scientific Publishing (2000).

[12] Y. Choquet-Bruhat, *General Relativity and the Einstein Equations*, Oxford University Press (2009).

[13] Y. Choquet-Bruhat, J. Isenberg, and J. M. York, *Einstein Constraints on Asymptotically Euclidean Manifolds*, Phys. Rev. D 61 (2000), 084034.

[14] S. Dain and H. Friedrich, *Asymptotically Flat Initial Data With Prescribed Regularity at Infinity*, Commun. Math. Phys. 222 (2001), pp. 569-609.

[15] W. de Sitter, *On the Relativity of Inertia: Remarks Concerning Einstein's Latest Hypothesis*, Proc. Kon. Ned. Akad. Wet. 19 (1917), pp. 1217-1225.

[16] P. Diener, E. N. Dorband, E. Schnetter, and M. Tiglio, *Optimized High-Order Derivative and Dissipation Operators Satisfying Summation by Parts, and Applications in Three-dimensional Multi-block Evolutions*, J. Sci. Comput. 32 (2007), pp. 109-145.

[17] G. Doulis and J. Frauendiener, *The Second Order Spin-2 System in Flat Space Near Space-Like and Null-Infinity*, Gen. Relativ. Gravitation 45 (2013), pp. 1365-1385.

[18] A. Einstein, *Die Feldgleichungen der Gravitation*, Sitzungsberichte der Preussischen Akademie der Wissenschaften zu Berlin (1915), pp. 844-847.

[19] A. Einstein, *Über Gravitationswellen*, Sitzungsberichte der Königlich Preussischen Akademie der Wissenschaften zu Berlin (1918), pp.154-167.

[20] A. Einstein and N. Rosen, *On Gravitational Waves*, Journal of the Franklin Institute 223 (1937), pp. 43-54.

[21] B. Fornberg, *A Practical Guide to Pseudospectral Methods*, Cambridge University Press (1998).

[22] J. Frauendiener, *Numerical Treatment of the Hyperboloidal Initial Value Problem for the Vacuum Einstein Equations. I. The Conformal Field Equations*, Phys. Rev. D 58 (1998), 064002.

[23] J. Frauendiener, *Numerical Treatment of the Hyperboloidal Initial Value Problem for the Vacuum Einstein Equations. II. The Evolution Equations*, Phys. Rev. D 58 (1998), 064003.

[24] J. Frauendiener, *Numerical Treatment of the Hyperboloidal Initial Value Problem for the Vacuum Einstein Equations. III. On the Determination of Radiation*, Class. Quantum Grav. 17 (2000), pp. 373-387.

[25] J. Frauendiener, *The Spin-2 Equation in Spherical Symmetry*, unpublished notes.

[26] A. Friedman, *Über die Krümmung des Raumes*, Zeitschrift für Physik 10 (1922), pp. 377-386.

[27] A. Friedman, *Über die Möglichkeit einer Welt mit konstanter negativer Krümmung des Raumes*, Zeitschrift für Physik 21 (1924), pp. 326-332.

[28] H. Friedrich, *On the Regular and the Asymptotic Characteristic Initial Value Problem for Einstein's Vacuum Field Equations*, Proc. R. Soc. Lond. A 375 (1981), pp. 169-184.

[29] H. Friedrich, *The Asymptotic Characteristic Initial Value Problem for Einstein's Vacuum Field Equations as an Initial Value Problem for a First-Order Quasilinear Symmetric Hyperbolic*, Proc. R. Soc. Lond. A 378 (1981), pp. 401-421.

[30] H. Friedrich, *Cauchy Problems for the Conformal Vacuum Field Equations in General Relativity*, Commun. Math. Phys. 91 (1983), pp. 445-472.

145

[31] H. Friedrich, *On Static and Radiative Space-Times*, Commun. Math. Phys. 119 (1988), pp. 51-73.

[32] H. Friedrich, *Einstein Equations and Conformal Structure: Existence of Anti-de Sitter-Type Space-Times*, J. Geom. Phys. 17 (1995), pp. 125-184.

[33] H. Friedrich, *Gravitational Fields Near Space-Like and Null Infinity*, J. Geom. Phys. 24 (1998), pp. 83-163.

[34] H. Friedrich, *Conformal Einstein Evolution*, in The Conformal Structure of Space-time: Geometry, Analysis, Numerics, eds. J. Frauendiener and H. Friedrich, Springer (2002), pp. 1-50.

[35] H. Friedrich, *Conformal Geodesics on Vacuum Space-Times*, Commun. Math. Phys. 235 (2003), pp. 513-543.

[36] H. Friedrich, *Spin-2 Fields on Minkowski Space Near Spacelike and Null Infinity*, Class. Quantum Grav. 20 (2003), pp. 101-117.

[37] H. Friedrich, *Smoothness at Null Infinity and the Structure of Initial Data*, in The Einstein Equations and the Large Scale Behavior of Gravitational Fields, eds. P. Chruściel and H. Friedrich, Birkhäuser Verlag (2004), pp. 121-204.

[38] H. Friedrich and B. G. Schmidt, *Conformal Geodesics in General Relativity*, Proc. R. Soc. Lond. A 414 (1987), pp. 171-195.

[39] R. Geroch, *Structure of the Gravitational Field at Spatial Infinity*, J. Math. Phys. 13 (1972), pp. 956-968.

[40] R. Geroch, *Asymptotic Structure of Space-time*, in Asymptotic Structure of Space-time, eds. T. P. Esposito and L. Witten, Plenum Press (1977), pp. 1-105.

[41] J. Gong and J. Nordström, *Interface Procedures for Finite Difference Approximations of the Advection-Diffusion Equation*, J. Computational Applied Mathematics 236 (2011), pp. 602-620.

[42] B. Gustafsson, H. O. Kreiss, and J. Oliger, *Time Dependent Problems and Difference Methods*, John Wiley & Sons (1995).

[43] E. Hairer, S. P. Norsett, and G. Wanner, *Solving Ordinary Differential Equations I: Nonstiff Problems*, Springler-Verlag (1993).

[44] S. W. Hawking and G. F. R. Ellis, *The Large Scale Structure of Space-time*, Cambridge University Press (1973).

[45] F. John, *Partial Differential Equations*, Springer-Verlag (1982).

[46] D. Kennefick, *Travelling at the Speed of Thought: Einstein and the Quest for Gravitational Waves*, Princeton University Press (2007).

[47] M. Ko, E. T. Newman, and K. P. Tod, $\mathfrak{H}$-*Space and Null Infinity*, in Asymptotic Structure of Space-time, eds. T. P. Esposito and L. Witten, Plenum Press (1977), pp. 227-271.

[48] O. Korobkin, B. Aksoylu, M. Holst, E. Pazos, and M. Tiglio, *Solving the Einstein Constraint Equations on Multi-Block Triangulations Using Finite Element Methods*, Class. Quantum Grav. 26 (2009), 145007.

[49] H. O. Kreiss and O. E. Ortiz, *Finite Element and Finite Difference Methods for Hyperbolic Partial Differential Equations*, in The Conformal Structure of Space-Time: Geometry, Analysis, Numerics, eds. J. Frauendiener and H. Friedrich, Springer-Verlag (2002), pp. 359-370.

[50] H. O. Kreiss and G. Scherer, *Some Mathematical and Numerical Questions Connected With First and Second Order Time Dependent Systems of Partial Differential Equations*, in Mathematical Aspects of Finite Elements in Partial Differential Equations, ed. C. De Boor, Academic Press (1974).

[51] H. O. Kreiss and G. Scherer, *On the Existence of Energy Estimates for Difference Approximations for Hyperbolic Systems*, Technical Report, Dept. of Scientific Computing, Uppsala University (1977).

[52] L. Lehner, D. Neilsen, O. Reula, and M. Tiglio, *The Discrete Energy Method in Numerical Relativity: Towards Long-Term Stability*, Class. Quantum Grav. 21 (2004), pp. 5819-5848.

[53] L. Lehner, O. Reula, and M. Tiglio, *Multi-Block Simulations in General Relativity: High Order Discretizations, Numerical Stability, and Applications*, Class. Quantum Grav. 22 (2005), pp. 5283-5322.

[54] A. Lichnerowicz, *L'intégration des équations de la gravitation relativiste et le problème des n corps*, J. Math. Pures Appl. 23 (1944), 37-63.

[55] K. Mattsson, *Boundary Procedures for Summation-by-Parts Operators*, J. Sci. Comput. 18 (2003), pp. 133-153.

[56] K. Mattsson and J. Nordström, *Summation by Parts Operators for Finite Difference Approximations of Second Derivatives*, J. Comput. Phys. 199 (2004), pp. 503-540.

[57] K. Mattsson, F. Ham, and G. Iaccarino, *Stable Boundary Treatment for the Wave Equation on Second-Order Form*, J. Sci. Comput. 41 (2009), pp. 366-383.

[58] K. Mattsson, *Summation by Parts Operators for Finite Difference Approximations of Second-Derivatives with Variable Coefficients*, J. Sci. Comput. 51 (2012), pp. 650-682.

[59] E. T. Newman and R. Penrose, *An Approach to Gravitational Radiation by a Method of Spin Coefficients*, J. Math. Phys. 3 (1962), pp. 566-578.

[60] P. O'Donnell, *Introduction to 2-Spinors in General Relativity*, World Scientific Publishing (2003).

[61] E. Pazos, M. Tiglio, M. D. Duez, L. E. Kidder, S. A. Teukolsky, *Orbiting Binary Black Hole Evolutions With a Multipatch High Order Finite-Difference Approach*, Phys. Rev. D 80 (2009), 024027.

[62] R. Penrose, *Asymptotic Properties of Fields and Space-Times*, Phys. Rev. Lett. 10 (1963), pp. 66-68.

[63] R. Penrose, *Zero Rest-Mass Fields Including Gravitation: Asymptotic Behaviour*, Proc. R. Soc. Lond. A 284 (1965), pp. 159-203.

[64] R. Penrose, *Structure of Space-Time*, in Battelle Rencontres, eds. C. M. deWitt and J. A. Wheeler, W. A. Benjamin, Inc. (1968), pp. 121-235.

[65] R. Penrose and W. Rindler, *Spinors and Space-Time*, Vol. 1, Cambridge University Press (1986).

[66] R. Penrose and W. Rindler, *Spinors and Space-Time*, Vol. 2, Cambridge University Press (1986).

[67] S. Persides, *A Definition of Asymptotically Minkowskian Space-Times*, J. Math. Phys. 20 (1979), pp. 1731-1740.

[68] S. Persides, *Structure of the Gravitational Field at Spatial Infinity. I. Asymptotically Euclidean Spaces*, J. Math. Phys. 21 (1980), pp. 135-141.

[69] S. Persides, *Structure of the Gravitational Field at Spatial Infinity. II. Asymptotically Minkowskian Space-Times*, J. Math. Phys. 21 (1980), pp. 142-151.

[70] F. A. E. Pirani, *Invariant Formulation of Gravitational Radiation Theory*, Phys. Rev. 105 (1957), pp. 1089-1099.

[71] E. Poisson, *A Relativist's Toolkit: The Mathematics of Black-Hole Mechanics*, Cambridge University Press (2004).

[72] H. Reissner, *Über die Eigengravitation des Elektrischen Feldes nach der Einsteinschen Theorie*, Annalen der Physik 50 (1916), pp. 106-120.

[73] M. Renardy and R. C. Rogers, *An Introduction to Partial Differential Equations*, Springer-Verlag (1993).

[74] O. Rinne, *Explicit Solution of the Linearized Einstein Equations in TT Gauge for All Multipoles*, Class. Quantum Grav. 26 (2009) 048003.

[75] R. K. Sachs, *Gravitational Waves in General Relativity. VI. The Outgoing Radiation Condition*, Proc. R. Soc. Lond. A 264 (1961), pp. 309-338.

[76] R. K. Sachs, *Gravitational Waves in General Relativity. VIII. Waves in Asymptotically Flat Space-Time*, Proc. R. Soc. Lond. A 270 (1962), pp. 103-126.

[77] B. G. Schmidt, *A New Definition of Singular Points in General Relativity*, Gen. Relativ. Gravitation 1 (1971), pp. 269-280.

[78] B. G. Schmidt, *Asymptotic Structure of Isolated Systems*, in Isolated Gravitating Systems in General Relativity, ed. J. Ehlers, North-Holland Pub. Co. (1979), pp. 11-49.

[79] B. G. Schmidt, *Conformal Geodesics*, in Conformal Groups and Related Symmetries, Physical Results and Mathematical Background, ed. A.O. Barut and H.D. Doebner, Springer (1986), pp. 135-137.

[80] E. Schnetter, P. Diener, E. N. Dorband, and M. Tiglio, *A Multi-Block Infrastructure for Three-Dimensional Time-Dependent Numerical Relativity*, Class. Quantum Grav. 23 (2006), pp. S553-S578.

[81] K. Schwarzschild, *Über das Gravitationsfeld eines Massenpunktes nach der Einsteinschen Theorie*, Sitzungsberichte der Königlich Preussischen Akademie der Wissenschaften zu Berlin (1916), pp. 189-196.

[82] P. Sommers, *The Geometry of the Gravitational Field at Spacelike Infinity*, J. Math. Phys. 19 (1978), pp. 549-554.

[83] B. Strand, *Summation by Parts for Finite Difference Approximations for d/dx*, J. Comput. Phys. 110 (1994), pp. 47-67.

[84] S. A. Teukolsky, *Linearized Quadrupole Waves in General Relativity and the Motion of Test Particles*, Phys. Rev. D 26 (1982), pp. 745-750.

[85] G. F. Torres del Castillo, *3-D Spinors, Spin-Weighted Functions and Their Applications*, Birkhäuser (2003).

[86] A. Trautman, *Radiation and boundary conditions in the theory of gravitation*, Bull. Acad. Polon. Sci., sér. sci. math., astr. et phys. 6 (1958), pp. 407-412.

[87] J. W. York, *Conformally invariant orthogonal decomposition of symmetric tensors on Riemannian manifolds and the initial-value problem of general relativity*, J. Math. Phys. 14 (1973), pp. 456-464.

[88] J. A. Valiente Kroon, *Polyhomogeneous Expansions Close to Null and Spatial Infinity*, in The Conformal Structure of Space-Time: Geometry, Analysis, Numerics, eds. J. Frauendiener and H. Friedrich, Springer-Verlag (2002), pp. 135-160.

[89] J. A. Valiente Kroon, *Time asymmetric spacetimes near null and spatial infinity: I. Expansions of developments of conformally flat data*, Class. Quantum Grav. 21 (2004), pp. 5457-5492.

[90] J. A. Valiente Kroon, *Time asymmetric spacetimes near null and spatial infinity: II. Expansions of developments of initial data sets with non-smooth conformal metrics*, Class. Quantum Grav. 22 (2005), pp. 1683-1707.

[91] R. B. Wald, *General relativity*, The University of Chicago Press (1984).